INFORMATION TO USERS

This manuscript has been reproduced from the microfilm master. UMI films the text directly from the original or copy submitted. Thus, some thesis and dissertation copies are in typewriter face, while others may be from any type of computer printer.

The quality of this reproduction is dependent upon the quality of the copy submitted. Broken or indistinct print, colored or poor quality illustrations and photographs, print bleedthrough, substandard margins, and improper alignment can adversely affect reproduction.

In the unlikely event that the author did not send UMI a complete manuscript and there are missing pages, these will be noted. Also, if unauthorized copyright material had to be removed, a note will indicate the deletion.

Oversize materials (e.g., maps, drawings, charts) are reproduced by sectioning the original, beginning at the upper left-hand corner and continuing from left to right in equal sections with small overlaps. Each original is also photographed in one exposure and is included in reduced form at the back of the book.

Photographs included in the original manuscript have been reproduced xerographically in this copy. Higher quality 6" x 9" black and white photographic prints are available for any photographs or illustrations appearing in this copy for an additional charge. Contact UMI directly to order.

UMI

A Bell & Howell Information Company
300 North Zeeb Road, Ann Arbor MI 48106-1346 USA
313/761-4700 800/521-0600

Antennas for Personal Communication Systems

by

Mark Gordon Douglas
B.Eng., University of Victoria, 1990
M.Sc., University of Calgary, 1993

A Dissertation Submitted in Partial Fulfillment of the
Requirements for the Degree of

DOCTOR OF PHILOSOPHY

in the Department of Electrical and Computer Engineering

We accept this dissertation as conforming to the required standard

---

Dr. M.A. Stuchly, Supervisor (Department of Electrical and Computer Engineering)

Dr. S.S. Stuchly, Supervisor (Department of Electrical and Computer Engineering)

Dr. V.K. Bhargava, Departmental Member (Dept. of Electrical and Computer Eng.)

Dr. J. Bornemann, Departmental Member (Dept. of Electrical and Computer Eng.)

Dr. D. Olesky, Outside Member (Department of Computer Science)

Dr. R.H. Johnston, External Examiner (Dept. of Electrical and Computer Engineering, University of Calgary)

Supervisors: Dr. Maria A. Stuchly and Dr. Stanislaw S. Stuchly

Abstract

The worldwide demand for personal communication system (PCS) devices is motivating the development of compact, high-performance antennas. It is also prompting a better understanding of the effects of the user and the mobile communication environment on the antenna performance. The objective of this dissertation is to add to the current knowledge in both areas. Using the Finite-Difference Time-Domain (FDTD) technique, a monopole antenna and a diversity antenna were modeled for PCS applications. Also, techniques were developed and applied to facilitate the accurate numerical analysis of PCS antennas and to investigate the electromagnetic interaction between PCS antennas and the mobile communication environment.

A monopole antenna and a polarization diversity antenna (PDA) were investigated at frequencies near 900 MHz. Antenna performance was evaluated in terms of the far-field radiation patterns, the mean effective gain (MEG), the radiation efficiency and the specific absorption rate (SAR) of energy in the user's body. For the diversity antenna, the statistical independence of the two diversity branches was determined from the correlation coefficient. The antenna modeling incorporated the antenna, a cellular telephone handset, models of the user's head and hand, and a statistical model of the mobile environment. Two mobile environments, an urban outdoor environment and a suburban outdoor environment, were modeled. The results show that (i) changing the antenna configuration from the monopole antenna to the PDA significantly affects the

antenna efficiency and SAR in the user's body; (ii) the type of mobile communication environment chosen (urban or suburban) has a pronounced effect on the correlation coefficient of the PDA and on the MEGs of the PDA and the monopole antenna; (iii) in terms of the MEG, the PDA is more sensitive than the monopole antenna to the presence of the user's body; and (iv) overall, the PDA performs better than the monopole antenna in terms of antenna efficiency, peak averaged SAR in the head, and MEG.

The accurate FDTD modeling of wires is crucial to the FDTD analysis of PCS antennas, particularly as monopole antennas and other linear wire antennas are often used with PCS devices. A study of the FDTD modeling of thin wires is included in this dissertation. The accuracy of the wire models was determined by calculating the input impedance of a dipole antenna over a broad range of dipole radii and comparing with the results of a Method of Moments formulation. Two existing thin wire models were analyzed and found to be inaccurate for some purposes. This finding led to the development of a new model, which includes a special treatment of the field components at the wire ends and a model of the source region. The proposed wire model is more accurate than the two existing wire models for a given spatial resolution. Thus, this new wire model facilitates accurate computations of input impedance and resonant frequency for linear wire antennas. The stability of the wire model was addressed, and a formulation for the maximum stability coefficient to be used with the proposed thin wire model was developed.

Examiners:

Dr. M.A. Stuchly, Supervisor (Department of Electrical and Computer Engineering)

Dr. S.S. Stuchly, Supervisor (Department of Electrical and Computer Engineering)

Dr. V.K. Bhargava, Departmental Member (Dept. of Electrical and Computer Eng.)

Dr. J. Bornemann, Departmental Member (Dept. of Electrical and Computer Eng.)

Dr. D. Olesky, Outside Member (Department of Computer Science)

Dr. R.H. Johnston, External Examiner (Dept. of Electrical and Computer Engineering, University of Calgary)

Table of Contents

List of Tables

List of Figures

Chapter 1 Introduction

1.1 Motivation

Due to the current demand for personal communication systems (e.g. cellular telephones, mobile data systems and global positioning systems), there is a need for compact, high-performance antennas. The requirements of high performance and compact size are often conflicting, which makes the design of these antennas very challenging. In addition, the interaction of the antenna with its environment, and the effects of this interaction on antenna performance must be understood. The close proximity of the user in the antenna near field, the small antenna ground plane, and the surrounding multipath environment all need to be taken into consideration. When numerical techniques are used to model and design antennas, the accuracy of the numerical model must also be considered.

The objective of the research is to expand the current knowledge of the electromagnetic interaction between a personal communication system (PCS) antenna and its environment. Investigated in this research are the effects of the user proximity and the multipath environment on antenna performance. The absorption of electromagnetic energy in the user's body is also studied. The emphasis of the antenna analysis is on a microstrip antenna and a monopole antenna on a PCS handset. While the monopole

antenna is the prevailing design, microstrip antennas are attracting increasing attention in PCS due to their light weight and thin profile. Antennas are investigated with the use of numerical techniques, particularly the Finite-Difference Time-Domain (FDTD) method. The FDTD method is a widely-used technique that is increasingly applied to the analysis and design of antennas. It has also recently been accepted by the Standards Committee of the Institute of Electrical and Electronics Engineers (IEEE) as the standard numerical technique for the evaluation of SAR due to human exposure to radio frequency (RF) fields from PCS devices. In this research, developments of the FDTD code have been made to improve the analysis of antennas. These include an improved FDTD algorithm for the analysis of wire antennas.

The antenna of a PCS device is typically only a few centimeters away from the user's body. This has consequences for both the antenna and the user. Since the user's body behaves as a lossy dielectric at microwave frequencies, its presence modifies the far-field radiation pattern and other antenna characteristics. A significant fraction of the radiated energy is absorbed by the body, resulting in lower antenna efficiency and possible health risks for the user. Most previous work in PCS antenna development has not taken the proximity of the user into account due to the complexity of modeling a human body. However, recent advances in numerical electromagnetic modeling techniques, including the FDTD method, have made this viable. The effect of the user's body on the antenna efficiency and the specific absorption rate (SAR) of energy in the body will be analyzed in this work using the FDTD method.

The performance of a PCS antenna is also influenced by the multipath environment. In this environment, objects such as buildings, cars and people scatter RF signals from transmitting antennas into many signal components. Thus the signal incident on the receiving antenna is composed of many components which have travelled along different paths. These signal components may combine destructively at the receiving antenna, resulting in random signal fading and other signal distortions. The effects of the multipath environment on antenna performance will be analyzed using the FDTD method and statistical techniques. The use of diversity antennas to alleviate multipath fading will be addressed, and a polarization diversity antenna (PDA) will be investigated. The performance of the PDA will be compared to that of a monopole antenna.

The FDTD analysis of antennas relies on the accurate FDTD modeling of wires and other objects. When at least one dimension of a modeled object is small compared to a practical size for the FDTD cells, subcell modeling can be performed in the cells adjacent to the object to improve the accuracy of the FDTD field update equations. The subcell modeling of thin wires in the FDTD technique is addressed in this dissertation. It will be shown that although FDTD wire modeling has been applied successfully in the past to scattering and radiation problems, there has not been a thorough investigation of the accuracy of FDTD wire models in calculating the antenna input impedance. A detailed numerical evaluation of the input impedance of dipole antennas is provided in the dissertation. Two currently used subcell wire models are investigated, including a model considered to be the standard in many present FDTD programs, and it is shown

that these models are not sufficiently accurate for some purposes, even when relatively fine spatial discretizations are used. In response to these findings, a new subcell wire model is proposed which includes special modeling of the wire ends and the source region. The improved accuracy of the new subcell wire model compared to that of the other models will be demonstrated.

1.2 Contributions

There are two major contributions of this dissertation to the numerical analysis and design of antennas for PCS devices. The first major contribution is the analysis of two practical PCS antennas, using numerical and statistical techniques, to investigate the effects of the PCS user and surrounding environment on antenna performance. The second major contribution is a thorough analysis of the accuracy of FDTD wire models and the development of a new wire model which facilitates the accurate computation of the input impedance of linear wire antennas. Specific contributions of the dissertation are:

- the further development of a novel polarization diversity antenna for practical application on a PCS device (this antenna was invented by the author and his supervisor during the course of the Master's thesis work),
- the application of statistical techniques, in concert with the FDTD technique and an accurate biological model of the user, to form a qualitative evaluation of the performance of PCS antennas which takes into account the proximity of the user and the multipath environment,
- the comparison of numerical and experimental results of the diversity antenna and a

performance comparison of the diversity antenna and a monopole antenna,

- an analysis of how the following factors influence the antenna performance and the absorbed power in the user: the type of antenna, the type of environment (urban or suburban), and the presence of parts of the user's body (head and hand).
- a method of analyzing the accuracy of FDTD subcell wire models based on the calculated input impedance of a dipole antenna,
- the application of this method to analyze the accuracy of two existing wire models,
- the development of a stable FDTD model for a resistive excitation inside a wire, and
- the development of a novel subcell wire model for the FDTD technique which allows for the more accurate calculation of the input impedance of linear wire antennas.

1.3 Outline of the Dissertation

Chapter 2 reviews the background material relevant to the development of microstrip antennas for PCS. The advantages and limitations of microstrip antennas are discussed and the basic theory of microstrip antennas is presented, including the radiation mechanism and the relationships between physical and electrical parameters. As microstrip antennas typically have narrow input impedance bandwidths, some attention is devoted to techniques of improving their bandwidths. The contributions of other researchers in this area are reviewed.

Chapter 3 addresses the electromagnetic interaction between a PCS antenna and its surroundings. The interaction between the antenna and the PCS user is treated in Section 3.1, beginning with an overview of the known health effects and the protective standards

of human exposure to RF fields. Also discussed is the biological model of the PCS user utilized in this research. In the remainder of Chapter 3, the current knowledge on how the performance of a PCS antenna is affected by the proximity of the user, the small ground plane and the multipath environment is discussed.

The numerical modeling techniques used in this work are described in Chapter 4. This chapter introduces the main concepts of the FDTD technique and the Method of Moments (MoM) and discusses their suitability to the research.

The research results are presented in Chapters 5 and 6. Chapter 5 provides the results of the interaction between two PCS antennas and the user's body. A polarization diversity antenna and a monopole antenna are analyzed at frequencies near 900 MHz to investigate the effects of the proximity of the user's body and the multipath environment on the antenna performance. The absorption of energy in the user's body is also evaluated. The two antennas are analyzed in terms of the radiation patterns, the mean effective gain (MEG), the correlation coefficient (for the diversity antenna), the SAR in the user and the antenna efficiency.

In Chapter 6, the subcell modeling of wires in the FDTD technique is introduced, and a test is defined for the evaluation of wire model accuracy. This test is applied to two currently used wire models, and it is shown that the accuracy of both models is poor. A new wire model is proposed which includes special treatments of the wire ends and the source region. The results demonstrate that the new wire model has good accuracy over

a broad range of wire radii. The stability of the proposed wire model is also addressed.

Chapter 2 Microstrip Antennas

As cellular telephones and other PCS devices have become smaller and more portable, the demand for microstrip antennas has increased. Their light weight, thin profile, and ease of fabrication make microstrip antennas attractive alternatives to other antenna configurations. In addition, microstrip antennas are mechanically rigid, which makes them less susceptible to damage than wire antennas. Microstrip antennas can also be designed and positioned on a cellular telephone handset to minimize the amount of radiation absorbed by the user. The analysis of microstrip antennas was important for the dissertation research. One microstrip antenna, a polarization diversity antenna, is presented in Chapter 5.

In the following sections, information relevant to the development of microstrip antennas for personal communication systems (PCS) is presented. This includes the historical development of microstrip antennas, their advantages and limitations, and microstrip antenna theory. For the development of microstrip antennas, the relationships between physical and electrical parameters are provided and techniques of improving the impedance bandwidth are reviewed.

2.1 Microstrip Antenna Background

Before reviewing the historical developments and the advantages and limitations of microstrip antennas, a brief description of the microstrip antenna is presented here. An example of a rectangular microstrip antenna and its feed network is illustrated in Fig. 2.1. Microstrip antennas consist of one or more conducting patches, a dielectric substrate and a ground plane, as shown. The conducting patch resonates at a frequency at which the characteristic length of the antenna (*b* in Fig. 2.1) is on the order of one-half wavelength [1]. The top surface of the antenna is accessible, so circuits (e.g. matching networks, phasing circuits and power splitters) can be built onto the top surface. In microstrip antenna design, there are many choices for the patch size, the number of patch elements and the feed configuration.

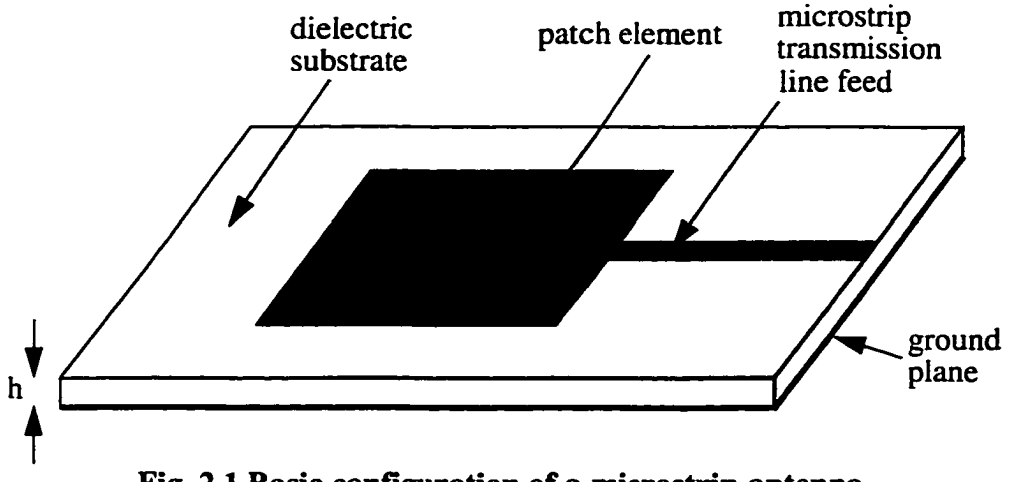

Fig. 2.1 Basic configuration of a microstrip antenna.

2.1.1 Historical Developments

Microstrip technology was initially applied to the design of non-radiating circuits, such as filters and couplers, where radiation represents loss and should be suppressed.

However, in the early 1950s, Deschamps studied ways of enhancing this radiation and introduced the concept of microstrip circuits as antennas [2]. Although this concept later became very popular, it did not initially attract significant attention for over two decades. The United States military developed the first practical use of microstrip antennas during the mid 1970s, realizing that their thin profile made microstrip antennas attractive for installations on missiles or other aircraft without affecting their aerodynamics. Commercial interest in the microstrip antenna followed by the late 1970s. This interest was slow at first [3], but it gained momentum once inexpensive, low-loss substrate materials became available, the cost of manufacturing was reduced, analytical and numerical analysis techniques were developed, and markets for these antennas emerged. Electronic circuit miniaturization also played an important role. One of the first markets for microstrip antennas was satellite communication [3]. Due to strict size and weight requirements and the need for mechanical rigidity on satellites, microstrip antennas were favoured over other antenna configurations (such as monopoles, helices, horns and parabolic reflectors). Today, microstrip antennas are used in a variety of applications, including air navigation and radar [3],[4], and there is increasing interest in them for PCS. Microstrip antennas are used at frequencies from 100 MHz to 50 GHz [1].

2.1.2 Advantages and Limitations

Microstrip antennas have many advantages which make them preferable in many applications. These advantages include [1]:

- *light weight and compact size*. Microstrip antennas can be made of light weight

dielectric substrates, and they usually have low profiles. Therefore, they can be used in systems where there are weight or size constraints. The low profile adds to the mechanical rigidity of the antenna. Microstrip antennas can also be made unobtrusive if aerodynamics or aesthetics are important.

- *low manufacturing cost.* A simple etching process is used to fabricate microstrip antennas, making them amenable to mass production. Feed lines and matching networks can also be fabricated at the same time.
- *easy mounting.* The antenna can be mounted onto planar or non-planar surfaces with minor alterations.
- *different polarizations possible.* The polarization of a patch antenna can be easily modified to any of a number of linear or circular polarizations with a change in the feed positions or a change in the phase relationships between feeds.
- *dual-frequency operation possible.* This advantage can offset the problem of narrow impedance bandwidths.
- *compatibility with integrated circuits.* Circuit elements can be deposited directly onto the antenna surface at the time of fabrication.

Microstrip antennas also have limitations compared with other antennas. These include:

- *narrow bandwidth.* The impedance bandwidth of a microstrip antenna (usually defined as the bandwidth within which the voltage standing wave ratio, *VSWR*, is no more than two) is typically in the range of 1 to 3% [5]. However, bandwidths greater than 30% have been reported [6]-[11].
- *higher losses*, notably in the antenna substrate and in the feed network.

- *lower power handling capability*, due to dielectric breakdown.
- *electrical properties which are difficult to analyze*, due to the fact that the antenna elements typically rest between two media of different dielectric constants.
- *the possible excitation of surface waves*, which results in distortion of the radiation pattern, unwanted coupling between antenna elements, and power loss.
- *poor isolation* between the feed and the radiating elements.

For many applications, the advantages of microstrip antennas outweigh their limitations. In fact, it is expected that in the future, microstrip antennas will replace conventional antennas in many applications [1]. There is increasing interest in microstrip antennas for mobile communication, where light weight, compact size and low manufacturing cost are desired, and bandwidth and power handling capacity are not critical.

2.2 Microstrip Antenna Theory

This section provides the theoretical background necessary for understanding the general aspects of microstrip antenna analysis. The section begins with a description of the basic radiation mechanism of microstrip antennas. Essential relationships between physical parameters and electrical properties are discussed. Previously used methods to increase the bandwidth of microstrip antennas are also reviewed.

2.2.1 Radiation Mechanism

Despite the simple geometry of the microstrip antenna, its electrical behaviour is

complicated to analyze, due to the fact that the radiating elements typically rest between two media of different dielectric constants. Fields in the medium above the patch may have different velocities of propagation than the fields in the medium below the patch. Also, the analysis of microstrip patch antennas requires an understanding of dielectric and conductor losses, scattering and refraction at the dielectric boundary, and the excitation of surface waves [1].

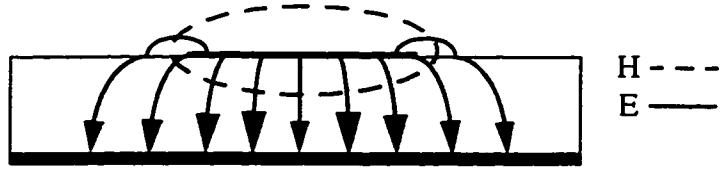

Fig. 2.2 Cross-section of a microstrip circuit showing field lines.

Figure 2.2 presents a cross-sectional view of a microstrip patch antenna, showing the distribution of the electric and magnetic fields. An electric field is excited between the patch and the ground plane when there is a potential difference between them. Far from the patch edges the electric field under the patch is directed vertically towards the ground plane, but near the patch edges, fringing of the fields results. Some of the fringing fields separate from the antenna to become radiating fields. As described in the next section, radiation from the patch is strongly affected by the physical parameters of the patch (including the patch size and the substrate thickness). Understanding the relationships between the physical parameters of the antenna and its electrical properties can be difficult, particularly if the patch shape is not simple. As a consequence, although patch conductors can be designed to have any flat shape, much of the previous work on microstrip antennas was restricted to patches with simple shapes, such as rectangles and

circles. Recently however, the development of numerical electromagnetic techniques, together with the increased memory and computing power of computers, have made it possible to explore more complex structures.

2.2.2 Relationships Between Physical and Electrical Parameters

This section describes how the physical properties of a microstrip antenna affect the antenna electrical characteristics (such as bandwidth, efficiency, radiation pattern and centre frequency).

The dielectric constant of the substrate influences the antenna resonant frequency, bandwidth, efficiency and most other antenna parameters. For a given antenna size, the operating frequency is inversely proportional to the square root of the dielectric constant. For example, the resonant frequency, f_r, of the fundamental mode of a rectangular patch is [4]:

$$f_r = \frac{c}{2\,(b + 2\Delta l)\,\sqrt{\varepsilon_e}} \tag{2.1}$$

where c is the speed of light in free space, b is the length of the patch (from Fig. 2.1), $2\Delta l$ is the effective increase in the patch length due to fringing fields, and ε_e is the effective dielectric constant of the antenna (the composite relative dielectric constant of both the fields in the substrate and the fields above the patch). The values of Δl and ε_e are difficult to determine, as they depend on the fringing of the fields, and only empirical

formulas exist for simple geometries. An approximate formula for ε_e of a rectangular patch antenna with an air superstrate and a dielectric substrate with relative dielectric constant of ε_r is [1]:

$$\varepsilon_e = \frac{\varepsilon_r + 1}{2} + \frac{\varepsilon_r - 1}{2\sqrt{1 + 12h/a}} \tag{2.2}$$

where h and a are the thickness and width of the antenna (see Fig. 2.1) and $a \geq h$. Thus, the effective dielectric constant of the antenna has a value between the relative dielectric constants of the air and the substrate (i.e. $1 \leq \varepsilon_e \leq \varepsilon_r$). At a given resonant frequency, the size of the antenna can be reduced by increasing ε_r, as evident from (2.1). However, a larger dielectric constant results in the reduction of the bandwidth, gain and efficiency [4].

Temperature and anisotropy of the substrate can cause changes in the dielectric constant. For example, anisotropy in ceramic polytetrafluoroethylene (PTFE) and random fiber PTFE causes typical variations in the dielectric constant of 2.4% and 1.7%, respectively [12]. Changes to the dielectric constant affect other parameters. For example, the sensitivity of the operating frequency to changes in the dielectric constant can be derived from (2.1). It can be expressed as [12]:

$$\frac{df_r}{f_r} = -\frac{1}{2}\frac{d\varepsilon_r}{\varepsilon_r} \tag{2.3}$$

The substrate dielectric constant also determines which parameter tolerances affect the antenna resonant frequency. For substrates with low dielectric constants (e.g. $\varepsilon_r \leq 2.5$), the resonant frequency is strongly affected by tolerances in the antenna size. For antennas with high dielectric constant substrates ($\varepsilon_r \geq 10$), the resonant frequency is sensitive to tolerances in the dielectric constant. In some cases, the manufacturer tolerance on ε_r can be insufficient for accurate design [12].

Dielectric substrates are available today with dielectric constants that vary over a wide range [12]. Materials from dielectric foams (e.g. polymethacrylamid hard foam: ε_r = 1.07) to ceramics (e.g. silicone resin ceramic: $\varepsilon_r = 25$) are used [1], and materials with ε_r > 50 are available [13]. Frequently used substrates include RT/duroid-5880 PTFE ($\varepsilon_r \approx 2.2$), K-6098 teflon/glass cloth ($\varepsilon_r \approx 2.5$) and alumina ceramic substrates ($9.7 < \varepsilon_r < 10.3$) [1].

The low efficiency of small patch antennas can be improved by increasing the substrate thickness. The thicker the substrate, the more loosely coupled the fields are to the ground plane. Thus, fringing fields are more likely to become radiating fields. An increase in the fringing of the fields causes an increase in the effective size of the antenna which leads to a lower resonant frequency. However, this effect is not significant. For example, the resonant frequency of a square patch antenna with a very thick substrate (thickness = 6% λ_0, where λ_0 is the wavelength in free space) is only 8%

lower than that of the same size square patch with a very thin substrate (thickness < 0.1% λ_0) [12]. Thicker antennas also typically have wider bandwidths [4].

A disadvantage of using thick substrates is that surface waves are generated [4]. Surface waves travel in the substrate and are scattered at discontinuities. Therefore they can degrade the radiation pattern. They also extract power from the radiating waves and thus lower the antenna efficiency. As the polarization of a surface wave is difficult to control, surface waves also cause an increase in cross-polarization. Other disadvantages of using thick substrates include added bulk and increased cost. Furthermore, patches on thick substrates are more difficult to feed, and additional losses may result [1].

Due to the size restrictions imposed on handset antennas by PCS devices, methods of decreasing the antenna size are of interest. However, for a given patch shape, decreasing the size can result in higher resonant frequencies, narrower bandwidths, lower radiation efficiency, and changes in the input impedance and radiation patterns [1]. The effect on bandwidth and efficiency is significant, due to the relatively narrow bandwidths and high losses of microstrip antennas (as discussed in Section 2.1.2). Smaller antennas are also more susceptible to manufacturing tolerances [1]. For many patch shapes, resonance in the dominant mode is achieved when the characteristic length of the patch is of the order of one half wavelength long (for rectangular patches, the characteristic length is the length of the longer side, for circular patches it is the diameter) [4].

It has been demonstrated that for a given patch size, the resonant frequency can be

lowered by inserting shorting posts between the patch and the ground plane [14],[15]. The shorting posts change the current distribution on the patch by providing new current paths to the ground plane. This technique has been applied to circular patches [14] and square patches [15] to decrease the patch size to approximately one-third the original size.

Dielectric superstrates are often used to protect the antenna from damage. However, a dielectric superstrate also significantly affects the performance of the antenna. It influences the characteristic impedance, lowers the resonant frequency, widens the bandwidth, increases dielectric losses, and increases the peak power-handling capability of the antenna [16]. Numerical and experimental results have been reported on the effects of a dielectric superstrate on the effective dielectric constant, resonant frequency and bandwidth of a rectangular microstrip antenna [16]. The antenna had a polystyrene substrate ($\varepsilon_r = 2.5$) of height 0.159 cm. The increase in ε_e was significant if the superstrate was thick or had a high value of ε_r. An increase in ε_e lead to a decrease in the resonant frequency, and the fractional change in resonant frequency depended on the resonant frequency itself. Using superstrate materials of polystyrene ($\varepsilon_r = 2.5$), ice ($\varepsilon_r = 3.2$) or beryllium oxide ($\varepsilon_r = 6.6$), the fractional changes in a 10 GHz resonant frequency were as much as 5.8%, 7.8%, and 16%, respectively (for infinite superstrate thickness). At 2 GHz, the maximum changes in resonant frequency were 2.5%, 3.4% and 7.1%, respectively. It was also observed experimentally that the bandwidth of the antenna widened slightly when a superstrate was used. Using this information, one can reduce the patch size for a given frequency at the expense of increasing the volume of the

structure.

Selecting the type of antenna feed is as important as designing the antenna itself. The four most common feeds used for microstrip antennas are the coaxial feed, the microstrip transmission line feed (shown in Fig. 2.1), the proximity coupled feed and the aperture coupled feed. All four feeds are extensively covered in the literature (e.g. [1]). Each method has advantages and limitations in terms of impedance matching, feed point positioning, feed radiation, ease of fabrication and other factors.

Most analyses of microstrip antenna characteristics assume a flat perfectly conducting ground plane of infinite area. In practice, however, the ground plane may not be flat or perfectly conducting, and it is certainly not of infinite extent. The size and shape of a small ground plane can have significant effects on the electrical characteristics of the antenna (such as the radiation pattern, input impedance, efficiency and centre frequency). This topic is covered more extensively in Section 3.2.

2.2.3 Improvement of the Bandwidth of Microstrip Antennas

Bandwidth is generally defined as the range of frequencies within which an electrical characteristic of the antenna performs to a specified standard [17]. There is no unique characterization of antenna bandwidth. The many types of antenna bandwidth include impedance bandwidth, pattern bandwidth, polarization bandwidth and gain bandwidth. The type of bandwidth chosen for a particular antenna is usually the one corresponding to the antenna characteristic which is most strongly influenced by frequency. For simple

microstrip patch antennas, the input impedance is a strong function of frequency while the radiation pattern, polarization and gain are less affected. Thus in this dissertation, the term bandwidth refers to the impedance bandwidth, which is usually defined as the range of frequencies within which the voltage standing wave ratio (*VSWR*) does not exceed two. The impedance bandwidth is usually expressed as a ratio of this frequency range to the centre frequency. A typical impedance bandwidth for the basic microstrip patch element is 1 to 3% [5], compared with the 15 to 20% impedance bandwidths of dipole, slot and horn antennas [1]. The relatively narrow bandwidths of microstrip antennas can be explained by observing that the region between the patch and the ground plane acts as a lossy resonant cavity [4], and resonant cavities typically have high Q factors (i.e. narrow bandwidths). However, there has been extensive research on broadband microstrip antenna configurations recently, and bandwidths greater than 20% are possible. As discussed previously, the bandwidth can be widened by increasing the substrate thickness and lowering the substrate dielectric constant. Also, wide patches typically have wider bandwidths than narrow patches. Other techniques generally fall into three categories: external impedance matching, the use of multiple resonances, and adding losses (to sacrifice efficiency for bandwidth). These three techniques are discussed below.

External impedance matching is an effective and relatively simple method of widening the bandwidth because it usually does not require any modification of the antenna element itself. Impedance matching is typically achieved by adding a matching circuit into the feed network, usually on the same substrate as the antenna. Thus the matching

circuit can be fabricated conveniently with the antenna. The matching network may consist of tuning stubs, quarter-wave transformer sections, capacitively coupled lines, or active devices. Good results are achieved when the matching circuit is very close to the antenna element. However, care must be taken to prevent the matching circuit from interfering with the antenna radiation pattern. An impedance bandwidth of more than 25% has been obtained by matching the input impedance of a single microstrip element [18]. Using transistors in the matching network, matching combined with amplification achieved a bandwidth of 24% and an added gain of approximately 10 dB [19]. Impedance matching can also be achieved by modifying the antenna patch itself (e.g. by creating slots in the patch [20]).

Using two or more resonators that resonate at closely-spaced frequencies is another effective technique to widen the bandwidth. The bandwidths of each resonator should overlap to give an overall wide bandwidth. For microstrip antennas, the use of multiple resonances can be achieved using stacked patches [6], [8], parasitic patches [6] and slot loading (cutting slots into the patch) [7], [9], [10], [11]. The stacked patch configuration occupies less area than the parasitic patch configuration, and tight coupling is more easily achieved. However, using the stacked configuration makes fabrication, modifications, and adding components more difficult. The bottom and top patches are very close in size, with one patch smaller than the other to resonate at a higher frequency. Bandwidths of 10 to 20% have been achieved with stacked patches [6]. Using parasitic patches, bandwidths of up to 25% have been achieved [6]. To achieve close coupling between parasitic patches, very small gaps between the elements must be

used, which makes fabrication tolerances critical. It may also be difficult to position coplanar feed lines and matching networks on the board, since there is less room to mount them. Slot loading does not increase the size of the antenna, as do the other two methods. Therefore, it is preferable in applications where size is critical. Using slot loading, dual-band operation [7] and triple-band operation [9], [10] have been demonstrated, and bandwidths as wide as 47% have been reported [11]. The resonant frequencies and bandwidths can be adjusted by changing the depth and width of the notches.

Bandwidth improvement can also be achieved at the expense of efficiency by adding loss into the system. Losses can be added externally using attenuators, distributed using lossy substrate materials, or added to the antenna directly using chip resistors or other loads. This method is generally discouraged for microstrip antenna design however, due to the relatively low radiation efficiency of microstrip antennas.

2.3 Concluding Remarks

In this chapter, information relevant to the development of microstrip antennas for PCS is presented. This information is important to the research, which contributes to the analysis of small antennas for hand-held PCS devices. Microstrip antennas, due to their compact geometry and other advantages, are attractive for PCS. As discussed, the development of microstrip antennas for hand-held PCS devices faces many challenges, including technological limitations (e.g. bandwidth and efficiency) and physical constraints (e.g. size). The analysis of these antennas is also complicated by the effects

of the close proximity of the user's body, the small ground plane and the multipath environment, as discussed in more detail in the next chapter.

Chapter 3 Antenna Interaction with the User and Surroundings

The antenna theory discussed in Chapter 2 is important for the analysis and design of microstrip antennas. However, many factors are not taken into account in this theory, such as the presence of the user and surrounding objects in the multipath environment. If the user is in the close proximity of the antenna, a significant amount of radiated power from the antenna may be absorbed in the user's body. This reduces the antenna efficiency and may have adverse health effects for the user. Surrounding objects in the far field of the antenna, such as buildings and vehicles, scatter RF signals, causing multipath distortion of the received signal. This distortion typically varies randomly in time due to the movement of the PCS device with respect to the surrounding objects. Another factor to consider is that the antenna ground plane (the PCS handset) is small compared to the wavelength. Field diffraction from the ground plane edges significantly affects the far-field radiation pattern and other electrical characteristics of the antenna.

The first section of this chapter describes the antenna interaction with the user, including the known biological effects of RF fields, health standards for human exposure to RF radiation from PCS devices, and the effects of the user proximity on the electrical characteristics of the antenna. It also defines the specific absorption rate (SAR) of energy in the body

and the antenna efficiency, which are used in the antenna analysis in Chapter 5, and it describes a biological model of the user used in the FDTD analysis. The effects of the small antenna ground plane on a PCS antenna are described in Section 3.2. Section 3.3 discusses the effects of the multipath environment on the antenna and derives an expression for the mean effective gain (MEG) of an antenna. The use of diversity to alleviate multipath fading is also addressed, and a performance measure for diversity antennas, the correlation coefficient, is derived. The work of this chapter is important for the results in Chapter 5 on the performance of PCS antennas and their interaction with the user and the multipath environment.

3.1 Antenna Interaction with the User

The antenna of a cellular telephone handset is typically within centimeters of the user's head. As a result, there are concerns about health effects for the user and degraded signal quality for the PCS system. This section addresses both areas. It begins with an overview of the known biological effects of RF fields and a review of some of the protective standards related to PCS devices. The effects of the body proximity on the antenna are then presented. These effects include reduced antenna efficiency and distortion of the radiation pattern. At the end of this section, the biological model of the user utilized in this research is described.

3.1.1 Biological Effects of RF Fields and Health Standards

Rapid technological development during this century has led to the widespread use of RF fields in various applications, including PCS systems (which operate at frequencies

between 40 MHz to 6 GHz [21]). Our daily exposure to RF fields has raised public concern and stimulated scientific inquiry into the possible health effects of these fields. This section briefly reviews the current body of knowledge on the biological effects of RF fields, with emphasis on biological effects which may lead to adverse health effects. A detailed review is outside the scope of this research but is available in the literature (e.g. [22],[23],[24]). Biological effects are analyzed in terms of the absorption of RF energy in the body. The standard dosimetric measure of RF exposure is the specific absorption rate (SAR), which is defined in this section. A review of health standards for RF exposure is also provided.

The biological effects of exposure to RF radiation are very different from the effects of extremely low frequency (ELF) radiation or ionizing radiation. In contrast with ionizing radiation, RF fields do not have sufficient quantum energy to break molecular bonds and damage genetic material. Therefore, the vast amount of research on the biological effects of ionizing radiation cannot be directly applied to RF radiation. Similarly, ELF data on biological effects cannot be directly extended to RF frequencies. Research on the biological effects of RF radiation has been conducted for over 40 years, and interest in the area heightened considerably in the early 1990s with the increase of cellular phone use. Multi-million dollar research studies around the world are currently on-going, but they will not conclude for several years [25].

To understand the biological effects of RF fields, it is first necessary to define a dosimetric measure of RF exposure. Unfortunately, there is no straightforward relationship between

the external RF field outside a biological body and the induced RF dose inside the body [21], due to the fact that dose distributions are highly dependent on the geometry of the body, the external field frequency and polarization, and other factors. Therefore, the safety evaluation of PCS devices cannot be based entirely on the external field. A generally accepted dosimetric measure of RF exposure is the specific absorption rate (SAR), which is defined as the power absorbed per unit mass of tissue. It can be calculated from the induced electric field $\overline{E}_i$ in biological tissue as [24]:

$$SAR = \frac{\sigma}{2\rho}\left|\overline{E}_i\right|^2 \qquad \text{(W/kg)} \tag{3.1}$$

where σ is the tissue conductivity and ρ is the tissue specific density. Evaluation of the SAR can be performed using numerical techniques such as the FDTD method, assuming that an accurate biological model is provided. The biological model used in this work is described in Section 3.1.3.

The thermal effects of exposure to RF fields are well established. Excessive exposure to RF fields for long durations can raise the body temperature and even cause burns. Studies on rodents indicate that an increase in body temperature from RF radiation can cause birth defects, temporary sterility and thermal stress [22]. However, at the low exposure levels induced from PCS devices, thermal effects are unlikely [23].

The non-thermal effects of RF exposure are currently under investigation, and few, if any, non-thermal effects have been found [26]. However, there may be non-thermal effects

associated with the exposure to RF signals that are amplitude modulated at ELF [23]. ELF-modulated RF field exposure is attracting increasing attention, due to the recent advent of digital communication systems. Many of these systems use time-division multiple access (TDMA) technology which divides channels into frames to allow many users to use the same channel. The frame rate used by the North American IS-54 TDMA standard results in the transmission of a 50 Hz field [23]. Experimental studies have identified a number of biological effects of ELF-modulated RF field exposure. One the reviews enumerates the following [23]:

> Major effects of these fields have been noted in 1) regulation of the immune system; 2) in modulation of brain and central nervous system functions...; 3) in regulation of cell growth...; and 4) in apparently acting at cell membranes with chemical cancer promoters, or with the body's intrinsic hormonal mechanisms, as co-factors in tumor promotion.

A limited number of epidemiological studies (studies of the occurrence of illness in populations) have also been undertaken over the last 30 years to evaluate the influence of human exposure to RF fields on human health. A review of these studies [27] suggests that RF exposure may influence paresthesia (pricking or tingling sensation on the skin), lung cancer and ocular lens changes in people. However, the review cautions that the groups in which these indications were found 'were probably exposed above current occupational exposure limits.' It also emphasizes that there is a lack of experimental studies supporting some of the epidemiological results, a lack of good exposure measurements, and inconsistency in the methodology of the studies. The review therefore concluded that there is no clear evidence 'suggesting an effect at RF exposure situations comparable to those encountered by common use of mobile communication systems.'

Research on the health effects of exposure to RF fields indicates a need for protective standards. Many national and international standards groups around the world have adopted safety standards for RF exposure. These include the Canadian standard, "Safety Code 6: Limits of Exposure to Radiofrequency Fields at Frequencies from 10 kHz - 300 GHz." [28], and the United States standard, "ANSI/IEEE C95.1-1991, IEEE Standard for Safety Levels with Respect to Human Exposure to Radio Frequency Electromagnetic Fields, 3 kHz to 300 GHz" [29]. These standards set maximum permissible levels of SAR (W/kg), incident power density (W/m^2) and other parameters, based on the known thermal effects of RF exposure. For PCS devices, SAR standards are of primary importance. The standards of different national and international groups are in good agreement.

Standards establish two types of exposure limits: one for RF workers and one for the general public. The SAR limits depend on the duration of exposure, the region of exposure (e.g. eyes compared to limbs), and the mass of tissue over which the SAR is averaged (e.g. one gram, 10 grams). For the general public, the Canadian standard requires that the SAR averaged over any 20% of the body mass cannot exceed 0.2 W/kg. Local SAR values cannot exceed 4 W/kg (averaged over 1 gram of tissue) except in the eye, where the SAR must be below 0.2 W/kg, and at the body surface and in the limbs, where the SAR must be less than 12 W/kg (averaged over 10 grams of tissue). For RF workers, who work in controlled environments, the SAR limits are approximately double those for the general public [28].

In Canada and the United States, a manufacturer of portable communication devices must

provide test results showing that the exposure standards are met before the device is allowed on the market. However, a device may be exempt from providing test results if the device output power is below a certain level [29]. According to the Canadian standard, all portable devices operating below 1 GHz are exempt if the output power is less than 7 W [28]. Most cellular telephones transmit less than one watt of output power.

3.1.2 Effects of the Body Proximity on the Antenna

Whether or not the user's health is adversely affected by the close proximity to the antenna, the performance of the antenna is adversely affected. The absorption of RF energy in the user's body reduces the antenna efficiency. The antenna far field patterns, input impedance, bandwidth and other parameters are also affected by the body proximity. In the context of the problems analyzed in this research, antenna efficiency is defined as the ratio of the power radiated to the total output power:

$$\eta = \frac{P_{rad}}{P_{rad} + P_{abs}} \tag{3.2}$$

where P_{abs} is the power absorbed in the volume V of the body:

$$P_{abs} = \frac{1}{2}\int_{V} \sigma |\bar{E}_i|^2 dv \tag{3.3}$$

and the radiated power P_{rad} is obtained as follows:

$$P_{rad} = \frac{1}{2}\iint_S Re\,(\bar{E} \times \bar{H}^*) \cdot d\bar{s} \tag{3.4}$$

where the surface S encloses the antenna-body configuration, $\bar{E}_i$ and σ are the induced electric field in biological tissue and the tissue conductivity, respectively, $\bar{E}$ and $\bar{H}$ are the total electric and magnetic fields, and dv and $d\bar{s}$ are the differential volume and the differential surface vector, respectively. The far-field radiation patterns are computed from the near-field vectors $\bar{E}$ and $\bar{H}$ using the surface equivalence theorem [30].

The effects of the user proximity on the antenna performance were investigated by several authors [31]-[36] using experimental and numerical techniques. Experimental work on a 600 MHz dipole antenna next to a human body model showed that scattering of fields by the body perturbs the current distribution on the antenna [31]. The body of the user was modeled as a rectangular cylindrical plexiglass container filled with saline solution.

Numerical analysis using the FDTD technique was performed to investigate the effects of the body proximity on the antenna resonant frequency, input impedance, efficiency and far-field patterns [33]. The numerical modeling included a monopole antenna mounted on a PCS device (metal box), a head (modelled as a sphere of muscle tissue) and a hand grasping the phone (modelled as a block of muscle tissue). Experimental measurements were also performed to verify the numerical analysis. Antenna characteristics were investigated at two frequencies, 914 MHz and 1890 MHz, which correspond to the frequencies used by European PCS systems (and are very close to the frequencies used by PCS systems in North America). The results showed that at 914 MHz, the presence of the head

and hand resulted in a decrease of the resonant frequency of 10% and an antenna efficiency of 55%. At 1890 MHz, the antenna efficiency was found to be 57%. A considerable distortion of the radiation patterns due to the presence of the body was also found, and diffraction and scattering from the head resulted in significant cross-polarization. The presence of the head resulted in a shadow effect, meaning that the magnitude of the far field radiation was less in the direction of the head compared to other directions (by 2 dB at 914 MHz and by 12 dB at 1890 MHz). Radiated power at a fixed receiving antenna was also measured as a person walked around an anechoic chamber holding the telephone at a natural speaking angle. Fades as deep as 15 dB were measured and the mean received power from the phone was 4.4 dB less than if the person was not present.

Similar tests were performed by others using an anatomically accurate head model (obtained from magnetic resonant images), a heterogeneous hand model and a variety of different antenna configurations mounted on a handset [34]. Results at 915 MHz indicated a similar decrease in resonant frequency and efficiencies between 32% and 52% due to the head and hand. Four antenna configurations were modelled, including a monopole and a planar inverted F antenna (PIFA). The numerical analysis, using an FDTD algorithm, was compared to experimental measurements. The authors observed that a PIFA mounted on the back of the handset (away from the head) gave the best results in terms of efficiency and SAR in the head.

3.1.3 A Biological Model Used in this Research

This research investigates the interaction between PCS antennas and the user's body using

numerical analysis. A biological model of the user is therefore needed to study this interaction and to evaluate the SAR in the user's body. As the antenna is held next to the user's head by a hand, both the head and hand should be modeled.

In terms of macroscopic electromagnetic behaviour, a biological body is a volume of lossy dielectric material, and each tissue type has a complex permittivity $\hat{\varepsilon}$:

$$\hat{\varepsilon} = \varepsilon_0 (\varepsilon_r' - j\varepsilon_r'') = \varepsilon_0 \varepsilon_r' - j\frac{\sigma}{2\pi f} \tag{3.5}$$

where ε_0 is the permittivity of free space (F/m), ε_r' and ε_r" are the real and imaginary parts of the relative permittivity of the medium, σ is the conductivity (S/m) and f is the frequency (Hz). At a given frequency, the complex permittivity is completely described by ε_r' and σ. Accurate values of ε_r' and σ for many human tissues and over many frequency ranges are available in the literature (e.g. [37]).

Various models of the head have been investigated, ranging in complexity from homogeneous boxes and spheres [32],[33] to heterogeneous and anatomically accurate models [34]-[36]. Anatomically accurate models are desired, as spherical models yield overestimated SAR values and box models provide distorted and unreliable results for the antenna far-field pattern [36].

Table 3.1 Dielectric properties of the tissues in the head model at 915 MHz [38].

Tissue	ε_r'	σ (S/m)	Tissue	ε_r'	σ (S/m)
skin	35	0.6	skull	8	0.11
spinal cord	49	1.1	spine	8	0.11
brain - white matter	38	0.8	brain - gray matter	49	1.1
jaw bone	8	0.11	muscle	58	1.4
parotid gland	55	1.0	lacrimal glands	55	1.0
spinal canal	72	2.1	tongue	55	1.0
pharynx	35	0.6	esophagus	35	0.6
nasal septum	35	0.6	fat	6	0.08
blood	62	1.5	CSF	78	2.1
eye - sclera	66	1.7	eye - humor	74	2.0
lens	44	0.8	bone marrow	42	0.8
cartilage	35	0.6	pituitary gland	55	1.0
ear bones	35	0.6	trachea	35	0.6

The head model used in this research is based on a model developed at the Radiology Department at Yale University using CT and MRI scans [39]. Improvements to the original Yale model were made at the University of Victoria. Twenty six tissue types are assigned to 3.6 mm cubes of the head model (see Table 3.1). The hand model used in this research consists of three blocks of bone surrounded by skin for the fingers, palm and base of the hand. The bone thickness is 0.4 - 0.6 cm and the thickness of the surrounding skin is 0.2 - 0.6 cm. The hand model holds the lower portion of the handset as shown in Fig. 3.1, with the fingers and the base of the hand touching the plastic casing, and the palm separated from the casing by a small air gap (1.1 cm). The whole configuration, including the

head, hand and communications handset, is shown in Fig. 3.1.

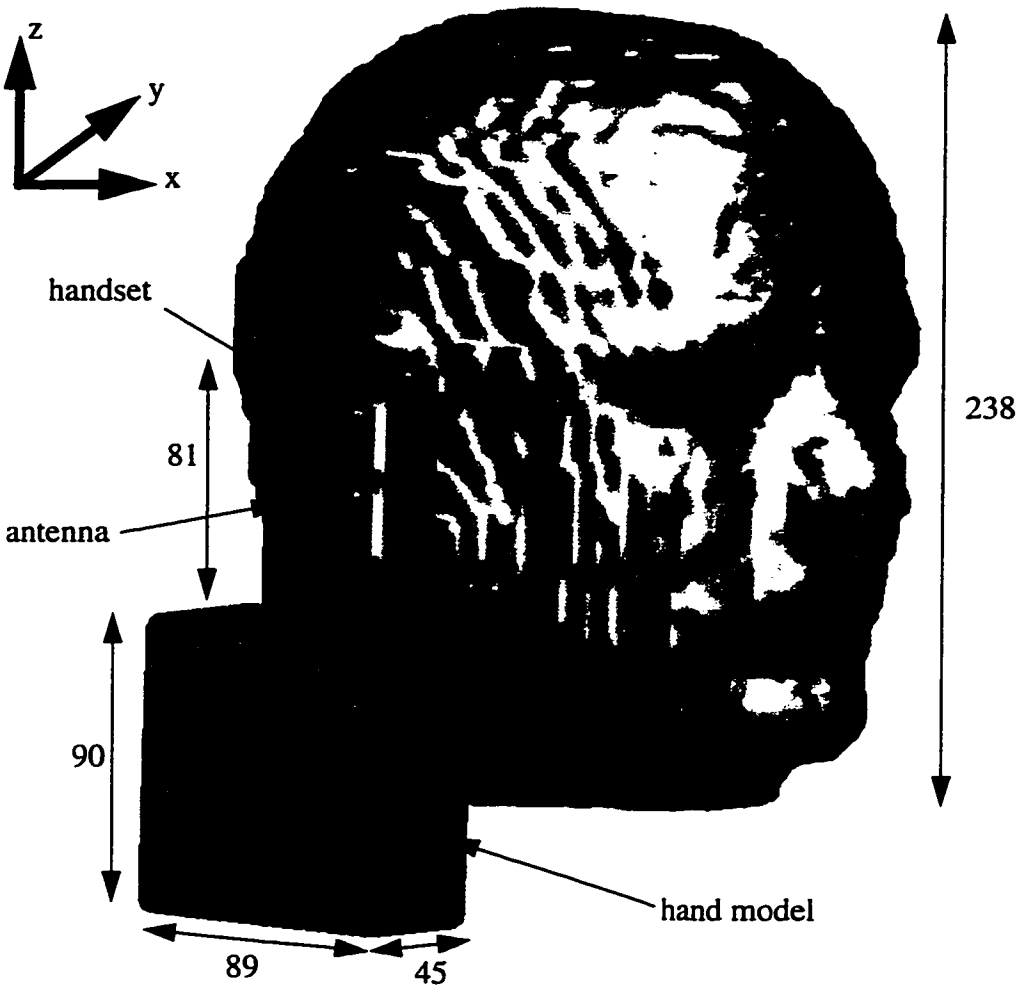

Fig. 3.1 Antenna-handset configuration with head and hand models (dimensions in millimeters).

3.2 Effects of the Small Antenna Ground Plane

Each antenna investigated in this research is installed on a handset, and the metal casing of the handset acts as the antenna ground plane. Due to the fact that the handset is small compared to the wavelength, the edges of the handset can have significant effects on the electrical characteristics of the antenna. These effects are important to consider in the antenna analysis.

If an infinitely large ground plane is assumed (the ideal case), the radiated fields can be determined using image theory [40]. Using image theory, the induced currents on the ground plane do not need to be computed, as the contribution of the induced currents on the ground plane to the radiated fields is the same as that of the mirror image of the equivalent current sources on the antenna. Antenna parameters are relatively easy to determine in this case. For example, a monopole antenna may be modeled by image theory as a dipole with one-half of the input impedance and double the peak directivity of the dipole [41].

In practice, however, a finite ground plane is used. The edges of the ground plane are scatterers which may diffract the incident field. Diffraction alters the radiation pattern, causing scalloping [42] or nulls [43] in the forward radiation, the presence of back radiation (i.e. radiation behind the ground plane) [41], and higher cross-polarization levels [43]. Other antenna parameters may be affected as well. The degree to which the edges of the ground plane change the antenna behaviour is largely a function of the distance from the antenna to the ground plane edges. It has been shown that the circular ground plane of a quarter-wavelength monopole antenna should be at least two wavelengths in radius for input impedance measurements to accurately resemble those of the same antenna with an infinite ground plane [44]. Such a large ground plane is necessary to ensure that the edges of the ground plane are not in the near field. For smaller ground planes, the diffraction of radiation at the edges modifies the currents on the ground plane [41]. Because the current must be zero at an edge, the currents on the front and back faces near the edge are equal in

magnitude and opposite in phase. The smaller the ground plane, the stronger the currents on its back side, resulting in stronger back radiation. Ground plane edge effects can be reduced by adding resistance to the edges. This can be achieved with the addition of a resistive coating [45] or resistively loaded wire radials (wire elements which extend the size of the ground plane) [44].

Many analytical tools can be used to model the diffraction of fields from ground plane edges. These include such techniques as the method of moments (MoM) [46], the geometrical theory of diffraction (GTD) [47] and the physical theory of diffraction (PTD) [47]. The MoM and the GTD are often used together.

The most studied antenna configuration is the monopole in the centre of a thin disk. The radius of the disk was found to have a very significant effect on the input impedance and on the current distributions on the monopole antenna and the ground plane [41],[48]. The effect of the ground plane thickness on the monopole antenna radiation patterns has also been studied [49]. A pronounced distortion of the E_θ radiation pattern was observed when the thickness of the circular ground plane was varied between $\lambda/100$ and $\lambda/2$. A monopole antenna on a conducting cube has been studied [43],[50]. As the monopole antenna was moved from the centre of the top surface towards the edge or a corner, the Q factor decreased by 60-70%, the magnitude of the conductance decreased by 50%, the resonance frequency increased by a few percent and deep nulls in the radiation pattern were produced.

For a helical antenna, a reduction of the ground plane radius to approximately the radius of the helix resulted in a transition from forwardfire radiation to backfire radiation [51],[52].

Patch antennas with finite ground planes have also been studied. For rectangular patches with rectangular ground planes, the slot theory and the modal expansion theory have been used to describe the fields impressed by the patch, and the GTD has been used to analyze diffraction by the ground plane [53]. For patches and ground planes that are circular, a method of moments formulation based on the equivalence principle [54] and a formulation based on the vector potential technique [55] have been used. Smaller circular ground planes result in beamwidths that are narrower in the E plane and broader in the H plane [54]. Thus pattern symmetry can be improved by modifying the ground plane size. The radiation pattern, directive gain and input impedance are strongly affected by the size of the circular ground plane [55]. Also, the height of the substrate and the distance between the patch edge and ground edge affect the excitation of surface waves which significantly affects the radiation efficiency [55]. For planar arrays of microstrip patch elements, scattering by the edges of a ground plane caused an increase in the cross-polarization and a decrease in the peak directivity of the antenna array [56]. It also resulted in a shifting of the scanned beam peak to a higher elevation angle [56].

3.3 Effects of the Multipath Environment

The environment surrounding a PCS antenna is often called a multipath environment due to the fact that a received signal is composed of many signal components, each of which

has traveled along a different path from the transmitter to the receiver. The scattering of the transmitted signal into its components is caused by reflection, refraction and diffraction by objects in the multipath environment such as buildings, cars and trees [57],[58]. Each signal component has its own amplitude, phase, polarization, angle of arrival and time of arrival. At the receiving antenna, the signal components may combine destructively, resulting in the fading of the received signal power, called multipath fading. A standard statistical model of multipath fading predicts that fades of 30 dB occur 0.1% of the time [57].

As the scattering objects in the multipath environment are typically in the antenna far-field, their presence does not affect the antenna efficiency, far-field patterns or other antenna parameters. However, multipath fading degrades the received signal quality, and proper design of the antenna can alleviate multipath fading. As described in Section 3.3.1, diversity antennas can alleviate multipath fading by combining the operation of two or more antennas in a constructive manner. A diversity antenna is analyzed in Chapter 5. The ability of a two-branch diversity antenna to alleviate multipath fading can be evaluated by calculating its correlation coefficient. Also, the performance of any antenna in a mobile communication environment can be assessed by calculating the antenna mean effective gain (MEG), which correlates the antenna power gains with patterns describing the distribution of incident waves. The MEG and the correlation coefficient between two antennas in diversity are described in Section 3.3.2.

3.3.1 Antenna Diversity

Antenna diversity systems employ M antennas ($M > 1$), instead of one antenna, to receive M different signals. Switching or combining circuitry in the receiver combines the M signals constructively, thus mitigating the effects of destructive interference. The combined signal fades less frequently and less severely than a signal incident on one antenna [57]. Ideally, a diversity system would receive each signal component separately and multipath fading would be removed entirely. However, such a scheme is unworkable in practice, as the number of signal components and their angles and times of arrival cannot be known in advance. Most diversity systems use $M = 2$ to $M = 4$ antennas, due in part to the trade-off between signal quality improvement and cost of implementation [59]. If the diversity system is designed well, the fading characteristics of the M received signals will be statistically independent (i.e. the signals will not likely fade at the same time). Statistical independence is evaluated using the correlation coefficient, ρ, as described in Section 3.3.2.

A number of diversity schemes can be employed to ensure a certain measure of statistical independence. Six of these schemes are space diversity, frequency diversity, time diversity, angle diversity, field component diversity and polarization diversity [57]. The first three of the methods are impractical for PCS handsets due to limitations in space, bandwidth and circuit complexity, respectively. The most favoured of the methods is polarization diversity, which is a specific case of field component diversity. Many diversity antenna configurations use a combination of angle diversity and polarization diversity.

Angle diversity makes use of the observation that the signal components arriving along different paths often have different angles of arrival, and signals with different angles of arrival are likely to have statistically independent fading patterns [57]. Diversity can therefore be achieved using directional antennas to isolate the signal components. The beamwidths of the antennas must be selected to give the optimum trade-off between statistical independence (using narrow beams) and signal coverage (using wide beams).

A wave travelling in space has a maximum of six field components, three electric field components (E_x E_y and E_z) and three magnetic field components (H_x H_y and H_z). A field component diversity antenna is one which receives two or more of the six field components independently. Polarization diversity is a specific form of field component diversity where the components are of the same field. These are typically E_z and a combination of E_x and E_y. Many studies on polarization diversity are available, and the results conclude that polarization diversity offers a substantial improvement in outdoor systems in suburban areas and in indoor systems where there is no line-of-sight propagation [60],[61]. Polarization diversity antennas also provide protection from signal loss due to random handset orientation [61]. Polarization diversity has been studied using cross dipole antennas [62], passive microstrip antennas [58], and active microstrip antennas [40],[63]. Energy density antennas have also been studied [64],[65]. Energy density antennas exhibit field-component diversity by receiving one or more components of the electric field plus one or more components of the magnetic field (typically E_z, H_x and H_y are received).

3.3.2 Mean Effective Gain and Correlation Coefficient

The mean effective gain (MEG) is a statistical measurement of the antenna performance in a multipath environment. For a two-branch diversity antenna, performance is evaluated using the MEG of each branch and the correlation coefficient, ρ, between the branches. The derivations of the MEG and ρ are given in this section.

The MEG correlates the antenna far-field patterns with patterns describing the mean power of incident waves on the antenna from the surroundings. Evaluation of the MEG can be evaluated experimentally [66] or it can be computed from the antenna far-field patterns and knowledge of the propagation characteristics of the surrounding environment. Mathematically, the MEG, denoted by G_e, can be expressed as [67]:

$$G_e = \eta\left[\int_0^{2\pi}\int_0^{\pi}\frac{XPR}{1+XPR}G_\theta(\theta,\phi)\,P_\theta(\theta,\phi)\sin\theta d\theta d\phi + \int_0^{2\pi}\int_0^{\pi}\frac{1}{1+XPR}G_\phi(\theta,\phi)\,P_\phi(\theta,\phi)\sin\theta d\theta d\phi\right] \tag{3.6}$$

where

η is the antenna efficiency.

XPR is the crosspolarization power ratio, defined as the ratio of the mean received power in the vertical polarization to the mean received power in the horizontal polarization. Over the range of angles of interest in mobile communications, the vertical and horizontal polarizations are equivalent to the θ and ϕ polarizations, respectively.

$G_\theta(\theta,\phi) = |E_\theta(\theta,\phi)|^2$ and $G_\phi(\theta,\phi) = |E_\phi(\theta,\phi)|^2$ are the antenna power gains in the θ and ϕ polarizations, respectively.

P_θ and P_ϕ are the probability distributions of power incident on the antenna in the θ and ϕ polarizations, respectively.

The XPR varies considerably, depending on the surrounding environment. In suburban outdoor environments [68] and in indoor environments [61] where there is no direct line of sight between the transmitter and receiver, measurements indicate that the XPR is approximately 1 (0 dB). However, in urban outdoor environments where there is a high density of tall buildings and in areas where there is a strong line-of-sight signal from a vertically-polarized transmitting antenna, the vertical polarization is stronger than the horizontal polarization. In two dense urban areas of Tokyo, Taga [67] measured XPR values of 3.2 (5.1 dB) and 4.8 (6.8 dB). Lee and Yeh [69] also showed that the XPR in urban areas is between 2.5 (4 dB) and 7.9 (9 dB). For this dissertation, a suburban area (XPR = 0 dB) and an urban area (XPR = 5 dB) were modeled.

The antenna power gains $G_\theta(\theta,\phi)$ and $G_\phi(\theta,\phi)$ satisfy the condition:

$$\int_0^{2\pi}\int_0^{\pi} \left(G_\theta(\theta,\phi) + G_\phi(\theta,\phi)\right) \sin\theta d\theta d\phi = 4\pi \tag{3.7}$$

P_θ and P_ϕ can be modeled as having uniform distributions in the ϕ direction and Gaussian distributions in the θ direction [67]. For $0 \le \theta \le \pi$:

$$P_\theta(\theta,\phi) = A_\theta \exp\left(-\left(\theta - \left[\frac{\pi}{2} - m_V\right]\right)^2 / \left(2\sigma_V^2\right)\right) \tag{3.8}$$

$$P_{\phi}(\theta,\phi) = A_{\phi}\exp\left(-\left(\theta-\left[\frac{\pi}{2}-m_H\right]\right)^2/\left(2\sigma_H^2\right)\right) \tag{3.9}$$

where:

m_V and σ_V are the mean and standard deviation of the incident angle of arrival of vertically-polarized waves and m_H and σ_H are likewise for horizontally-polarized waves (the mean angles are observed upward from the horizontal direction).

A_θ and A_ϕ are the amplitudes of P_θ and P_ϕ, which satisfy:

$$\int_0^{2\pi}\int_0^{\pi} P_\theta(\theta,\phi)\sin\theta d\theta d\phi = \int_0^{2\pi}\int_0^{\pi} P_\phi(\theta,\phi)\sin\theta d\theta d\phi = 1 \tag{3.10}$$

For the urban outdoor environment modeled in this dissertation, values of $m_V = 19°$, $\sigma_V = 20°$, $m_H = 32°$ and $\sigma_H = 64°$ were used, corresponding to measurements [67]. For suburban outdoor environments, no published results of typical mean and standard deviation of incident angles have been found. However, it is clear that the incident waves in suburban outdoor environments arrive closer to the horizontal plane than incident waves in urban outdoor environments, and that the standard deviation of arrival angles will also be smaller. In this dissertation, values of $m_V = \sigma_V = m_H = \sigma_H = 10°$ are used. Polar plots of P_θ in the elevation plane for the urban and suburban environments are shown in Fig. 3.2. Note from the MEG condition of equation (3.6) that an ideal PCS antenna does not have to have a far-field radiation pattern that is omnidirectional in the horizontal plane, as some antenna designers assume. A highly directional antenna could also receive the same average signal power. This has been observed in measurements [70].

The correlation coefficient, ρ, of a two-branch diversity antenna is given in [62] as:

$$\rho = \frac{|R_{12}|^2}{G_{e1} G_{e2}} \tag{3.11}$$

where G_{e1} and G_{e2} are the MEGs of antennas 1 and 2 of the diversity system as given by (3.6), and R_{12} is the cross-correlation between the two antennas in diversity:

$$\begin{aligned} R_{12} = & \sqrt{\eta_1 \eta_2} \int_0^{2\pi} \int_0^{\pi} \frac{XPR}{1+XPR} E_{\theta 1}(\theta,\phi) E^*_{\theta 2}(\theta,\phi) P_{\theta}(\theta,\phi) \sin\theta d\theta d\phi \\ & + \sqrt{\eta_1 \eta_2} \int_0^{2\pi} \int_0^{\pi} \frac{1}{1+XPR} E_{\phi 1}(\theta,\phi) E^*_{\phi 2}(\theta,\phi) P_{\phi}(\theta,\phi) \sin\theta d\theta d\phi \end{aligned} \tag{3.12}$$

where the subscripts 1 and 2 refer to the first and second branch of the diversity antenna and $E^*(\theta,\phi)$ denotes the complex conjugate of $E(\theta,\phi)$. The best results are achieved when the far-field patterns of the two antennas are orthogonal. In this case, $\rho = 0$.

3.4 Concluding Remarks

In this chapter, the biological effects of RF fields and the effects of the user proximity, the small ground plane and the multipath environment on the antenna performance were described. The background information presented on these effects is important for the antenna analysis undertaken in this research. One of the main projects of this research is an analysis of two PCS antennas: a monopole antenna and a polarization-diversity

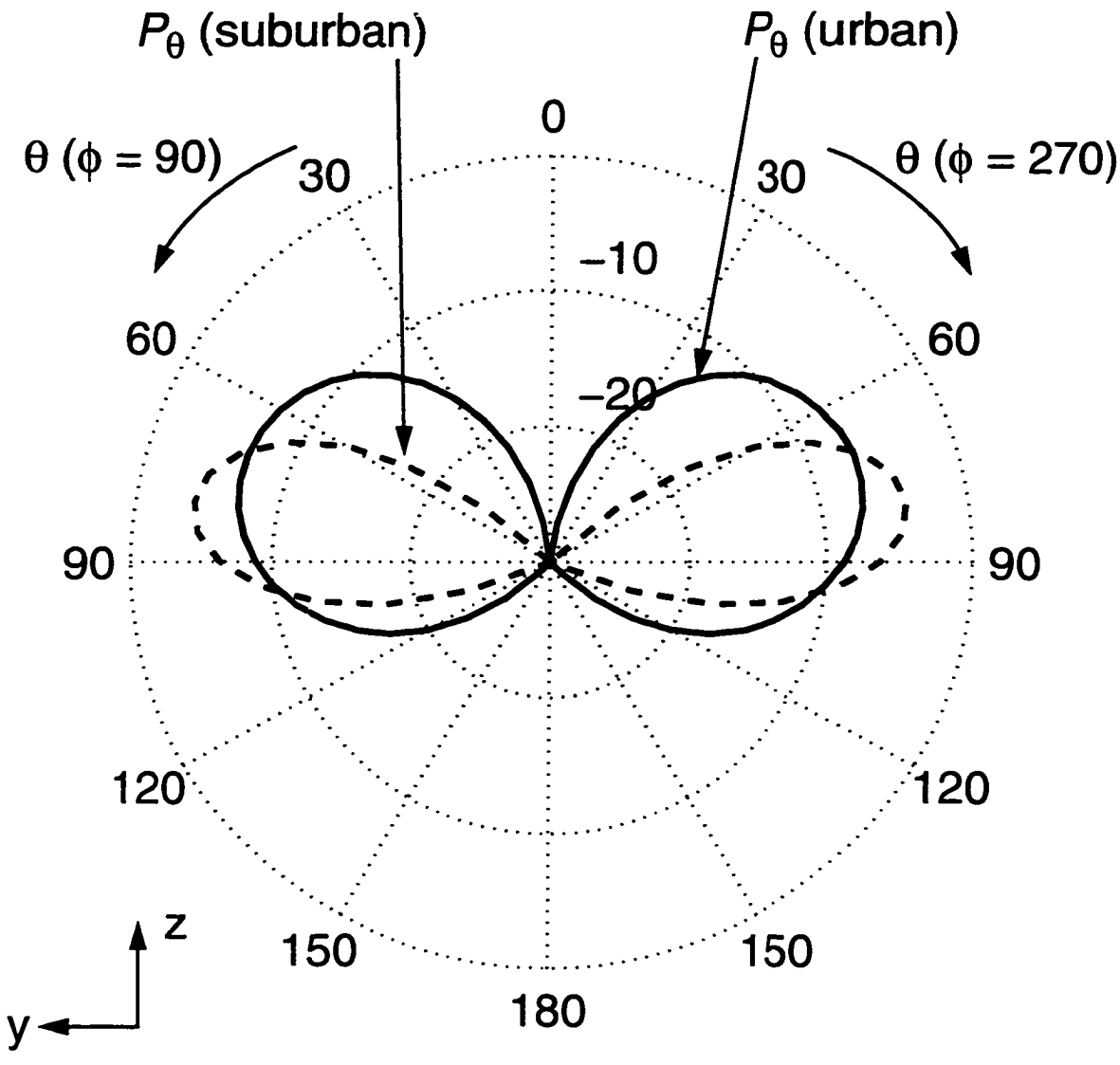

Fig. 3.2 Probability distributions of power incident on an antenna (θ-polarization only) in the urban and the suburban environments. Shown in the elevation plane with $\phi = 90°$ and $270°$.

antenna. Using the FDTD technique, both antennas are analyzed in terms of the SAR in the body, the antenna efficiency, the far-field patterns and the mean effective gain (MEG). For the diversity antenna, the statistical independence of the two branches is determined using the correlation coefficient.

Chapter 4 Numerical Modeling

The analysis of PCS antennas for this dissertation is performed using two numerical electromagnetic techniques: the finite-difference time-domain (FDTD) method and the method of moments (MoM). The FDTD method can be readily applied to complex geometries of inhomogeneous dielectrics and metals. Thus it is well-suited to the analysis of the interaction between a PCS antenna and the user, presented in Chapter 5. A widely-used MoM computer program called the Numerical Electromagnetic Code (NEC) [71] is used in this research to verify the accuracy of FDTD wire modeling. As the NEC program was written 'for analysis of the electromagnetic response of antennas and other metal structures' [71], and as it is largely based on specialized formulations for wires, it is a good standard for comparison with FDTD wire models using calculations of the input impedance of a dipole antenna. This chapter introduces the main concepts of the FDTD technique and the Method of Moments (MoM) and discusses their suitability to the research.

4.1 Finite-Difference Time Domain Method

The Finite-Difference Time-Domain method is a popular numerical electromagnetic technique that is based on solving the differential forms of Maxwell's equations [72]. The FDTD method is a time-domain technique which requires the discretization of both time

and space. The method iterates through time for a given number of time steps, and at each time step, the field components are updated using relatively simple linear equations. The memory requirements of the FDTD method are not as restrictive as those of the MoM for large problems, and complex inhomogeneous structures are readily implemented.

The FDTD method, introduced to electromagnetics by Yee in 1966 [73], is a direct solution of Maxwell's differential equations. Two of the differential equations are [74]:

$$\nabla \times \bar{H} = \bar{J} + \frac{\partial \bar{D}}{\partial t} \tag{4.1}$$

$$\nabla \times \bar{E} = \bar{M} - \frac{\partial \bar{B}}{\partial t} \tag{4.2}$$

where $\nabla \times \bar{A}$ is the curl of $\bar{A}$, $\bar{E}$ and $\bar{H}$ are the electric and magnetic field intensities, $\bar{J}$ and $\bar{M}$ are the electric and magnetic current densities, and $\bar{D}$ and $\bar{B}$ are the electric and magnetic flux densities [74]. All of the field variables are functions of space and time, $f(x,y,z,t)$. To solve the differential equations numerically, space and time are discretized and differentiation is performed using finite-difference approximations. A commonly used finite-difference approximation is the central finite-difference formula, shown below for differentiation in the x direction:

$$\frac{\partial f(x,y,z,t)}{\partial x} \approx \frac{f\left(x+\frac{\Delta x}{2},y,z,t\right) - f\left(x-\frac{\Delta x}{2},y,z,t\right)}{\Delta x} \tag{4.3}$$

where Δx is an increment in the x direction. It can be shown that applying the central finite-difference formula to (4.1) and (4.2) produces a set of six scalar equations in which the field values at each point in time and space are related only to field values at neighbouring points [72]. Thus, the solution of each field value does not depend on the formulation of large matrices, which is a great advantage of the FDTD method. However, $\overline{E}$ and $\overline{H}$ must be evaluated at all nodes in the computational space, not just at the nodes of interest. It accomplishes this by iterating through space along a regular grid. A unit cell of the grid, known as a Yee cell, is shown in Fig. 4.1. As shown in Fig. 4.1, $\overline{E}$ and $\overline{H}$ field components are evaluated at different locations on the grid. They are also evaluated at alternate time steps. This results in savings of memory and computation time.

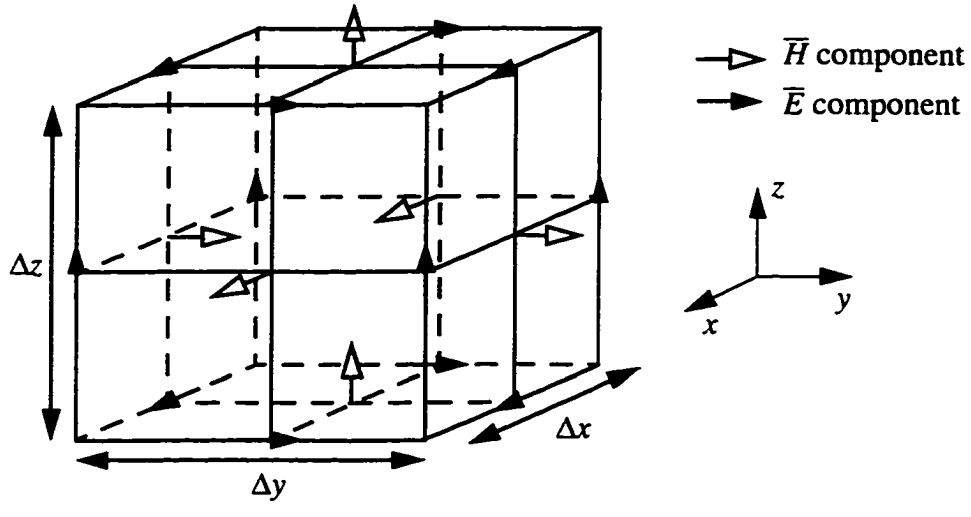

Fig. 4.1 Yee cell in the FDTD method.

To ensure the numerical stability of the FDTD method, the time stepping increment, Δt, must be less than the Courant limit [75]:

$$\Delta t = S\sqrt{\mu\varepsilon}\left[\frac{1}{\Delta x^2}+\frac{1}{\Delta y^2}+\frac{1}{\Delta z^2}\right]^{-1/2} \tag{4.4}$$

where μ and ε are the permeability and permittivity of the medium, respectively, and $S \leq 1$ is the stability coefficient. Also, for sufficient accuracy of the results, spatial increments in the Yee grid (Δx, Δy, Δz) must be small compared to the smallest wavelength used and a sufficient number of time steps must be chosen [72]. Accuracy also depends on the proper application of boundary conditions and the accurate modeling of metals and dielectric materials. The application of boundary conditions is particularly difficult when the structure of interest is to be modeled in an unbounded region. A region of infinite size cannot be implemented in the FDTD method. However, absorbing boundary conditions (ABCs) have been formulated which simulate the effect of an unbounded region [76]. One of the most popular ABCs is the perfectly matched layer (PML) boundary [77] which is used in this research.

The accurate modeling of metal and dielectric objects is an important issue in the FDTD method, particularly if the FDTD grid does not conform to the shape of the object or if the object is small compared to the size of the Yee cell. A two-dimensional example of the latter situation is shown in Fig. 4.2a. In this geometry, two metal sheets are modeled whose thickness is smaller than the height of the Yee cell. Conventional FDTD update equations for this geometry will either ignore the metal sheets or assume that they occupy the entire areas of their cells. Either approach would result in a considerable error. A finer spatial discretization may be used, as shown in Fig. 4.2b, but this may place impractical

demands on computer memory or computation time.

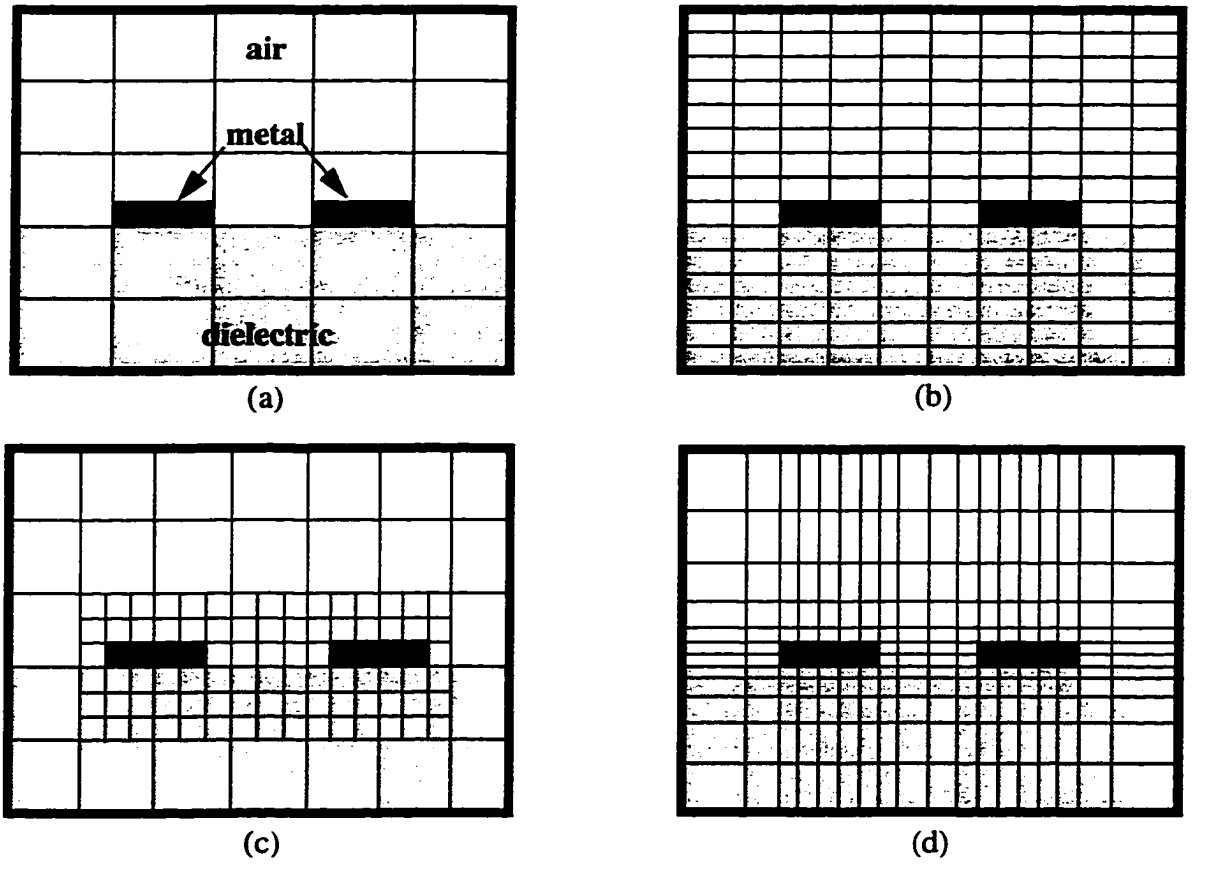

Fig. 4.2 FDTD modeling of coplanar lines using (a) a coarse grid, (b) a fine grid, (c) a subcell grid, and (d) a nonuniform grid.

Improvements can be made to the conventional FDTD algorithm which increase the modeling accuracy while maintaining the computational efficiency. These improvements include subcell gridding, using nonuniform grids and subcell modeling [78]. In the subcell gridding method, shown in Fig. 4.2c, a fine grid is used around the small features while the regular coarse grid is used in the remaining region. Nonuniform grids, as shown in Fig. 4.2d, are made gradually denser near the small features.

Subcell modeling is often used when it is impractical to decrease the mesh size to the dimensions of the object, even if subcell gridding or nonuniform grids is used. Wires [79], sheets [80] and slots [81] are often modeled using the subcell modeling technique. The approach of subcell modeling is to modify the update equations near the object of interest rather than modifying the grid. The new update equations are typically based on the integral forms of Maxwell's equations, taking into account assumptions of field behaviour in the region of interest. The subcell modeling of thin wires is described in Chapter 6.

4.2 Moment Method

Moment methods typically use the integral formulations of Maxwell's equations to solve electromagnetic field problems. Applying a moment method (MoM) involves three main steps: formulating an integral equation (IE) for the particular problem, discretizing the integral equation into a series of linear equations, and evaluating and solving the linear equations for the unknown parameters [46]. The particular choice of IE depends on the structure to be modeled. For example, Hallén and Pocklington have developed IEs that are well-suited to the modeling of thin-wire structures [82]. Other IEs have been developed to model metal plates, homogeneous dielectrics and other objects [46]. A one-dimensional IE has the general form:

$$E(z) = \int I(z')\, K(z, z')\, dz' \tag{4.5}$$

where $E(z)$ is the known excitation, $K(z,z')$ is the known kernel of the IE and $I(z)$ is the unknown function to be determined. Although the unknown function $I(z)$ is inside the

integral, it can be solved for by first discretizing the linear space into N segments and approximating $I(z)$ as a series of known basis (or expansion) functions $u_n(z)$:

$$I(z) = \sum_{n=1}^{N} I_n u_n(z) \tag{4.6}$$

where I_n are the unknown expansion coefficients. Many choices of basis functions are possible [82], but the basis functions must be linearly independent. Substituting (4.6) into (4.5) gives:

$$E(z_m) = \sum_{n=1}^{N} I_n \int u_n(z') K(z_m, z')\, dz' = \sum_{n=1}^{N} I_n g_m \tag{4.7}$$

where $z = z_m$ is a matching point where (4.7) is enforced. Thus the integral equation has been converted into a linear equation with N unknowns. To solve for the coefficients I_n, N simultaneous equations must be found. This is achieved with the use of N weighting functions, w_n. Forming the inner product of w_n with both sides of (4.7) leads to the expression:

$$\langle w_m, E(z_m) \rangle = \sum_{n=1}^{N} I_n \langle w_n, g_m \rangle \qquad m = 1, 2, ..., N \tag{4.8}$$

which can be represented in the matrix form as:

$$[V] = [Z][I] \tag{4.9}$$

where $V_m = \langle w_m, E(z_m) \rangle$ and $Z_{mn} = \langle w_n, g_m \rangle$. The solution of $[I]$ is obtained by pre-multiplying both sides of (4.9) by the inverse of $[Z]$:

$$[I] = [Z]^{-1}[V] \tag{4.10}$$

or by using a variety of other standard techniques [83]. A limitation of moment methods is that they are restricted to solving relatively simple geometries for which IEs can be derived. Also, the size of the problem is limited due to the memory requirements for the matrix storage and evaluation. However, for relatively simple problems, moment methods are much more efficient than many other numerical techniques. Moment methods are preferred for the modeling of structures that are electrically small (i.e. each dimension is small compared to the wavelength) and can be modeled as a composite of simple objects for which accurate IEs exist (e.g. an aircraft modeled as a grid of wires).

4.3 Concluding Remarks

The main concepts of the moment method and the finite-difference time-domain technique were introduced in this chapter. The Numerical Electromagnetic Code, a moment method program, can efficiently solve electromagnetic problems involving simple geometries such as wires. The FDTD method, on the other hand, is a robust technique that is capable of modeling complex geometries of inhomogeneous dielectrics. The NEC is used in this research to verify the FDTD method results and to assist in the development of subcell

wire modeling in the FDTD method. An FDTD-based computer program developed at the University of Victoria is used to analyze the effect of the user proximity and the multi-path environment on antenna performance and to develop the improved subcell wire model. Results of this work are provided in Chapters 5 and 6.

Chapter 5 Analysis of PCS Antennas in Mobile Environments

The development and widespread use of hand-held wireless communication systems has stimulated increasing interest in the electromagnetic interactions between the antenna and the surroundings. Of interest are the influence of the mobile communications environment and the close proximity of the user's body on antenna performance, the potential health effects of the radio frequency (RF) fields absorbed in the user's body [22]-[24] and compliance of the personal communication system (PCS) device with existing safety standards (e.g. [28],[29]). These issues must be addressed while also ensuring that the PCS antenna is small enough to be used on a PCS handset and has sufficient gain, bandwidth and efficiency.

In this chapter, the FDTD technique is used to analyze two PCS antennas at frequencies near 900 MHz. The research investigates the interaction between PCS antennas and mobile communications environments and addresses the following issues:

- how the proximity of the user's body affects the antenna performance,
- how the antenna performance is influenced by the type of mobile communication environment (urban outdoor vs. suburban outdoor), and
- how changing the antenna configuration can improve the antenna performance and

reduce the specific absorption rate (SAR) of energy in the user's body.

The two antennas under investigation are a monopole antenna and a polarization diversity antenna (PDA). The antenna modeling incorporates the antenna, a cellular telephone handset in the vertical orientation, models of the user's head and hand, and a statistical model of the mobile communication environment. Antenna performance is evaluated in terms of the far-field radiation patterns, the mean effective gain (MEG), the correlation coefficient, the radiation efficiency and the SAR in the user's body. For the PDA, the far-field radiation patterns are compared with experimental measurements which were conducted prior to this dissertation work [58]. Good agreement between the calculated and measured radiation patterns was observed.

Results indicate that the two modes of the PDA are sufficiently uncorrelated for diversity operation and that overall, the values of the MEG, the efficiency and the peak averaged SAR in the head are better for the PDA than for the monopole antenna. However, in terms of the MEG, the PDA is more sensitive than the monopole antenna to the presence of the user's body. For the PDA, most of the power absorbed in the user's body is deposited in the hand, whereas for the monopole antenna, most of the absorbed power is deposited in the head. For both antennas, the MEG is strongly influenced by the type of environment.

5.1 Description of Antennas

A monopole antenna is investigated in this dissertation because of its widespread use in personal communications systems. Its popularity is due to its attractive bandwidth and

radiation characteristics. However, monopole antennas are easily damaged, due to their nonrigid structure. Damage of the monopole antenna accounts for approximately one half of faults in vehicle-mounted cellular telephone use [84]. Also, more than half of the radiated power from a handset-mounted monopole antenna may be absorbed in the user's body [33],[85],[86]. The absorbed power is a potential health concern and it results in reduced antenna efficiency.

Microstrip antennas are attractive alternatives to monopole antennas, as outlined in Chapter 2. They can be made conformal with the handset for protection from damage. They can also be positioned away from the head and hand to reduce power deposition in the user's body. Many microstrip antenna configurations have been developed for personal communication systems [34],[87]-[91]. Microstrip antennas can also be used to provide antenna diversity. To date, there has been considerable research on polarization diversity antennas and many configurations have been proposed [40],[63]-[65],[92]. However, many of these configurations are not suitable for hand-held communications devices due to their inefficient use of space (space must often be sacrificed to minimize the coupling between the two polarization modes). A novel microstrip patch antenna that offers polarization diversity in a compact configuration is investigated in this dissertation [58].

An experimental model of the PDA is shown in Fig. 5.1. This antenna was developed for the author's Master's thesis [58]. It consists of two radiating patches on a polyethylene dielectric substrate ($\varepsilon_r = 2.5$). Each radiating patch is short-circuited to the ground plane on one side using a shorting patch. The use of the shorting patch reduces

the length of each radiating patch by 50%. The two patches are fed separately, and feeding the two feed points in phase or out of phase results in the radiation of horizontally-polarized (HP) or vertically-polarized (VP) fields, respectively [93],[94]. Impedance matching of the antenna was achieved by connecting each coaxial feed probe to a quarter-wave microstrip transformer underneath the ground plane [94]. To simultaneously transmit or receive both the HP and VP modes, the two quarter-wave transformers were connected to a two-way 0°/180° power combiner/splitter. Using this device, the sum of the signals from the two feed points (the HP mode) is received at one port and the difference between the signals (the VP mode) is received at the other port. The slots in the shorting patches help to bring the resonant frequencies of the two modes together. The dimensions of the PDA in Fig. 5.1 are for a resonant frequency of 856 MHz. Both experimental and numerical results are reported for this antenna configuration.

The numerical model of the PDA in a handset configuration is shown in Fig. 5.2a. For this configuration, a superstrate over the gap between the patches was used instead of slots in the shorting patches to bring the resonant frequencies of the two modes together. The dielectric constants of the substrate and superstrate are relatively high (9.3 and 15.0, respectively) to keep the antenna size small at 900 MHz. However, much lower dielectric constants can be used for resonance at PCS frequency bands near 1900 MHz. The monopole antenna is shown in Fig 5.2b. It consists of a thin wire with a gap excitation at the base of the wire.

Both antennas are situated on PCS handsets that are held next to the user's head by a hand, as described in Section 3.1.3 and shown in Fig. 3.1. PCS handsets typically consist of electronic circuitry, a metal casing which surrounds the circuitry and serves as the ground plane of the antenna, and a plastic covering layer. For this analysis, the PCS handsets are modeled as metal boxes (with dimensions as shown in Fig. 5.2) covered by a 2 mm thick layer of plastic material ($\varepsilon_r = 2.0$). The plastic layer did not cover the PDA. For both antennas, the height and width of the handset are identical. The thickness of the handset of the diversity antenna is smaller than that of the monopole antenna, however, to ensure a consistent distance between the head and the antenna feed points for SAR comparisons. For both antennas, the handset is placed against the ear of the user (i.e. with no gap between ear and handset). This results in a 1.4 cm distance between the head and the antenna feed. The handset is in the vertical orientation, as tilted orientations result in lower SARs [34]. The PDA is mounted on the back of the handset, away from the head. To avoid being near the hand, the PDA was also located at the top of the handset, opposite the earpiece. The monopole antenna is located in the middle of the top surface of the handset.

5.2 Modeling Configuration

Numerical modeling of the antennas is performed using the FDTD technique using 3 mm cubical Yee cells [73]. Due to the fact that the resolution of the head model (3.6 mm) and the size of the Yee cells (3 mm) are not equal, a dielectric averaging algorithm is used to convert the head model to the Yee cell resolution [36]. The computational space is terminated by a perfectly matched layer absorbing boundary with seven layers, a parabolic pro-

file, and 1 percent termination reflection, PML(7, P, 1) [77]. This ensures that reflections from the boundary walls are below -40 dB. For antenna feeding, gap excitations are used with the time-domain envelope of a frequency-shifted Gaussian pulse. The center frequency and bandwidth of the pulse are 900 MHz and 1 GHz, respectively. The number of time steps chosen for each simulation is sufficient to ensure that the pulse amplitude had decayed to a small fraction of its peak value.

5.3 Experimental Results

Experimental results of the PDA are provided in this section to demonstrate that the antenna works in practice and that experimental and numerical results are in agreement. The experimental measurements of the PDA were obtained for the author's Master's thesis [58]. Scattering parameters and far-field radiation patterns of the antenna were measured using a Hewlett-Packard 8510C Network Analyzer and an antenna test range [95]. Scattering parameter measurements indicate that the HP and VP modes had $VSWR \leq 2$ bandwidths of 2.0% and 3.9% and return losses of 12 dB and 23 dB at their centre frequencies, respectively. Bandwidths of approximately 5% for both modes are possible using better matching circuits [58]. The minimum isolation between the two modes was 20.2 dB. Free-space far-field radiation patterns of the antenna in the azimuth plane ($\theta = 90°$) are given in Fig. 5.3. When the patches are fed in phase, E_ϕ has an approximately omnidirectional pattern. On average, E_θ is 23.6 dB lower than E_ϕ. When the patches are fed out of phase, E_θ dominates, with an average power 19.9 dB greater than that of E_ϕ. Radiation of E_θ is nearly omnidirectional in the horizontal plane. Note that the radiation of the PDA behind the ground plane is very strong. This is due to the presence of currents

on the back face of the small ground plane, as discussed in Section 3.2.

For the same PDA configuration, numerical results of the radiation patterns are also shown in Fig. 5.3. Numerical and experimental results are in agreement for the dominant polarization of each mode. There is less agreement between the numerical and experimental results for the cross-polarization of each mode. However, this disagreement is not significant due to the low power levels involved, and it may be caused by the misalignment of the transmitting and receiving antennas in the experimental measurements.

5.4 Numerical Results

5.4.1 Antennas in Free Space

The free-space far-field radiation patterns (dominant polarizations only) of both antenna models are shown in the elevation plane in Fig. 5.4. The user is not included in the results of this subsection. For the handset-mounted monopole antenna, the E_θ pattern has a butterfly shape, as noted by others [36],[75]. Most of the radiation is directed below the horizon, whereas most of the incident power is arriving at the antenna from above the horizon (see plots of P_θ for urban and suburban environments in Fig. 3.2). As a result, the MEGs are low in both urban and suburban environments, as shown in Table 5.1. The MEG of the monopole antenna is higher in the urban environment than in the suburban environment because the dominant polarization radiated by the monopole (E_θ) corresponds to the polarization which is received with higher mean power in the urban environment. In the suburban environment, however, E_θ and E_ϕ are received with equal mean power (XPR = 0 dB). For the same reason, the MEG of the VP mode of the diversity antenna is higher in the

urban environment, and the MEG of the HP mode is higher in the suburban environment. Both modes of the diversity antenna radiate a significant amount of power above the horizontal plane, where P_θ and P_ϕ are strong, resulting in MEGs for the diversity antenna that are higher than those of the monopole antenna (Table 5.1).

Table 5.1 MEG and correlation coefficient of monopole and PDA in free space at 900 MHz.

antenna	MEG_{urban} (dBi)	$MEG_{suburban}$ (dBi)	ρ_{urban}	$\rho_{suburban}$
monopole	-1.5	-3.3	--	--
PDA (HP mode)	-0.9	+1.4	0.44	0.21
PDA (VP mode)	+2.2	+1.0		

Dominant mode radiation of the two modes of the PDA is approximately uniform over the azimuthal angles, as shown in Fig. 5.5. Also, the cross polarization level for the VP mode is very low. Thus, these radiation patterns are similar to those of the experimental PDA model. However, the cross polarization level of the HP mode is relatively high. It has been observed that the HP mode cross polarization level can be reduced by increasing the size of the antenna (i.e. by lowering the substrate dielectric constant). Correlation coefficients of the PDA (Table 5.1) are below 0.5 for both environments, indicating that both modes are sufficiently uncorrelated [60]. The correlation is higher in the urban environment due to the strong reception of E_θ and the high cross-polarization level of the HP mode.

5.4.2 Effects of the User's Head and Hand

When the user's head and hand are included in the model, the monopole antenna and the PDA have radiation patterns as shown in the azimuthal plane in Figs. 5.6 and 5.7, respectively. For both figures, the head is located at $\theta = 90°$, as indicated by the illustration in the bottom right corner. A comparison of the monopole far-field radiation patterns in free-space with the patterns in the presence of the user's body reveals three effects (Fig. 5.6). First, the magnitude of the dominant polarization, E_θ, has decreased due to absorption of radiation in the user's body. Second, the magnitude of the cross-polarization, E_ϕ, has increased substantially. Third, the E_θ pattern is distorted, particularly in the half-plane containing the head. Radiated power in the direction of the head is reduced, as expected. The same three effects are also observed for the diversity antenna (Fig. 5.7 vs. Fig. 5.5) except that the cross-polarization level of the HP mode has decreased.

Table 5.2 MEG and correlation coefficient of monopole and PDA in the presence of the user's body at 900 MHz.

antenna	MEG_{urban} (dBi)	$MEG_{suburban}$ (dBi)	ρ_{urban}	$\rho_{suburban}$
monopole	-3.3	-5.2	--	--
PDA (HP mode)	-5.0	-2.0	0.20	0.13
PDA (VP mode)	-1.6	-2.3		

Absorption of power in the user's body and distortion of the radiation pattern result in significantly lower MEGs for both antennas, as shown in Table 5.2. The decrease in MEG due to the presence of the user is similar in both urban and suburban environments, and the average decrease is 1.9 dB for the monopole antenna, 3.8 dB for the HP mode of the

PDA and 3.5 dB for the VP mode of the PDA. Thus in terms of the MEG, the PDA is more sensitive than the monopole antenna to the presence of the user. As explained in the next section, reduction in MEGs of the monopole antenna is largely due to power absorbed in the head, while for the PDA, reduction of MEGs is mainly due to power absorbed in the hand. This result makes sense, as the PDA is closer to the hand than the monopole antenna, and the PDA is somewhat shielded from the head by the handset whereas the monopole antenna is not.

As in free space, the MEGs of antennas in the presence of the user are strongly influenced by the type of environment. This is largely due to the difference in XPR levels of the urban and suburban environments, as explained earlier. Compared to the urban environment, the MEG in the suburban environment when the user is modeled is 1.9 dB lower for the monopole, 3.0 dB higher for the HP mode of the PDA and 0.7 dB lower for the VP mode of the PDA. The results are similar when the user is not modeled.

The correlation coefficients of the PDA have significantly improved compared to the case where the user is not present. This is mainly due to the reduction in magnitude of the cross-polarization of the HP mode. In all cases presented, at least one mode of the PDA has a higher MEG than the monopole antenna, and the two modes of the PDA are sufficiently uncorrelated. Although a combined MEG of both modes of the PDA cannot be determined without knowledge of factors such as the diversity combining scheme used, it is expected that the combined MEG would be greater than the MEGs for either of the two modes. Therefore, the diversity antenna has better overall MEG than the monopole, both

in the urban and suburban environments.

A study was performed to determine how small changes in the statistical model of the mobile environment affect the values of the MEG and the correlation coefficient. The purpose of this study is to analyze the sensitivity of the antenna performance to changes in the mobile environment. The statistical parameters of the urban and suburban environments were perturbed to simulate different urban and suburban environments. For the suburban environment, the values of m_V, σ_V, m_H and σ_H were increased by 10% to $m_V = \sigma_V = m_H = \sigma_H = 11°$ and the XPR was increased by 12% from 0 dB to 0.5 dB. For the urban environment, the values of m_V, σ_V, m_H and σ_H were decreased by 10% to $m_V = 17.1°$, $\sigma_V = 18.0°$, $m_H = 28.8°$ and $\sigma_H = 57.6°$ and the XPR was decreased by 12% from 5 dB to 4.5 dB. The values of MEG and ρ were calculated for the antennas in the presence of the user's body. These values are presented in Table 5.3 for the two environments.

Table 5.3 MEG and correlation coefficient of monopole and PDA in the presence of the user's body at 900 MHz for modified urban and suburban environments.

antenna	MEG_{urban} (dBi)	$MEG_{suburban}$ (dBi)	ρ_{urban}	$\rho_{suburban}$
monopole	-3.5	-5.2	--	--
PDA (HP mode)	-4.8	-2.2	0.19	0.14
PDA (VP mode)	-1.6	-2.2		

The changes in the MEG and the correlation coefficient are relatively small compared with the changes in the parameters of the mobile environment (Table 5.2 vs. Table 5.3).

The change in the MEG varies from 0 to 5.9%, with an average change of 3.0%. The correlation coefficients of the PDA in the modified urban and suburban environments changed by 4.5% and 7.0%, respectively. As expected, changing the parameters of the urban environment to be more like those of the suburban environment increased the MEG of the HP mode of the PDA, decreased the MEG of the monopole antenna and the VP mode of the PDA, and decreased the correlation coefficient of the PDA. The changes in the MEGs and the correlation coefficient by changing the suburban environment to be more like the urban environment are also as expected.

5.4.3 Efficiency and SAR

The antenna efficiency and the peak averaged SAR in the user for both antennas are shown in Table 5.4 for two cases: with only the hand modeled and with both the head and hand modeled. SAR calculations are normalized to 1W of total output power (i.e. the radiated power plus the absorbed power in the body equals 1 W). The results suggest that for the monopole antenna, most the power absorbed in the body is absorbed in the head, whereas for the PDA, most of the absorbed power is absorbed in the hand. In fact, it was found that when both the head and the hand are modeled, the percentage of absorbed power that is deposited in the head is 91.2% for the monopole antenna, 38.5% for the HP mode of the PDA and 33.9% for the VP mode of the PDA. Thus the efficiency of the monopole antenna is more strongly influenced by the presence of the head than by the presence of the hand, whereas the opposite is true for the PDA. SAR values are much higher in the head when the monopole antenna is used and higher in the hand when the PDA is used. Overall, the PDA has higher antenna efficiency and lower SAR in the head

than the monopole antenna. SAR in the head is of greater concern than SAR in the hand due to the importance of organs in the head and their sensitivity to electromagnetic fields.

Table 5.4 Efficiency of antennas and peak SAR (averaged over 1g and 10g of tissue) at 900 MHz.

	antenna	η (%)	SAR (1g), (W/kg)		SAR (10g), (W/kg)	
			in hand	in head	in hand	in head
with hand model only	monopole	87.2	2.52	--	1.61	--
	PDA, HP mode	66.0	14.4	--	8.52	--
	PDA, VP mode	58.5	19.7	--	11.9	--
with hand and head models	monopole	44.4	1.57	8.44	0.94	5.04
	PDA, HP mode	51.9	14.4	2.63	8.48	1.34
	PDA, VP mode	55.4	15.7	3.91	9.64	1.87

5.5 Concluding Remarks

When analyzing antennas for PCS devices, it is important to take the mobile communication environment into consideration. The type of mobile communication environment chosen (urban or suburban) has a pronounced effect on the correlation coefficient of the polarization diversity antenna (PDA) and on the MEGs of the PDA and the monopole antenna. It is interesting to note that while a vertically-polarized antenna, such as the monopole antenna, should perform well in urban environments (due to the presence of a strong vertically-polarized component of the received signal), the handset-mounted monopole antenna did not perform as well as the PDA. The monopole antenna performed relatively poorly in the urban environment because most of the radiated power was directed downward, away from the incoming signals. The performance of the PDA relative to that

of the monopole antenna was better in the suburban environment than in the urban environment. The better performance is a result of the fact that the both the vertically-polarized and horizontally-polarized components of the electric field are received with approximately the same mean power in the suburban environment, and the PDA receives both components. The fact that the PDA receives both components is also beneficial if handset orientations other than the vertical orientation are studied.

The presence of the user's body distorts the far-field radiation patterns, particularly in the direction of the head, and generally increases the magnitude of the cross polarization radiation. The antenna type and geometry significantly affect the antenna efficiency and SAR in the user's body. When the monopole antenna is used, most of the absorbed power is dissipated in the head while a relatively small amount of power is dissipated in the hand. The opposite is true for the diversity antenna. Overall, the PDA performs better than the monopole antenna in terms of antenna efficiency, peak averaged SAR in the head, and MEG. Also, the two modes of the PDA are sufficiently uncorrelated for diversity operation in both environments. However in terms of the MEG, the PDA is more sensitive than the monopole antenna to the presence of the user's body. Note that the antenna efficiency computed in this dissertation is strictly a measure of how much power is not absorbed in the user's body. A more practical measure of efficiency would also take into account other antenna losses (including dielectric losses and mismatch losses).

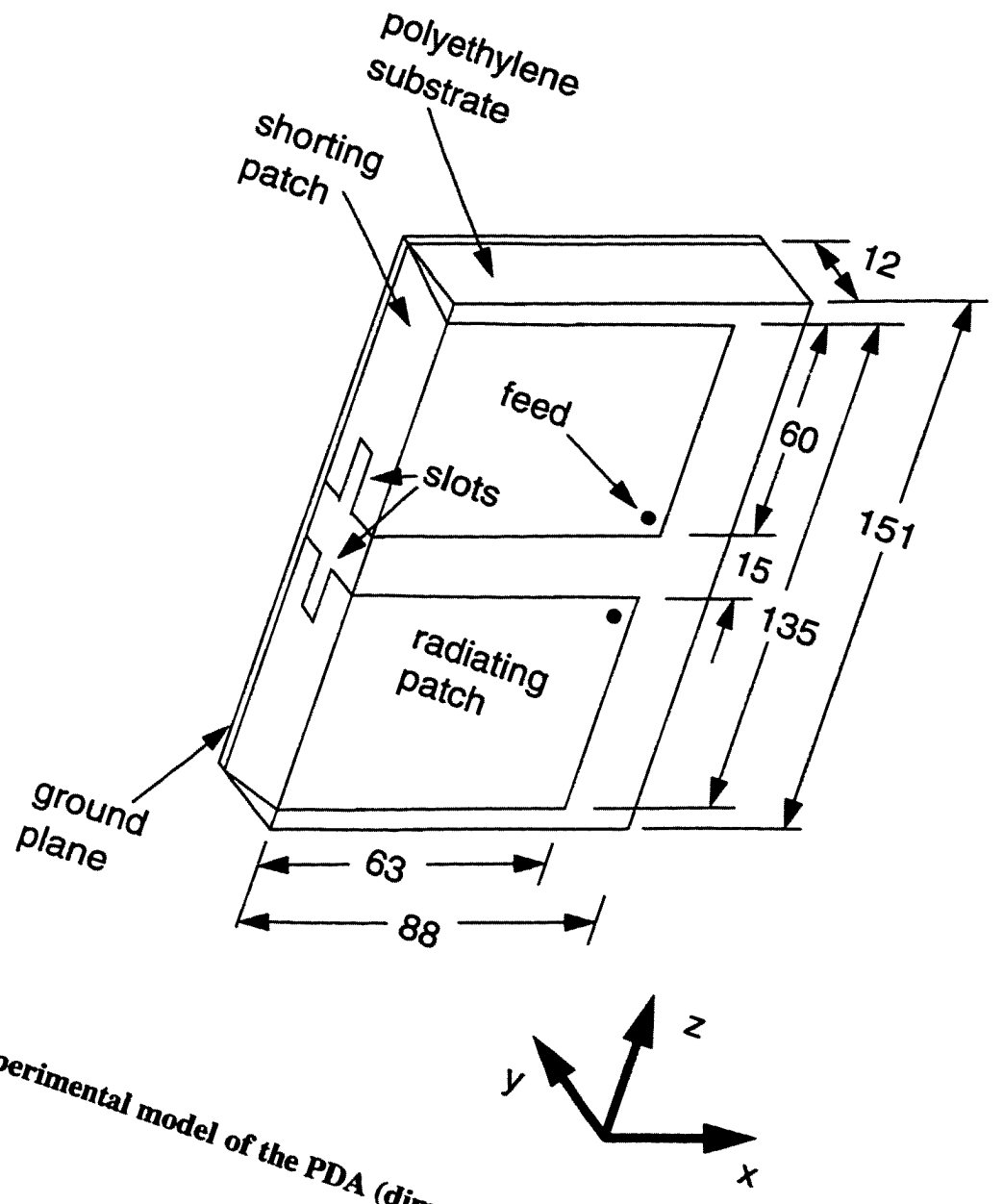

Fig. 5.1 Experimental model of the PDA (dimensions in millimeters).

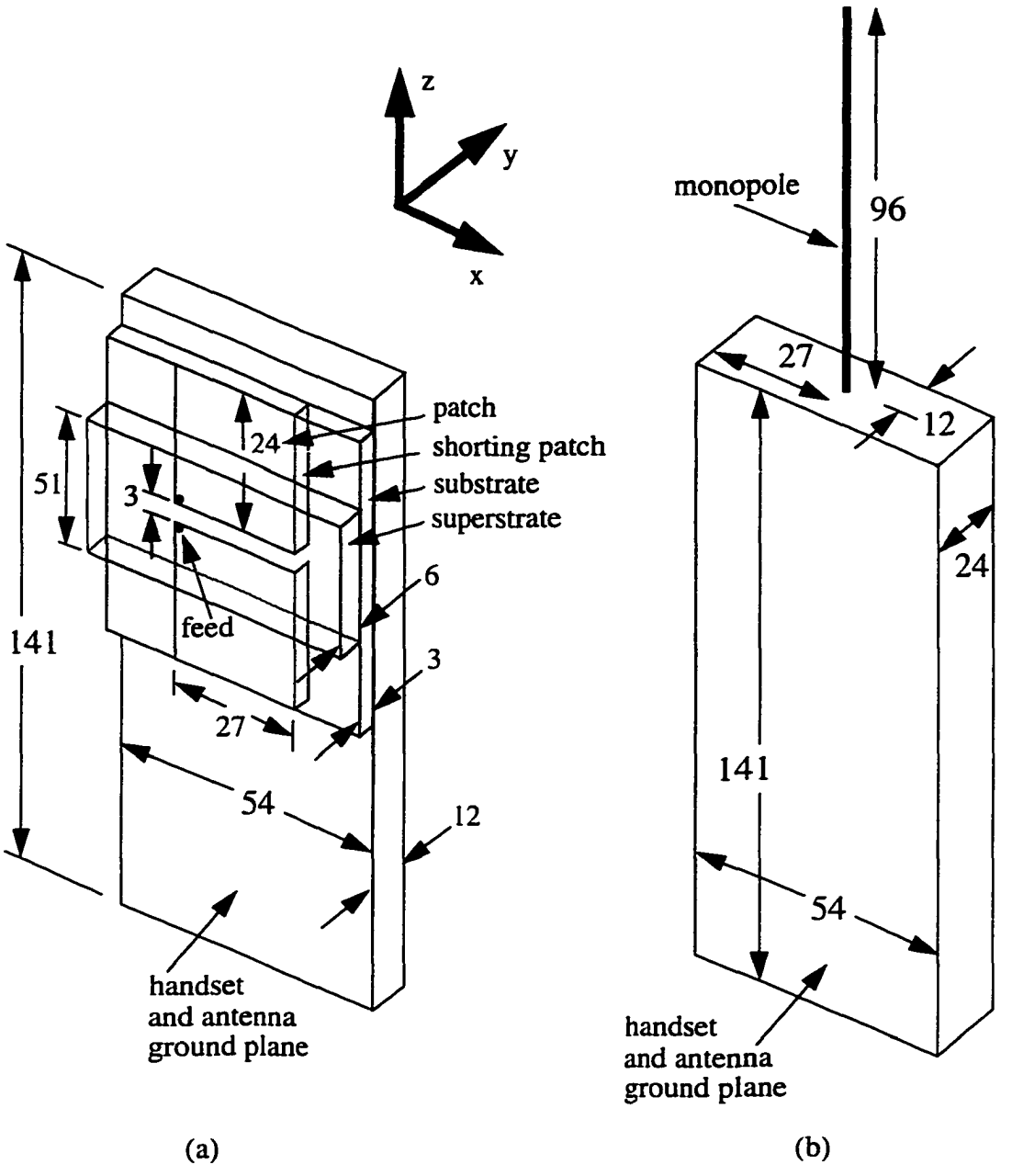

Fig. 5.2 Antenna-handset configuration for (a) the PDA, and (b) the monopole antenna (dimensions in millimeters).

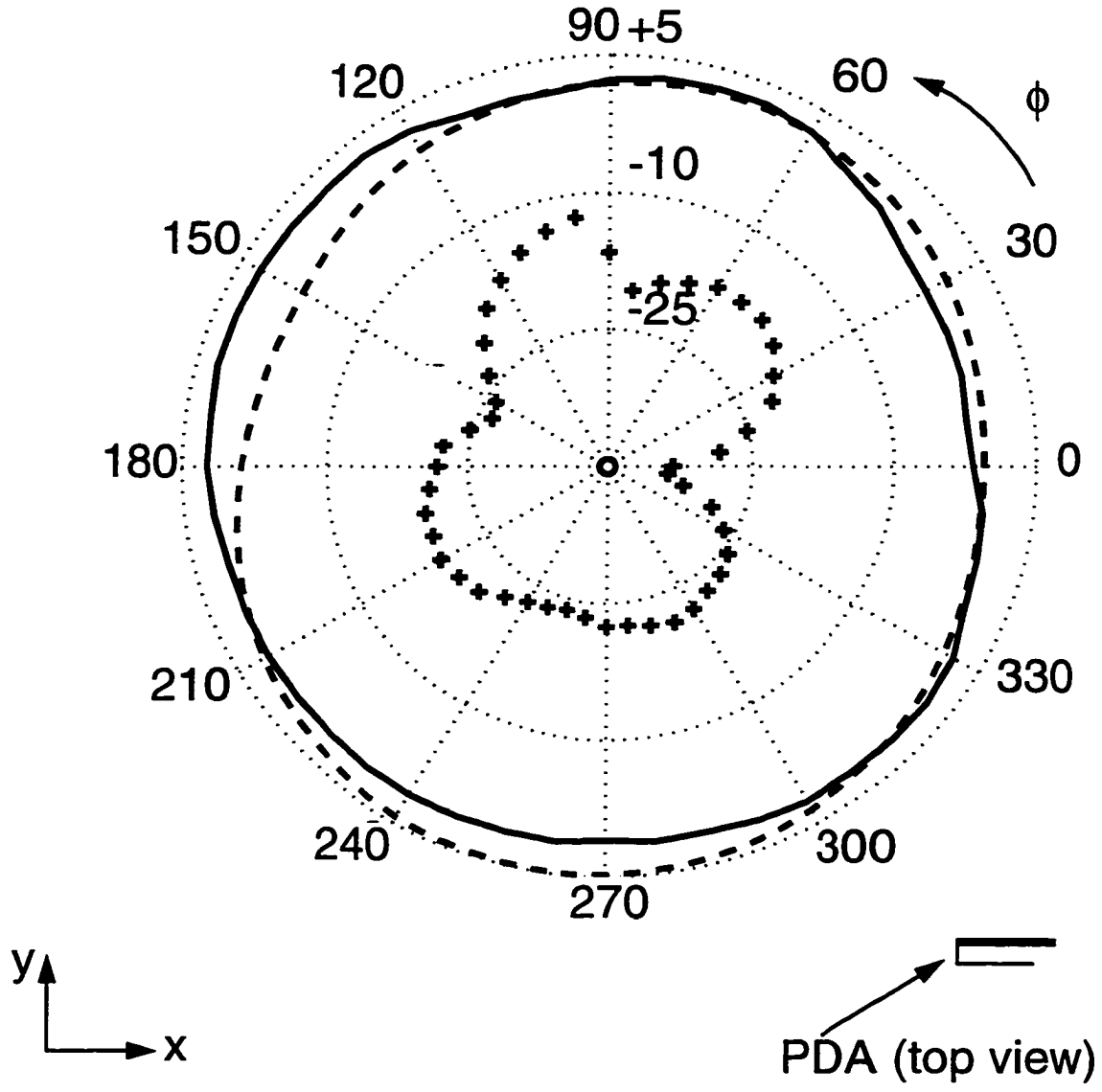

Fig. 5.3 Free-space far-field radiation patterns of the experimental PDA in the azimuth plane (in dBi). (a) HP mode.

+ + + E_θ, measured
o o o E_θ, calculated
——— E_ϕ, measured
- — — - E_ϕ, calculated

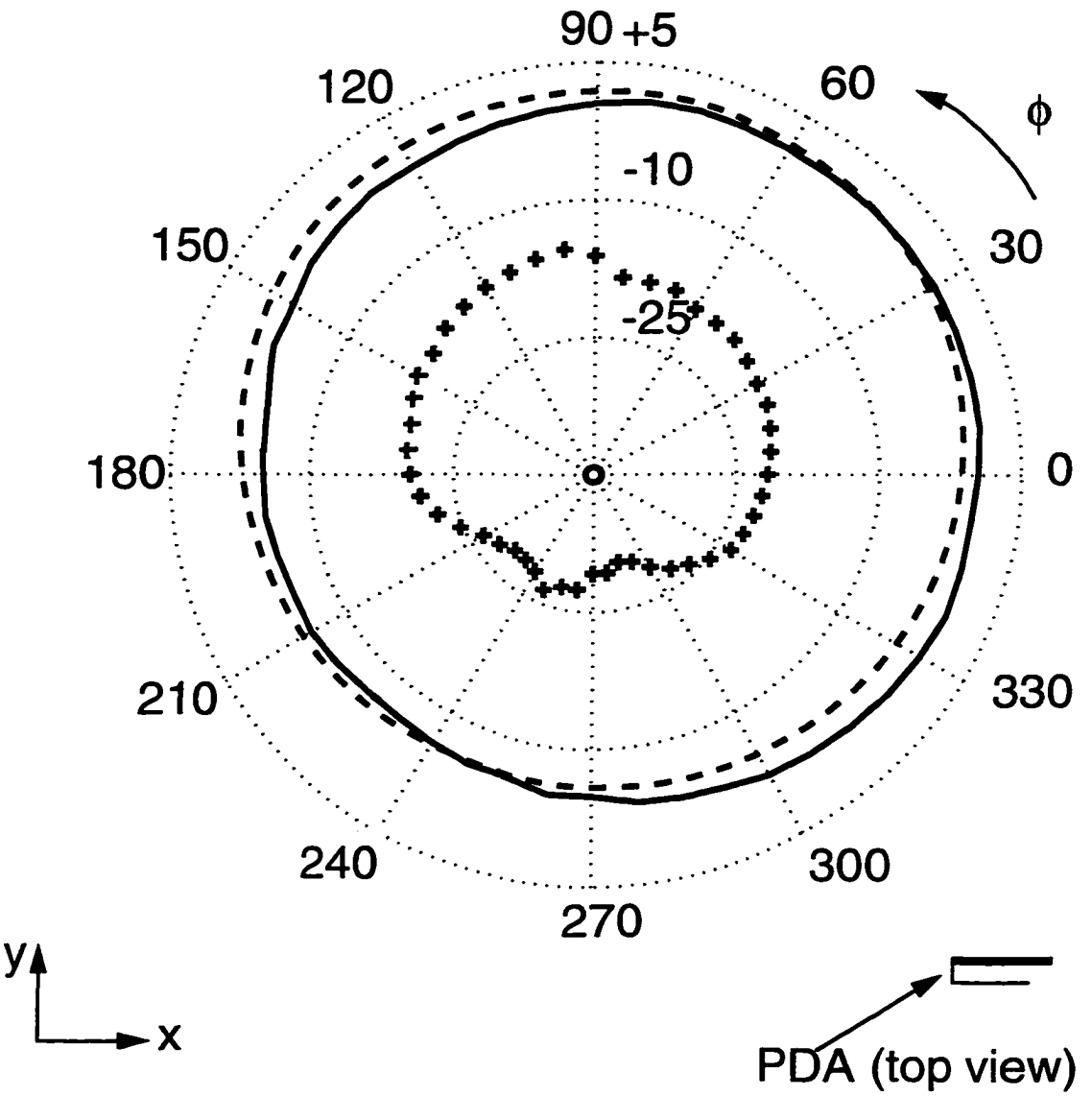

Fig. 5.3 Free-space far-field radiation patterns of the experimental PDA in the azimuth plane (in dBi). (b) VP mode.

——— E_θ, measured
- — — - E_θ, calculated
+ + + E_ϕ, measured
o o o E_ϕ, calculated

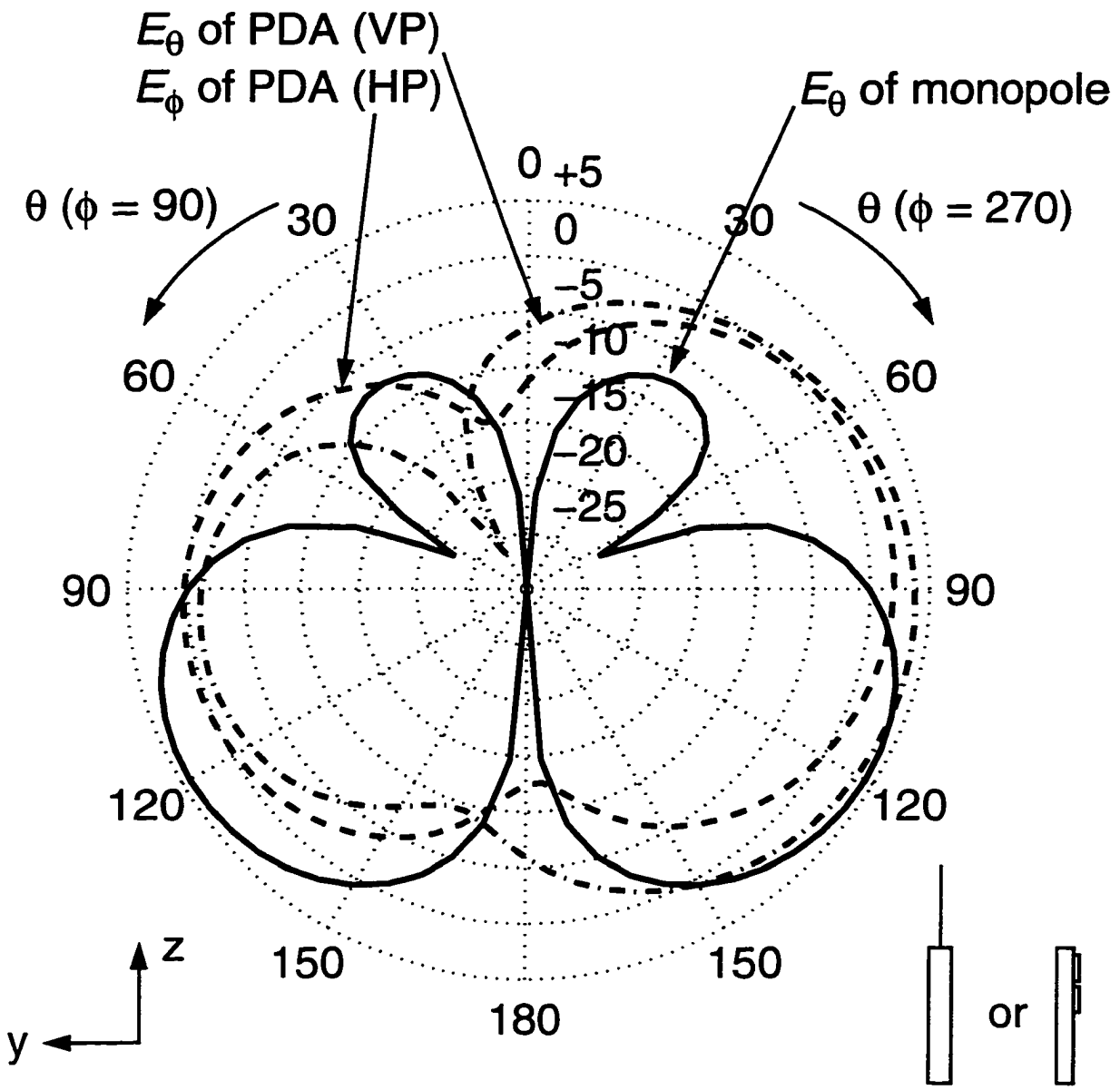

Fig. 5.4 Free-space far-field radiation patterns of the antenna models in the elevation plane (in dBi). Dominant polarizations only.

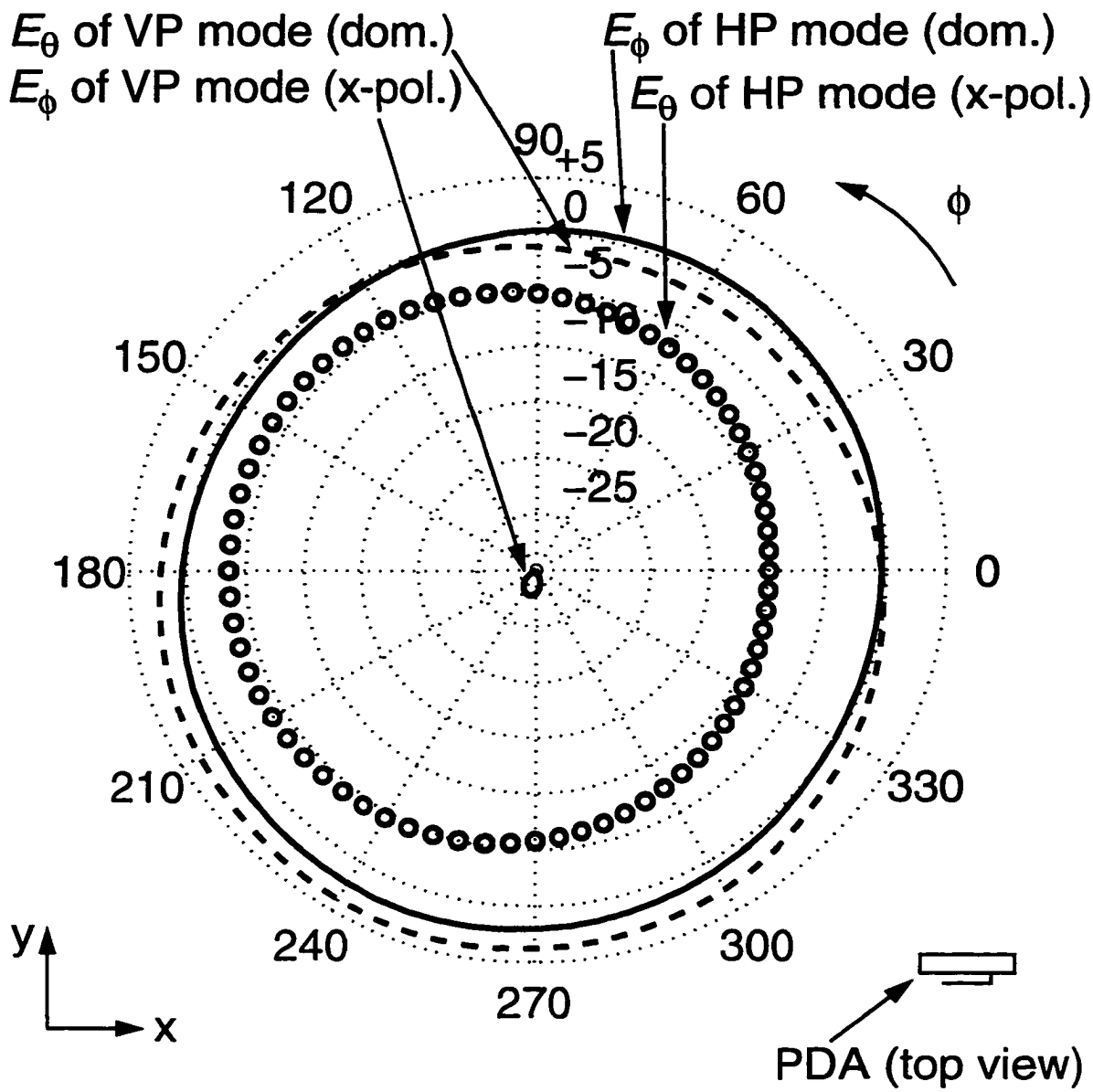

Fig. 5.5 Free-space far-field radiation patterns of the PDA in the azimuth plane (in dBi).

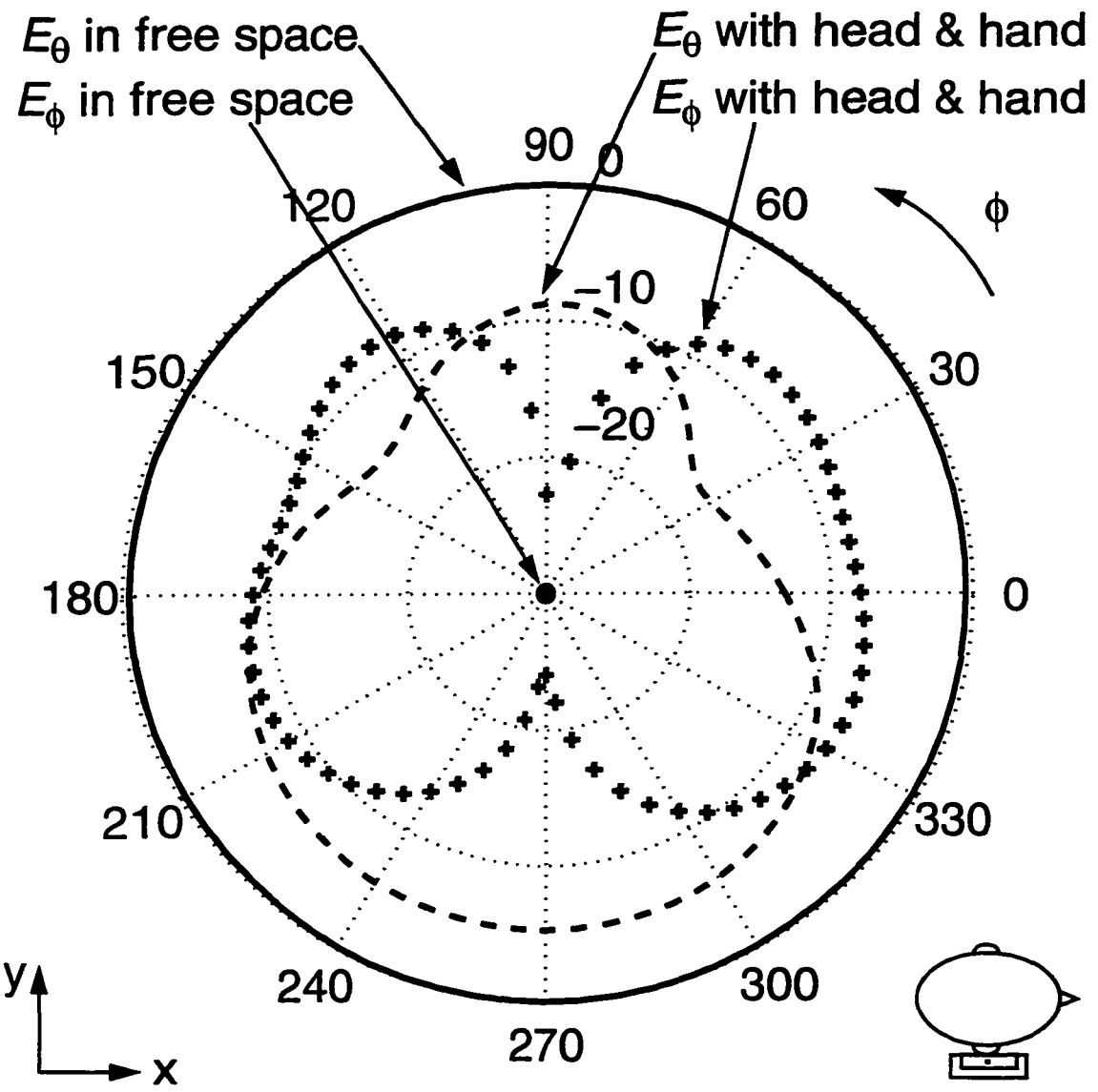

Fig. 5.6 Far-field radiation patterns of the monopole antenna in the presence of the user's body (in dBi). Shown in the azimuth plane.

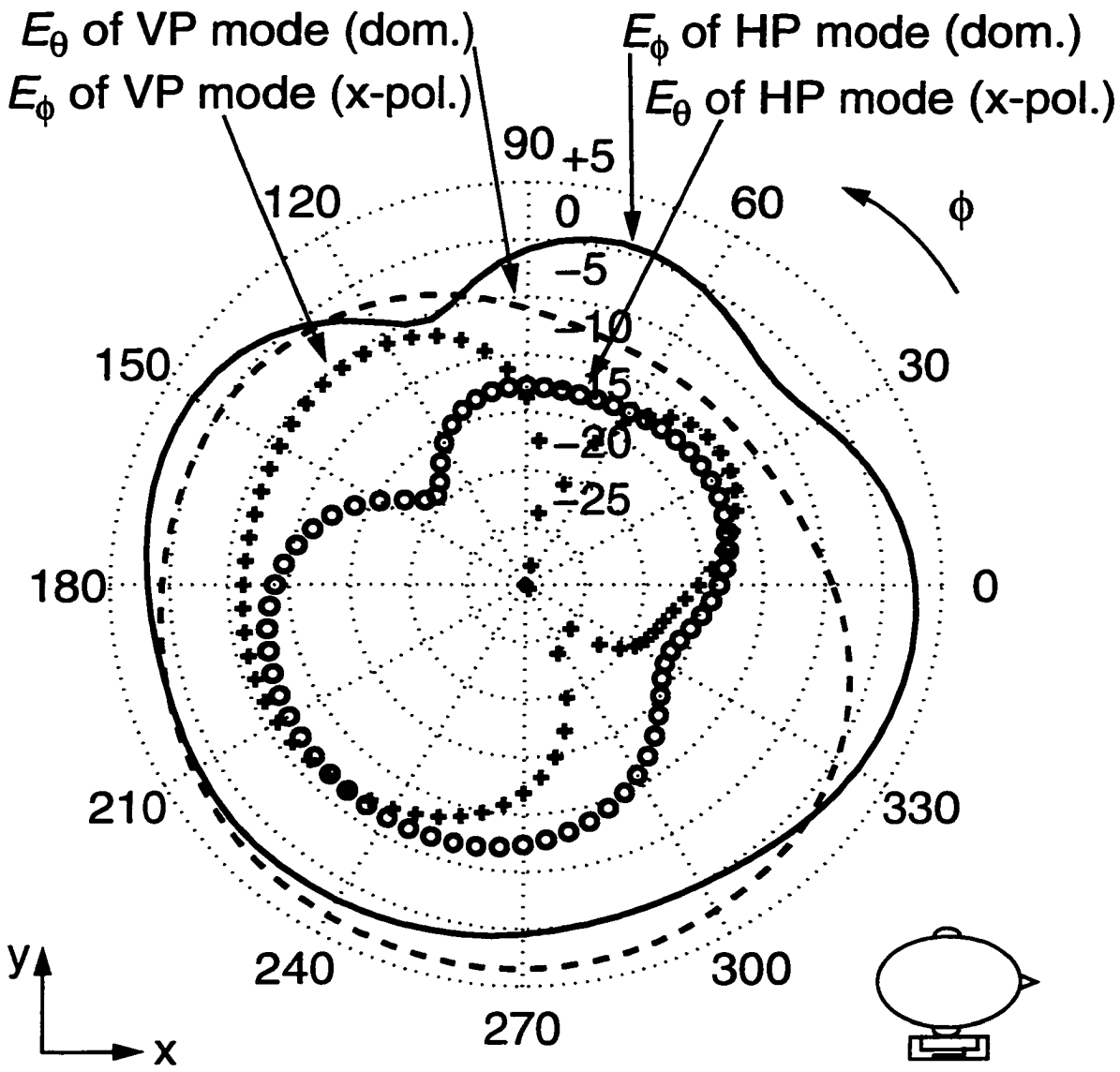

Fig. 5.7 Far-field radiation patterns of the PDA in the presence of the user's body (in dBi). Shown in the azimuth plane.

Chapter 6 Linear Wire Antenna Modeling in FDTD

The accurate FDTD modeling of wires is critical to many areas of FDTD modeling, particularly to linear wire antenna design and to the study of the human-antenna interaction for PCS systems. The modeling of wires is complicated by the fact that the wire radius is typically smaller than a practical size for the FDTD Yee cells, and therefore, the wire does not conform to the FDTD mesh. This chapter presents a thorough investigation of the accuracy of wire models. The calculated input impedance of dipole antennas is used to evaluate model accuracy. A summary of wire modeling in FDTD is provided in Section 6.1, along with a justification of why the antenna input impedance is used to evaluate the accuracy of wire models. Two currently-used wire models are then described: a standard wire model (Section 6.2) and a modified wire model (Section 6.3). It is shown in these sections that to the best of the author's knowledge there has not been a thorough investigation of wire model accuracy in FDTD. After describing the relevant details of the tests used to evaluate the accuracy of the FDTD wire models (Section 6.4), it is shown that the standard and modified wire models are not sufficiently accurate for some purposes, even with spatial discretizations smaller than $\lambda/40$ (Section 6.5). A new subcell wire model is proposed in Section 6.6. In the development and implementation of the algorithm, special attention is paid to two factors that affect the accuracy, namely the thin wire model and the

source model. The stability of the wire model is also addressed. Using the proposed wire model, parameters of the input impedance are calculated over a broad range of wire radii and are found to be more accurate than those obtained using the standard or modified wire model (Section 6.7).

6.1 Background

Wire modeling has been investigated mathematically for over a century [96] and has been applied to the FDTD technique for over 20 years [97]. Most of the practical work is focussed on thin wires, in which the radius of the wire is a very small fraction of the wavelength. In this dissertation, a thin wire is defined as a wire with a radius less than the selected FDTD mesh size. While accurate results are possible by setting the wire radius equal to one cell width [98], this approach often results in a very fine discretization and excessive computational resources.

In early work on FDTD wire modeling, wires with zero thickness were investigated [97], [99],[100]. However, a zero-thickness model does not accurately calculate parameters that are sensitive to the radius, such as the input reactance and the antenna bandwidth. The FDTD modeling of wires with radii greater than zero and less than one cell width requires modifying Yee's standard FDTD update equations [73] in the cells adjacent to the wires. The modifications are typically made by using the integral forms of Maxwell's equations instead of the differential forms [101]. In free space, the integral and differential forms yield the same update formulas for the $\overline{E}$ and $\overline{H}$ fields [102]. However, when performing subcell modeling, the integral formulations allow for the incorporation of the field distri-

butions along the contours of integration, which is very effective in improving the accuracy of FDTD in regions of high field variation [103].

A small number of FDTD thin wire models have been reported in the literature. One of these is a formulation based on the 'in-cell inductance' of the wire [104]. This complicated model does not appear to have sufficient accuracy (a 7% error observed in the calculation of the source current could not be improved) and it has not been found in later papers. Two other models are described in Sections 6.2 and 6.3.

FDTD wire modeling was initially applied to scattering problems [99],[79] and was later extended to include the radiation [100],[105],[106] and input impedance [106]-[109] of wire antennas. Good accuracy has been obtained for scattered fields and radiation patterns using relatively coarse spatial discretizations of $\lambda/10$ to $\lambda/20$. This accuracy is relatively easy to obtain, due in part to the fact that scattered fields and radiation patterns are not very sensitive to the wire dimensions. For example, a 10% increase in the length of a dipole antenna from $L = \lambda/2$ results in only a 3% reduction in the 3-dB beamwidth of the radiation pattern [110]. Also, 'the [radiation] pattern is essentially unaffected by the thickness of the wire in regions of intense radiation' [111]. The accurate calculation of the input impedance, however, requires spatial discretizations of $\lambda/40$ or finer [108]. At resonance, where $\lambda \approx 2L$, this means that each arm of a dipole antenna must be at least 10 cells long. Such a fine discretization is necessary to accurately represent the sinusoidal distribution of current along the antenna length. It will be shown in Section 6.5 that even with discretizations finer than $\lambda/40$, the input impedance calculated by currently-used wire

models is not sufficiently accurate for some purposes. The accurate calculation of antenna input impedance is critical to many areas of FDTD modeling, including the large body of work in antenna design and in the human-antenna interaction for PCS systems.

6.2 Standard Subcell Wire Model

In a paper by Umashankar *et al.* [79], a subcell wire model was presented that is now considered to be the standard in the FDTD community. A derivation of this wire model and a summary of relevant published work on the model is provided in this section.

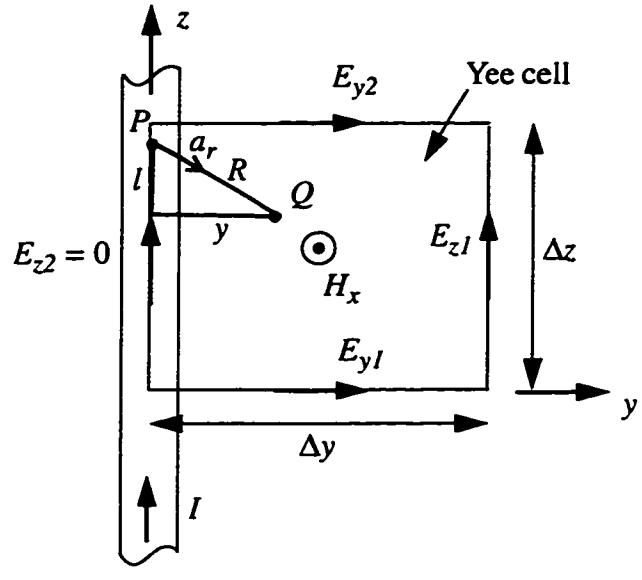

Fig. 6.1 Electric and magnetic field components in a Yee cell adjacent to a wire.

For a thin wire, the update formula for the circumferential $\overline{H}$ field component adjacent to the wire (H_x in Fig. 6.1) follows from Faraday's law [112]:

$$-\frac{d}{dt}\iint \mu \overline{H} \cdot d\overline{s} = \oint \overline{E} \cdot d\overline{l} \tag{6.1}$$

The magnetic field is integrated over the rectangular area of the Yee cell, and the electric field is integrated around the perimeter of the cell, as shown in Fig. 6.1. Expanding the integrals yields:

$$-\frac{d}{dt}\int_0^{\Delta z}\int_0^{\Delta y} \mu H_x dy dz = \int_0^{\Delta y} E_{y1} dy + \int_0^{\Delta z} E_{z1} dz - \int_0^{\Delta y} E_{y2} dy \qquad (6.2)$$

Unfortunately, each $\overline{E}$ or $\overline{H}$ field component of (6.2) is known only at the centre of the domain of integration. Therefore, assumptions must be made about their distributions before the integrals of (6.2) can be evaluated. Since the size of the Yee cell is small compared to the wavelength, static field approximations can be made, using the Biot-Savart law and Coulomb's law [113]. According to the Biot-Savart law, the magnetic field circumscribing a wire has the following relationship to the current I flowing in the wire:

$$\overline{H} = \int \frac{I d\bar{l} \times \bar{a}_r}{4\pi R^2} \qquad (6.3)$$

where R and $\bar{a}_r$ are the magnitude and direction of the vector between a point P on the wire and a point Q where the field is calculated, and $d\bar{l}$ is the differential length vector along the wire from P to Q, as shown in Fig. 6.1. Coulomb's law relates the electric field in the vicinity of the wire to the linear charge density ρ on the wire:

$$\bar{E} = \int \frac{\rho dl}{4\pi\varepsilon R^2} \bar{a}_r \tag{6.4}$$

where ε is the permittivity of the medium surrounding the wire. The standard subcell wire model assumes that both I and ρ are uniformly distributed along the wire and that the wire is infinite in extent. Using these assumptions in equations (6.3) and (6.4) leads to the following expressions for $\bar{E}$ and $\bar{H}$ in the yz plane:

$$\bar{H} = \frac{-I}{2\pi y} \bar{a}_x \tag{6.5}$$

$$\bar{E} = \frac{\rho}{2\pi\varepsilon y} \bar{a}_y \tag{6.6}$$

where $\bar{a}_x$ and $\bar{a}_y$ are unit vectors in the x and y directions, respectively. Thus, the circumferential component of the magnetic field and the radial component of the electric field vary as $1/r$ near the wire, where r is the radial distance from the wire axis ($r = y$ in this case). As neither $\bar{E}$ nor $\bar{H}$ exhibit variation in the z direction, it is assumed that both fields are uniformly distributed in z. The update formula for H_x in Fig. 6.1 is easily derived by incorporating (6.5) and (6.6) into (6.2) and evaluating (6.2). It should be noted that the standard wire formulation only applies the $1/r$ distributions of (6.5) and (6.6) to the updates of the $\bar{H}$ field components circumscribing the wire. There are no special update equations for any other field components and there is no treatment of the field singularities at the wire ends. An advantage of this is that the model is relatively easy to incorporate into an FDTD program.

The accuracy of this formulation on the scattering [99],[79], radiation patterns [105], [106] and input impedance [106],[109] of wire antennas has been investigated. However, the accuracy of the input impedance, by comparison with measurements [106] or with the moment method [109] was not investigated thoroughly. In both cases, the input impedance was plotted over a broad range of frequencies and it was merely observed that the FDTD and reference curves look similar. No numbers showing relative or absolute errors were provided. Neither were figures provided showing practical parameters of the input impedance, such as the resonant frequency or the resonant resistance. In this dissertation, a more thorough analysis of subcell wire model accuracy is provided.

6.3 Modified Subcell Wire Model

In the published FDTD literature, only one other significant paper was found that proposes a novel subcell wire model [108]. The model proposed in that paper is an extension of the standard wire model which includes a special treatment of the wire ends. Like the standard wire model, this modified model assumes a $1/r$ variation of the circumferential component of the $\overline{H}$ field and the radial component of the $\overline{E}$ field in the cells adjacent to the wire, and it incorporates these distributions into the update formulas for the circumferential $\overline{H}$ field components adjacent to the wire. Unlike the standard wire model, it also incorporates these distributions into the update formulas for the circumferential $\overline{H}$ fields one cell beyond the wire ends and the tangential $\overline{H}$ fields along the wire. However, there is still no treatment of the field singularities at the wire ends. These singularities are avoided by making the wire one-half unit cell longer on each end. The paper applies this model to

calculate the input impedance of a dipole antenna. However, a qualitative error analysis of the results is not given. Such an analysis is important for the dissertation, so it is provided in Section 6.5.

6.4 Geometry and Computational Methods

This section describes the relevant details of the tests used to evaluate the accuracy of FDTD wire models. The accuracy is determined from calculations of the input impedance of a dipole antenna. Antenna far-field patterns are not compared as the differences due to the various wire treatments are negligibly small. FDTD wire model results are compared with the results of the Numerical Electromagnetics Code [71], a widely-used method of moments program that is largely based on specialized formulations for wires. A second method of moments technique was also used for comparison. This technique is based on the Galerkin formulation with a piece-wise sinusoidal distribution along the wire [114]. The differences in the dipole antenna input impedance calculated by the NEC code and the Galerkin-based code were negligible compared to the differences between NEC and the FDTD wire models. Therefore, the Galerkin results are not shown. Analytical formulations for wires of finite thickness could not be used as they are not available.

The thin wire algorithms were tested for a centre-fed dipole of length $L = 0.21$ m. The radius of the wire was varied from $r_0 = 2L/10^6$ to $r_0 = 2L/100$ (at the fundamental resonance of the dipole antenna, $\lambda \approx 2L$). The upper limit for r_0 corresponds to the suggested maximum radius of $r_{0max} = \lambda/100$ for thin wires [115]. For wires thicker than r_{0max}, the assumption of a sinusoidal distribution of current along the wire becomes inaccurate.

Also, circumferential currents, which are not taken into account in the NEC thin wire formulation, may exist on thicker wires. The lower r_0 limit corresponds to a wire radius of 0.42 μm, which is an approximate practical lower limit for wires used in microelectronics.

The NEC thin-wire formulation is based on Pocklington's integral equation [116]. This is a one-dimensional equation which considers only the axial currents on the wire. There are two choices for the kernel of the thin wire integral equation: a thin-wire kernel, in which the current on the wire is reduced to a filament of current along the wire axis, and an extended thin-wire kernel, where the current is uniformly distributed on the surface of the wire [71]. The extended thin-wire kernel was selected for all NEC calculations in this dissertation. In all NEC tests, the dipole antenna was excited in the centre cell using a voltage source with 1 V amplitude. The length, L, of the dipole antenna was discretized into N equal length segments. N was selected to be large enough to ensure a fine discretization of the antenna yet small enough to obey the limit of $\Delta z/r_0 > 2$ (where $\Delta z = L/N$) [71]. This limit ensures that errors in the NEC formulation are less than 1%. In practice, $N = 21$ was selected for the thickest wire and $N = 101$ was selected for the thinnest wires. It was observed that the difference in all input impedance parameters between using $N = 101$ and $N = 201$ segments was less than 0.2%.

In FDTD simulations, a fine resolution was chosen, with discretizations of $\Delta z = 10$ mm = $2L/42$ and $\Delta x = \Delta y = 7.5$ mm = $2L/56$ in every wire model except for the modified model, where $\Delta z = 8.75$ mm = $2L/48$ was chosen in order to keep the same dipole length while including the wire extension of one-half cell on each end. A relatively coarse resolution

was also chosen, with discretizations of $\Delta x = \Delta y = \Delta z = 19.1\text{mm} = 2L/22$ (it was not necessary to use the modified wire model for this resolution, as explained in Section 6.5). The discretizations used in the fine resolution correspond to the limit of $\Delta \leq \lambda/40$ for the accurate FDTD calculation of the input impedance of wire antennas [108]. The coarse resolution is another practical resolution for FDTD simulations that is used for comparison. Note that the results of the FDTD wire models do not change when the entire geometry is proportionally scaled (i.e. when the sizes of all spatial increments and physical objects are scaled by the same factor). This observation was tested and verified.

Across the centre cell of the dipole, a z-directed E_z spike was excited using a wide-bandwidth frequency-shifted Gaussian pulse. The center frequency and frequency range of the pulse were 1.2 GHz and 1.0 GHz, respectively. Other excitations could have been used instead (as long as they have sufficient power in the proper frequency range), as it was observed that the type of excitation did not affect the calculation of the fundamental resonance frequency. The impedance of the source was 50 Ω. The computational space was terminated by the PML(7,P,1) absorbing boundary (seven layers, a parabolic profile and one percent termination reflection) [77]. For modeling accuracy, the simulation time was chosen to ensure that the pulse amplitude decayed to below 0.001% of its maximum value.

The antenna input impedance was calculated from the $\overline{E}$ and $\overline{H}$ fields at the source cell of the dipole antenna. The $\overline{E}$ and $\overline{H}$ fields were observed in the time domain and integrated to obtain the source voltage $V(t)$ and the source current $I(t)$. For a z-directed dipole, $V(t)$ is obtained by integrating $E_z(t)$ along the length Δz of the source region. For the source exci-

tation chosen, $E_z(t)$ is constant along the length Δz. Therefore, $V(t)$ is expressed:

$$V(t) = \int_{z}^{(z+\Delta z)} E_z(t)\, dl = \Delta z\, E_z(t) \tag{6.7}$$

The source current $I(t)$ is calculated by integrating the $\overline{H}$ field along a closed contour around the wire source. Due to symmetry, the circumferential $\overline{H}$ component, $H_\phi(t)$, is uniform along a circular contour centered at the wire axis. In the yz-plane, $H_\phi(t) = H_x(t)$. If the radius of the circular contour is $r = \Delta y/2$, then $I(t)$ is expressed:

$$I(t) = \oint H_\phi(t)\, dl = 2\pi\left(\frac{\Delta y}{2}\right) H_x(t) \tag{6.8}$$

To determine the input impedance in the frequency domain, the time signals $V(t)$ and $I(t)$ are Fourier transformed to obtain $V(f)$ and $I(f)$. Then the input impedance, $Z(f)$, is calculated by dividing $V(f)$ by $I(f)$. However, in the FDTD algorithm $\overline{E}$ and $\overline{H}$ fields are computed at alternate half time steps. Therefore, time-shifting by one half time step, $\Delta t/2$, is needed to align the $V(t)$ and $I(t)$ measurements in time. In the frequency domain, this leads to the following expression for the input impedance:

$$Z(f) = \frac{V(f)}{I(f)} \exp\left(-j2\pi f\left(\frac{\Delta t}{2}\right)\right) \tag{6.9}$$

From the input impedance curves, four parameters are presented: the input resistance and

reactance when the dipole length is $L = \lambda/2$, and the wavelength and input resistance at the first dipole resonance (the lowest frequency where the input reactance is zero).

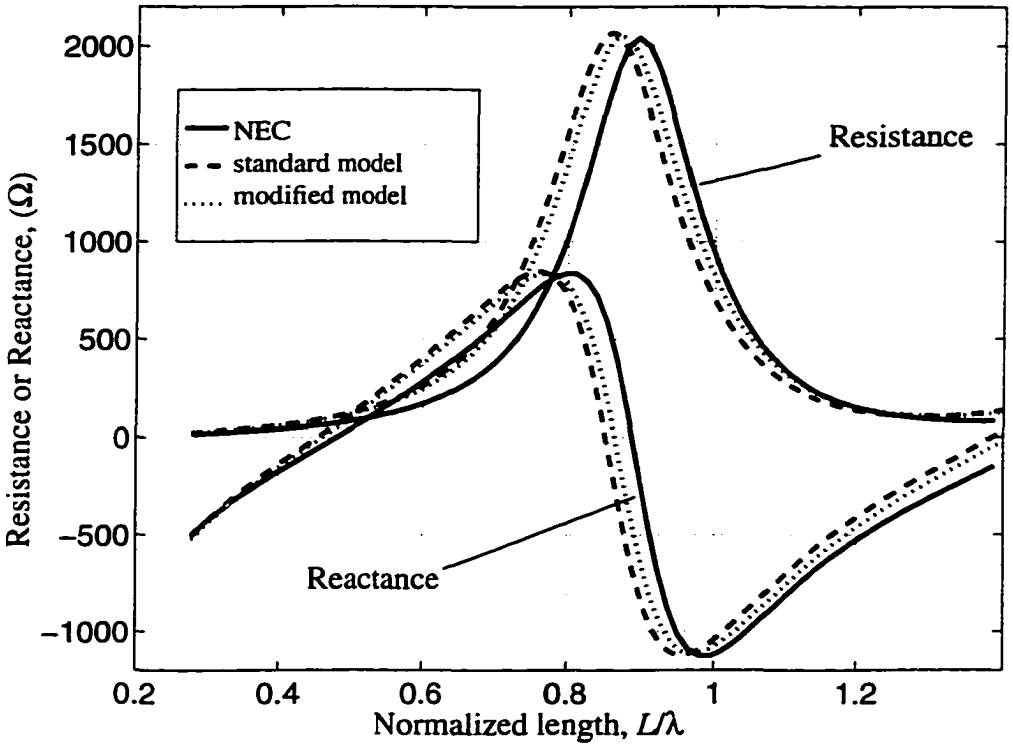

Fig. 6.2 Input impedance of the dipole antenna calculated by existing wire models. $r_0 = 2L/2100$.

6.5 Accuracy of Existing Wire Models

The accuracy of the two existing FDTD wire models is presented in Figs. 6.2 to 6.5. A general view of the agreement between the FDTD and NEC results over a broad frequency range is first presented. In Figs. 6.2 and 6.3, the dipole antenna input impedance is presented for wire radii of $r_0 = 2L/2100$ and $r_0 = 2L/10^5$, respectively. These figures can be compared with the results given in published papers. A more detailed illustration of model accuracy is presented in Figs. 6.4 and 6.5. Four parameters of the calculated input impedance are presented, as discussed in Section 6.4. For all of the data in this section,

the finer spatial resolution was used.

The impedance curves calculated by the two FDTD wire models have similar shapes as those calculated by NEC (Figs. 6.2 and 6.3). However, FDTD wire model results are scaled down in frequency compared to NEC results. Thus, the FDTD models predict lower resonant frequencies, as if a longer dipole antenna was modeled. This error has also been observed in published papers [99],[107],[108]. It is caused by the fact that the update formulas for the circumferential H field components assume that the wire is infinitely long (as discussed in Section 6.2). The finite length of the wire must be more properly taken into account to correct this problem.

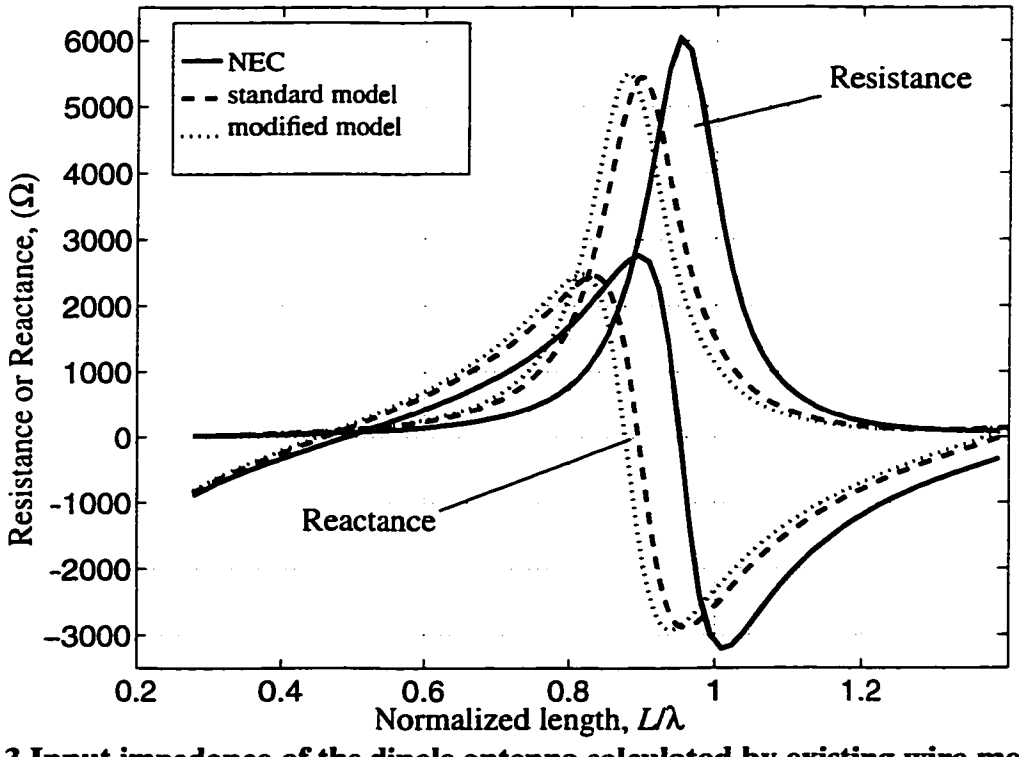

Fig. 6.3 Input impedance of the dipole antenna calculated by existing wire models. $r_0 = 2L/10^5$.

For the wire radius of $r_0 = 2L/2100$, the results of the modified wire model are somewhat better than the standard model results, although it is not known how much of the improvement is due to the model and how much is due to the finer Δz discretization used for the modified wire model. For a wire radius of $r_0 = 2L/10^5$, the errors in the FDTD results are even more pronounced (Fig. 6.3). The errors are due to frequency scaling, which is worse for this wire radius, and the smaller magnitudes of the FDTD curves. For this wire radius, the modified wire model results are worse than the results of the standard wire model. Given that the errors of the standard wire model are already quite large, there does not appear to be a significant benefit to using the modified wire model. Comparing Figs. 6.2 and 6.3, it appears that the accuracy of the input impedance calculated by the modified wire model is better than that of the standard model for thicker wires, and worse for thinner wires. This observation is confirmed by the results of Figs. 6.4 and 6.5.

For a more detailed evaluation of the wire model accuracy, four useful parameters of the dipole antenna input impedance are presented. The input resistance, R_{in}, and the input reactance, X_{in}, at the frequency where $L = \lambda/2$ are presented in Fig. 6.4. The normalized wavelength, $\lambda/2L$, and the input resistance at the first dipole resonance are shown in Fig. 6.5. All of the results are shown over a range of wire radii, and cubic splines were used to interpolate between the data points, shown as circles in the figures.

To verify the accuracy of the NEC results, the input impedance parameters were compared to their theoretical values when $r_0 = 0$. It was observed that when r_0 approaches zero, the NEC value for the input impedance at $L = \lambda/2$ converges to the theoretical value of $Z_{in} =$

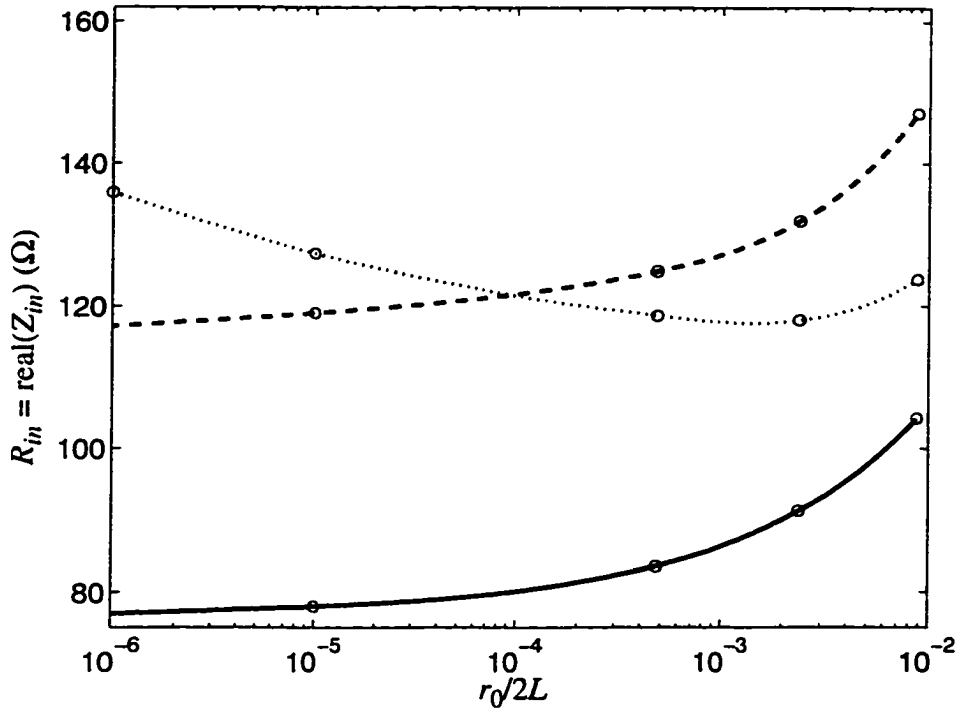

(a)

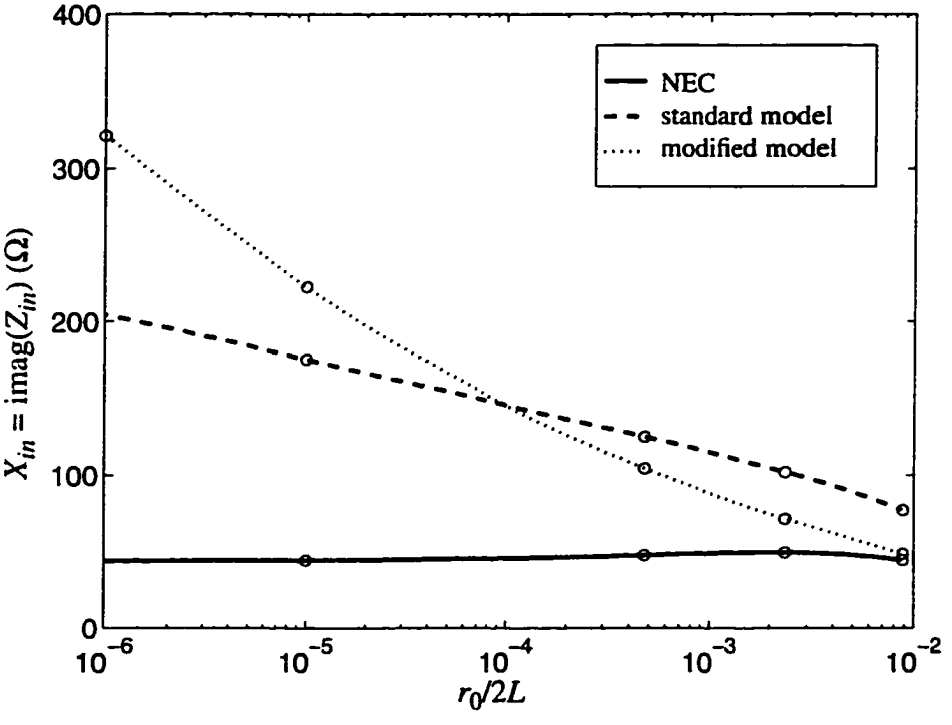

(b)

Fig. 6.4 (a) Input resistance and (b) input reactance of the dipole antenna at $L = \lambda/2$, calculated by existing wire models.

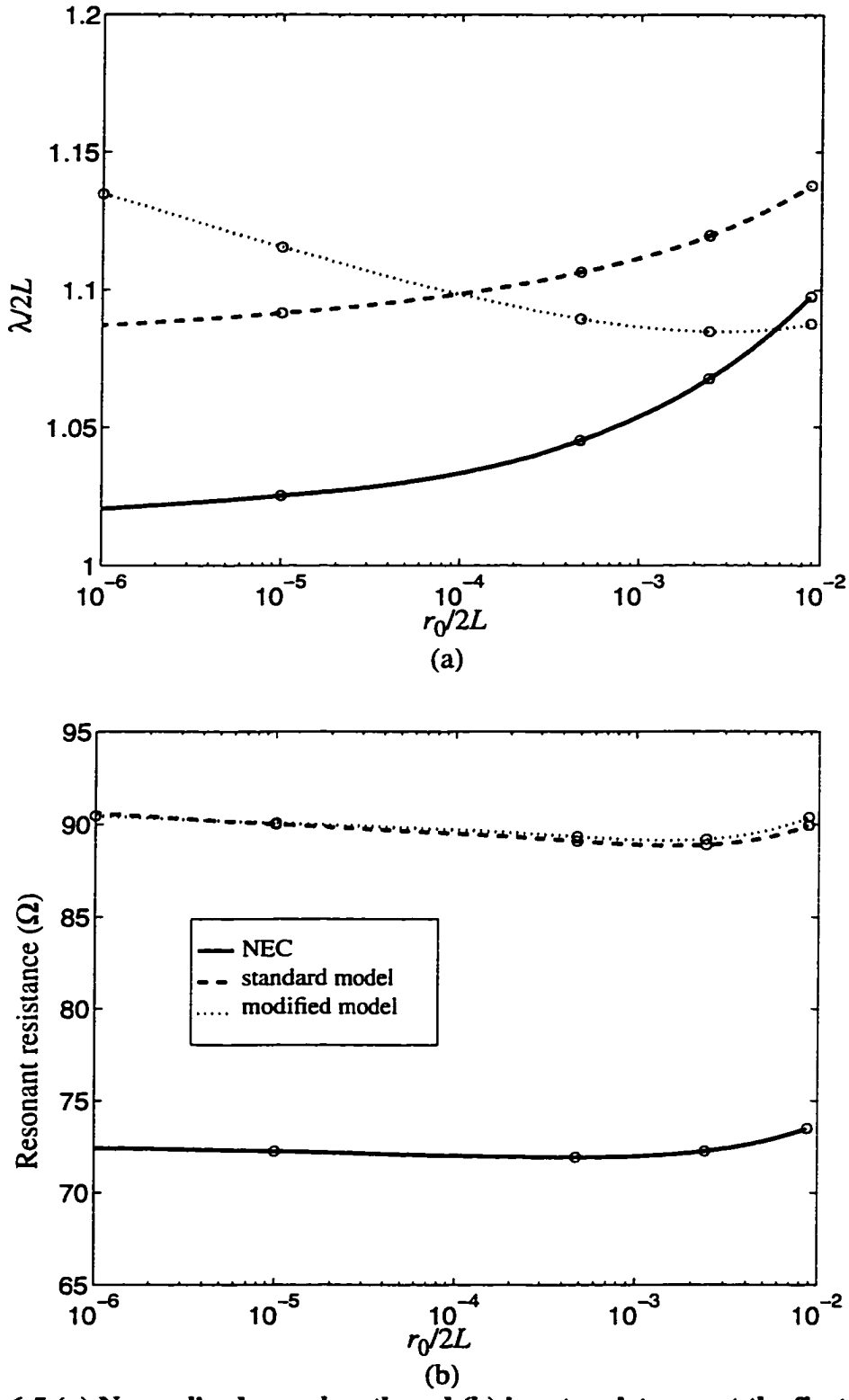

Fig. 6.5 (a) Normalized wavelength and (b) input resistance at the first dipole antenna resonance, calculated by existing wire models.

$R_{in} + jX_{in} = 73.1 + j42.5\ \Omega$ [117]. This can be observed in Fig. 6.4. The NEC values for $\lambda/2L$ and the resonant resistance converge to values of 1.01 and 72.8 Ω, respectively, which are close to their theoretical values of 1.04 [111] and 73 Ω (using the induced EMF formulation) [118].

As seen in Figs. 6.4 and 6.5, the errors in the results of standard wire model are large, even though a relatively fine resolution was used. The standard wire algorithm grossly overestimates the input resistance and reactance at $L = \lambda/2$. All errors are greater than 40% and the largest error in the input reactance is 358%. The resonant wavelength and input resistance are also overestimated. The resonant resistance calculated by the standard wire algorithm is consistently off by approximately 24%.

The results of the modified wire model are also not accurate, particularly for thin wire radii. Although the errors from the modified model are generally lower than those of the standard wire model for relatively thick wires, the errors become much greater as the wire radius is reduced. The errors in the input resistance and reactance at $L = \lambda/2$ are as high as 77% and 621%, respectively. The modified wire model errors in three of the four parameters are not consistent over the range of radii, which makes it difficult to use correction factors to scale the results to the correct values. For these reasons, the modified model is not recommended as an alternative to the standard wire model.

Out of the four parameters calculated by the two FDTD wire models, the input reactance at $L = \lambda/2$ is the most sensitive to the wire radius (Fig. 6.4(b)). For the modified wire

model, X_{in} varies from 48.7 Ω to 321.5 Ω. Interestingly, however, NEC values of X_{in} do not vary widely with wire radius. This results in errors which vary widely over the range of r_0 and become larger as the wire radius decreases. The reason for the large errors is that the value of X_{in} near $L = \lambda/2$ becomes increasingly sensitive to small changes in the antenna electrical length, L/λ, as the wire radius is reduced. For very thin dipole antennas, a relatively small error in $\lambda/2L$ can result in a large error of X_{in}. For example, using the standard wire model, a 3.7% error in $\lambda/2L$ at $r_0 = 2L/114$ results in a 73.8% error in X_{in}, while at $r_0 = 2L/10^5$, a 6.6% error in $\lambda/2L$ results in a 358% error of X_{in} (Figs. 6.4(b) and 6.5(a)). The errors in many parameters of the input impedance can be significantly reduced by accurately computing the electrical length of the antenna. This can be achieved by taking into account the proper field distributions at the wire ends.

6.6 Proposed Wire Model

The observations of the previous section motivated the development of a new FDTD wire model. This model takes into account the finite length of the wire and the field distributions beyond the wire ends. The assumed distributions of the field components used in the proposed wire model are described in Section 6.6.1, and two update equations are provided. In the implementation of the model (Section 6.6.2), two important issues are addressed: the model of the source and the model stability. The proposed wire model assumes that other objects in the computational space (e.g. metal objects) are not close enough to the wire to disturb the distributions of the field components in the cells adjacent to the wire. It also treats thin wires in which only axial currents exist on the wire.

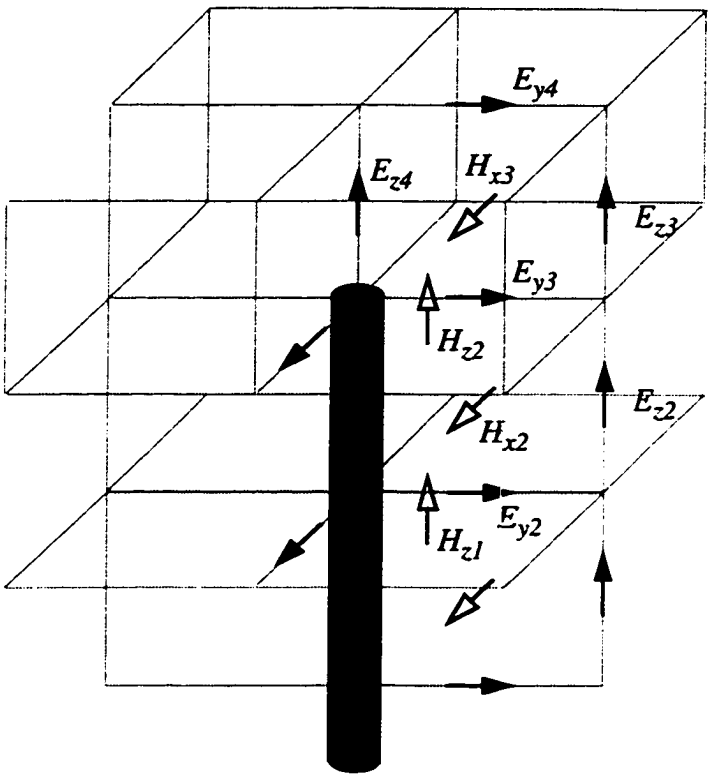

Fig. 6.6 Field components affected by the new wire model.

6.6.1 Algorithm

The proposed subcell algorithm for thin wires includes new update formulas in addition to the update formulas used by the standard wire formulation. There are two main differences between the proposed model and the standard model. First, the proposed algorithm incorporates the $1/r$ distributions of normal $\overline{E}$ and circumferential $\overline{H}$ field components into the updates of *all* field components adjacent to the wire (e.g. E_{y2} and H_{x2} in Fig. 6.6. The standard model only incorporates $1/r$ distributions into the updates of circumferential $\overline{H}$ field components). Second, the proposed model uses special update formulas for the field components one cell beyond the wire ends (e.g. E_{z4} and H_{x3} in Fig. 6.6. The standard model does not treat these components). The field distributions for the special update formulas are based on analytic expressions and NEC results, as described below. In one case, the

resulting field distribution was modified for the sake of numerical stability. As an example of how the algorithm is implemented, the update equations for two of the field components will be provided.

The field components affected by the proposed wire model are illustrated in Fig. 6.6 for a wire oriented in the z direction. For clarity, only the field components in one quadrant are shown, but the model applies to all four quadrants surrounding the wire. Of the field components shown in Fig. 6.6, the $1/r$ dependency is assumed to be the main influence on the field distributions of H_{x2}, E_{y2} and H_{x3} for line integrals and H_{x2}, E_{y2} and E_{y3} for surface integrals.

Table 6.1 Assumed distributions of field components in the proposed wire model.

field component	E_{z4}	E_{y3}	H_{x3}	H_{z1}, H_{z2}	all others
line integral distribution	$1/z^{0.6}$	$1/r^{1.3}$	$1/r$	0	$1/r$
surface integral distribution	eqn (6.10)	$1/r$	uniform	0	$1/r$

Other field distributions which require special treatment are summarized in Table 6.1. At the wire ends, some fields have a dependency that decreases more rapidly than $1/r$, due to singularities and the accumulation of charge there. Although analytic formulas do not exist for field distributions at the end of a wire of nonzero thickness, numerical techniques can give insight into the problem. Using the NEC program, the distribution of E_{y3} was observed to have a dependence close to $1/r^{1.1}$ for very thin wires and $1/r^{1.4}$ for wires with radii approaching maximum for thin wires. The distribution did not change significantly

with frequency or spatial resolution. A $1/r^{1.3}$ dependence was selected as it falls within the range given by NEC, and it was found to give very good results.

The accumulation of charge at the wire end is assumed to provide the main contribution to the distribution of E_{z4}. The wire end can be described as a circular disk. Assuming that the fields are quasi-static, the distribution of E_{z4} on a rectangular surface above the wire end can be evaluated from the following equation for the surface charge density on a thin circular disk [119]:

$$\rho_s(r) = \frac{4\varepsilon_0 V}{\pi\sqrt{r_0^2 - r^2}} \tag{6.10}$$

where r_0 is the radius of the disk, r is the radial distance from the centre of the disk to the point of interest, and V is the applied voltage. Coulomb's law is used to integrate the charge density to obtain the electric field distribution. As the surface integral of E_{z4} was found to vary only slightly with radius, a constant value was used corresponding to $r_0 = 2L/2100$.

The line distribution of E_{z4} for the update of H_{x3} is more challenging to obtain than its surface distribution. The difficulty is caused by the lower bound of $z = 0$ in the line integral. Many expressions were tried, based on solutions from NEC or analytic formulas for geometries similar to wires. However, these expressions, when integrated from $z = 0$ to $z = \Delta z$, resulted in numerical instabilities. Results from NEC simulations show that E_{z4} has a distribution of $1/z^p$ where $p > 1$. This formula does not have a finite integral, so values of $p <$

1 were chosen. A value of $p = 0.6$ was found to provide a good trade-off between stability and model accuracy.

The only other special treatment is the setting of $H_z = 0$ in the four Yee cells surrounding each wire section (this applies to H_{z1} and H_{z2} in Fig. 6.6). Theoretically, this should be the case for thin wires, as only axial currents exist on the wire, so there is no loss of generality of the model by imposing $H_z = 0$. It was also observed that there was no significant change in the numerical accuracy of the wire model when H_z was set to be zero. The reason for this treatment is that it improved the stability of the algorithm, particularly for very thin wires.

The FDTD update equations of the electric fields can be formulated from Ampere's law. For the update of E_{z4}, this requires knowledge of the surface distribution of E_{z4} and the line distributions of H_{x3} and the three other $\overline{H}$ field components surrounding the E_{z4} component. If the FDTD node at the wire end is located at $(x, y, z) = (i\Delta x, j\Delta y, k\Delta z)$, then implementing the $1/r$ dependence of H_{x3} and the E_{z4} distribution given from equation (6.10) results in the following update formula for a wire in free space:

$$E_z^{n+1}(i,j,k+1/2) = E_z^n(i,j,k+1/2) + \frac{\Delta t}{\varepsilon_0 K \Delta x \Delta y}\{ \tag{6.11}$$
$$\left(H_y^{n+1/2}\left(i+\frac{1}{2},j,k+\frac{1}{2}\right) - H_y^{n+1/2}\left(i-\frac{1}{2},j,k+\frac{1}{2}\right)\right)\Delta x \operatorname{atan}\left(\frac{\Delta y}{\Delta x}\right) -$$
$$\left(H_x^{n+1/2}\left(i,j+\frac{1}{2},k+\frac{1}{2}\right) - H_x^{n+1/2}\left(i,j-\frac{1}{2},k+\frac{1}{2}\right)\right)\Delta y \operatorname{atan}\left(\frac{\Delta x}{\Delta y}\right)\}$$

where the superscript n denotes the time step at which the field component is calculated (at time $t = n\Delta t$) and K is determined from the surface distribution of E_{z4}. In practice, $K \approx 0.7$.

Faraday's law in the integral form provides the update equations for the $\overline{H}$ field components. For the update of H_{x3}, the surface distribution of H_{x3} and the line distributions of E_{z4}, E_{y3}, E_{z3} and E_{y4} are needed. No special treatment of either E_{y4} or E_{z3} is given. Thus, they are assumed to vary uniformly along their lines of integration. This results the following update equation:

$$H_x^{n+1/2}(i, j+1/2, k+1/2) = H_x^{n-1/2}(i, j+1/2, k+1/2) - \frac{\Delta t}{\mu \Delta y \Delta z}\{ \quad (6.12)$$
$$(C_1 E_y^n(i, j+1/2, k) + \Delta z E_z^n(i, j+1, k+1/2) -$$
$$\Delta y E_y^n(i, j+1/2, k+1) - C_2 E_z^n(i, j, k+1/2)\ )\ \}$$

where:

$$C_1 = \frac{10}{3}\left(\frac{\Delta y}{2}\right)^{1.3}\left(r_0^{-0.3} - \Delta y^{-0.3}\right) \quad (6.13)$$

$$C_2 = \frac{2.5\Delta z}{2^{0.6}} \quad (6.14)$$

6.6.2 Implementation

Two important issues need to be addressed in the implementation of the wire model: the modeling of a source region inside the wire, and the model stability. The modeling of the source region should be based on the near-field physics of the region and consistent with

the model of the rest of the wire. This prevents non-physical reflections at the source region which would influence the input impedance and other parameters. The source model applies to all FDTD wire models presented in this dissertation. The stability analysis of the wire model provides information on how the stability of the model is influenced by the wire geometry and other model parameters. A formula is given which can be used to select a stability coefficient for the proposed wire model.

For the results presented in this dissertation, a dipole antenna is modeled with a 50 Ω source in the middle cell. A zero-impedance source gives the same value for the input impedance as a 50 Ω source, but it requires more iterations to achieve steady-state conditions. The dipole antenna is modeled as one continuous wire, rather than as two wires separated by a gap in the source region. This ensures that there are no discontinuities in the source region to influence the results.

The update equations for the source region are similar to those used along the wire. The E_z field in the source resistor is updated assuming a $1/r$ distribution of the circumferential H field, H_ϕ, and a uniform distribution of E_z. The update equations for the four H_ϕ components surrounding the source region are similar to those for the same components along the wire. Outside the resistor, the fields vary as $1/r$. However, inside the resistor, the H_ϕ components are nonzero. If the current density inside the wire is approximately uniform, then H_ϕ varies linearly from zero at the wire axis to a maximum value at the wire surface [113]. The maximum value is determined from continuity conditions at the resistor boundary. The assumption of a uniform current density inside the source resistor is accu-

rate when the skin depth of the resistor, δ_s, is large compared to the radius. For all of the results presented in this dissertation, $\delta_s > 1.6\, r_0$. Thus the current density at the centre of the resistor is at least $\exp(-r_0/\delta_s) = 54\%$ of its value at the resistor surface. Although the current density is not exactly uniform, the deviation between the true and assumed current distributions does not affect the results. This was tested and verified. It was also observed that using this distribution of H_ϕ (as opposed to assuming that $H_\phi = 0$) stabilized the source model for thick wires.

As explained in Chapter 4, the time stepping increment, Δt, must be less than the Courant limit to ensure the numerical stability of the FDTD method [75]. The stability coefficient, $S \leq 1$, can be selected to give a certain margin of stability, and values of $0.9 \leq S \leq 1$ are common in the FDTD method. Often when using subcell modeling, subcell gridding or other improvements to the conventional FDTD algorithm, lower stability coefficients must be used to ensure numerical stability. Both the modified and proposed wire models must be stabilized by reducing the stability coefficient as the wire radius is decreased. For the proposed wire model, the reason for this is that the scalar factor in front of E_{y3} (C_1 in equation (6.13)) increases exponentially as the wire radius is reduced, resulting in a non-physical accumulation of energy at the wire ends. Reducing the stability coefficient decreases the time increment between time steps, thus reducing the accumulation of energy at the wire ends. The only disadvantage of decreasing the stability coefficient is that the number of time steps must be increased to ensure that the same amount of time is simulated.

A formula has been derived that can be used to find the maximum stability coefficient, S_{max}, which guarantees the stability of the proposed wire algorithm. This formula was derived by fitting curves to a number of data points for S_{max} as a function of the wire radius and the spatial discretizations. The relationship between S_{max} and $\log(r_0)$ is approximately a straight line, and the slope and y-intercept of this line are functions of the spatial discretization. For a z-directed wire with $\Delta x = \Delta y$:

$$S_{max} = A \log(r_0) (B + (\Delta y/\Delta z)) + C (D - (\Delta z/\Delta y)) \tag{6.15}$$

where $A = 0.058951$, $B = 1.349891$, $C = 0.150746$, and $D = 10.334458$. Stability coefficients between 0.5 and 0.99 were used for the wires tested in this dissertation with the proposed algorithm. Lowering the stability coefficient was found to be the best way to guarantee stability and ensure consistent accuracy of the wire model. Other methods, including modifying the distributions of the field components or fixing the values of field components to those corresponding to using a thicker wire, were not as successful. The accuracy of the wire model is independent of the stability coefficient.

6.7 Accuracy of the Proposed Model

The accuracy of the proposed wire model is compared to the accuracy of the standard and modified models in this section. Wire model accuracy is evaluated using the same figures as shown in Section 6.5, with curves added for the proposed model. For the graphs of the four input impedance parameters, two other curves are also added to compare the accuracy of the standard and proposed wire models for a coarser spatial resolution ($\Delta x = \Delta y = \Delta z =$

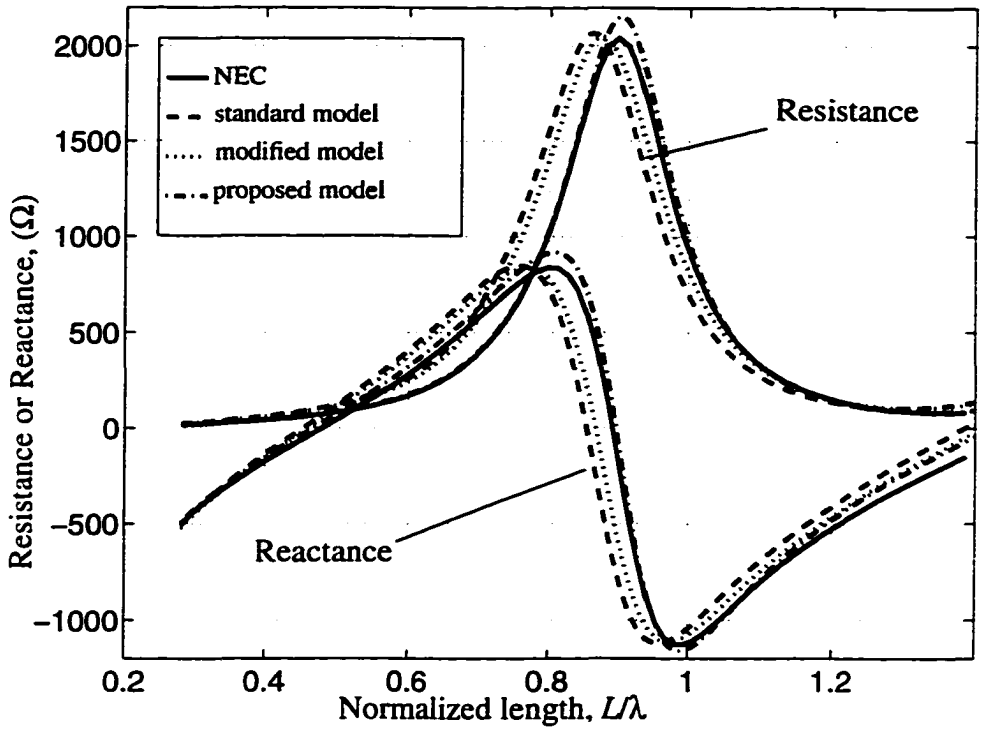

Fig. 6.7 Input impedance of the dipole antenna calculated by existing and proposed wire models. $r_0 = 2L/2100$.

19.1mm = $2L/22$). As the accuracy of the modified model was found to be unacceptable using the finer resolution, it is not compared to other wire models using the coarser resolution.

The input impedance of the dipole antenna is plotted over a broad frequency range in Figs. 6.7 and 6.8 for wire radii of $r_0 = 2L/2100$ and $r_0 = 2L/10^5$, respectively. For both wire radii, the input impedance curves calculated by the proposed wire model are in close agreement with NEC results. Due to the incorporation of more representative field distributions at the wire ends in the proposed model, the frequency scaling present in the results of the standard and modified wire models is nearly absent in the proposed wire model results. There is some amplitude error in the input impedance curves of the proposed wire model for $r_0 = 2L/2100$, but this error is not significant for $r_0 = 2L/10^5$. To further illustrate the improved

accuracy of the proposed wire model, the percent error in the input resistance (i.e. the percent deviation from the NEC input resistance) is shown in Fig. 6.9 for the three FDTD wire models. For both the standard and modified models, the error in the input resistance is greater than 40% for all values of L/λ below 0.8, and it is greater than 100% at values of L/λ near 0.8 (just below the second resonance). By comparison, the error in the input resistance of the proposed model is very small (less than 10% for all values of L/λ).

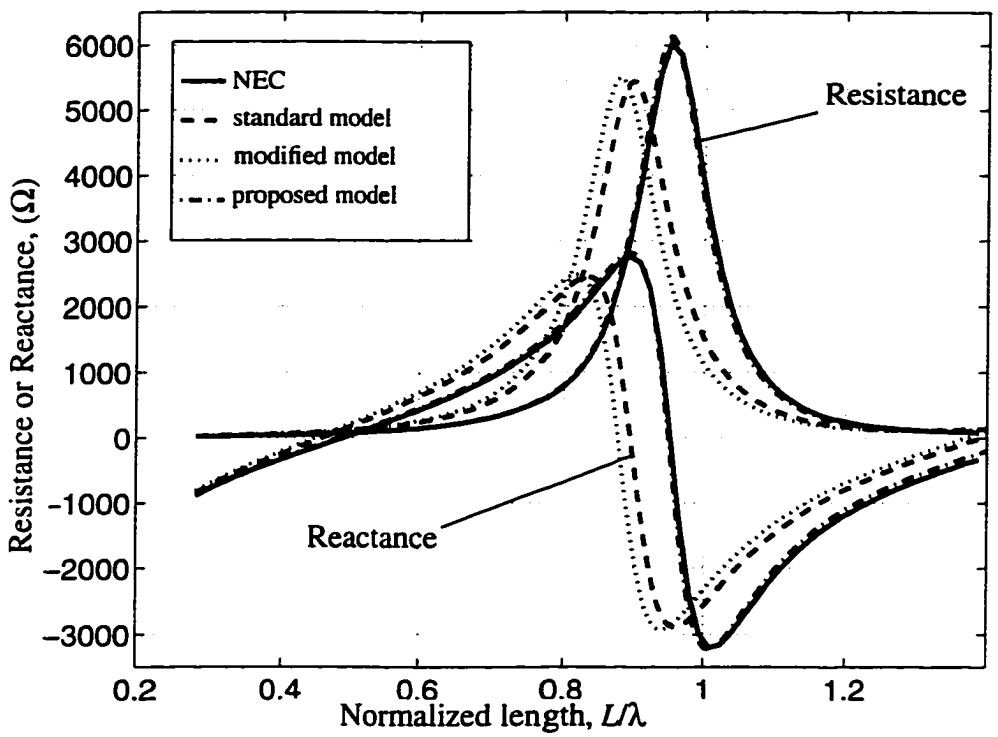

Fig. 6.8 Input impedance of the dipole antenna calculated by existing and proposed wire models. $r_0 = 2L/10^5$.

The input resistance, R_{in}, and the input reactance, X_{in}, at the frequency where $L = \lambda/2$ are presented in Fig. 6.10. The normalized wavelength, $\lambda/2L$, and the input resistance at the first dipole resonance are shown in Fig. 6.11. As in Section 6.5, the data points are shown as circles in the figures and cubic splines were used to interpolate between them. Bold lines indicate data using the finer spatial resolution and thin lines indicate data using the coarser

resolution.

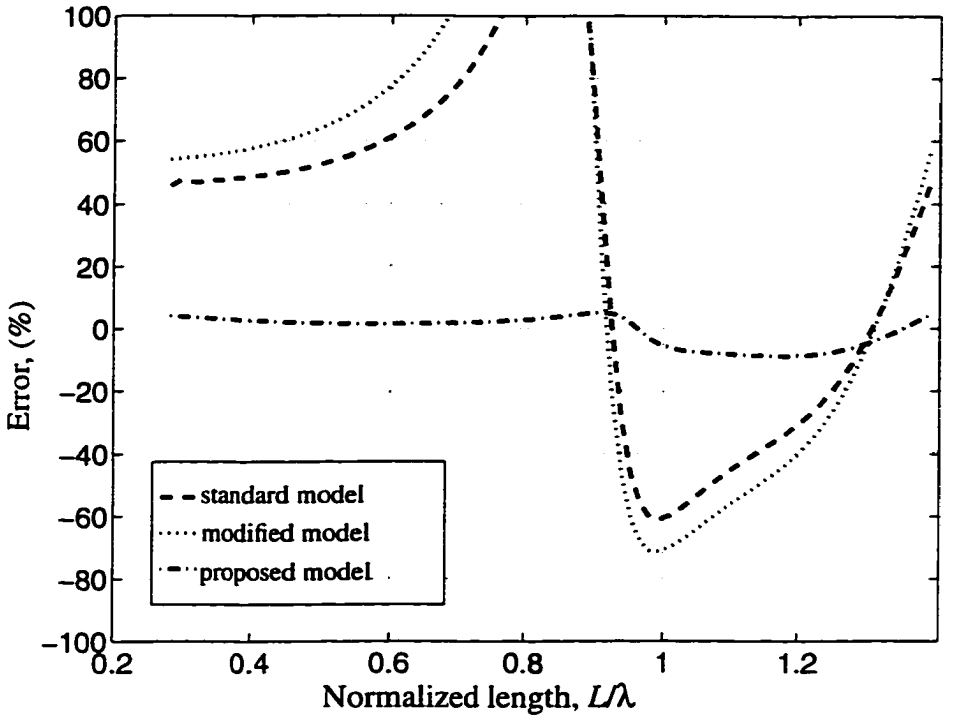

Fig. 6.9 Errors in input resistance of the dipole antenna calculated by existing and proposed wire models. $r_0 = 2L/10^5$.

With the finer spatial resolution, the results of the proposed model are much more accurate than those of the standard and modified models. The results of the proposed model are consistently more accurate than all of the standard model results and most of the modified model results. Although the errors in the modified model calculations of $\lambda/2L$ and X_{in} are smaller than those of the proposed model for the thickest wires studied, these errors increase dramatically as the radius is reduced. In contrast, the errors of the proposed model decrease as the wire radius is reduced. The maximum errors of R_{in} and X_{in} at $L = \lambda/2$ are 5.25% and 62.4%, respectively, using the proposed model, compared with maximum errors of 52.7% and 363% using the standard model and 76.6% and 629% using the modified model. For calculations of $\lambda/2L$ and the resonant resistance, the errors of the

proposed model are not greater than 3.01% and 5.09%, respectively. In comparison, the maximum errors are 6.53% and 25.1% using the standard wire model and 11.2% and 24.9% using the modified wire model. The significant improvements in the results are largely due to the modeling of the wire ends. While the modeling of the source region and the treatment of the field components along the length of the wire were important in improving the stability of the proposed wire model, the modeling of the wire ends affected the accuracy of the proposed wire model more significantly. At the wire ends, the $\overline{E}$ field components were more influential in improving the wire model accuracy than the $\overline{H}$ field components. This is due to the fact that the magnitudes of the $\overline{E}$ and $\overline{H}$ fields are proportional to the charge and current densities on the wire, respectively, and at the wire ends, the current density is at a minimum on the wire while the charge density is at a maximum. The distributions of E_{y3} and E_{z4} (Fig. 6.6) have the most pronounced effects on the model accuracy, and their effects are more pronounced for thinner wires.

With the coarser spatial resolution, the results of the standard and proposed wire models are less accurate than they are with the finer resolution, as expected. An interesting observation, however, is that in most cases, the accuracy of the proposed wire model with the coarser resolution is better than the accuracy of the standard wire model with the finer resolution. In fact, the proposed model results of R_{in} at $L = \lambda/2$ and the resonant resistance are still relatively close to the NEC values. From these observations, one could conclude that in order to achieve the same accuracy as the standard wire model, the proposed model may use a much coarser spatial resolution, resulting in large savings of computer memory and time.

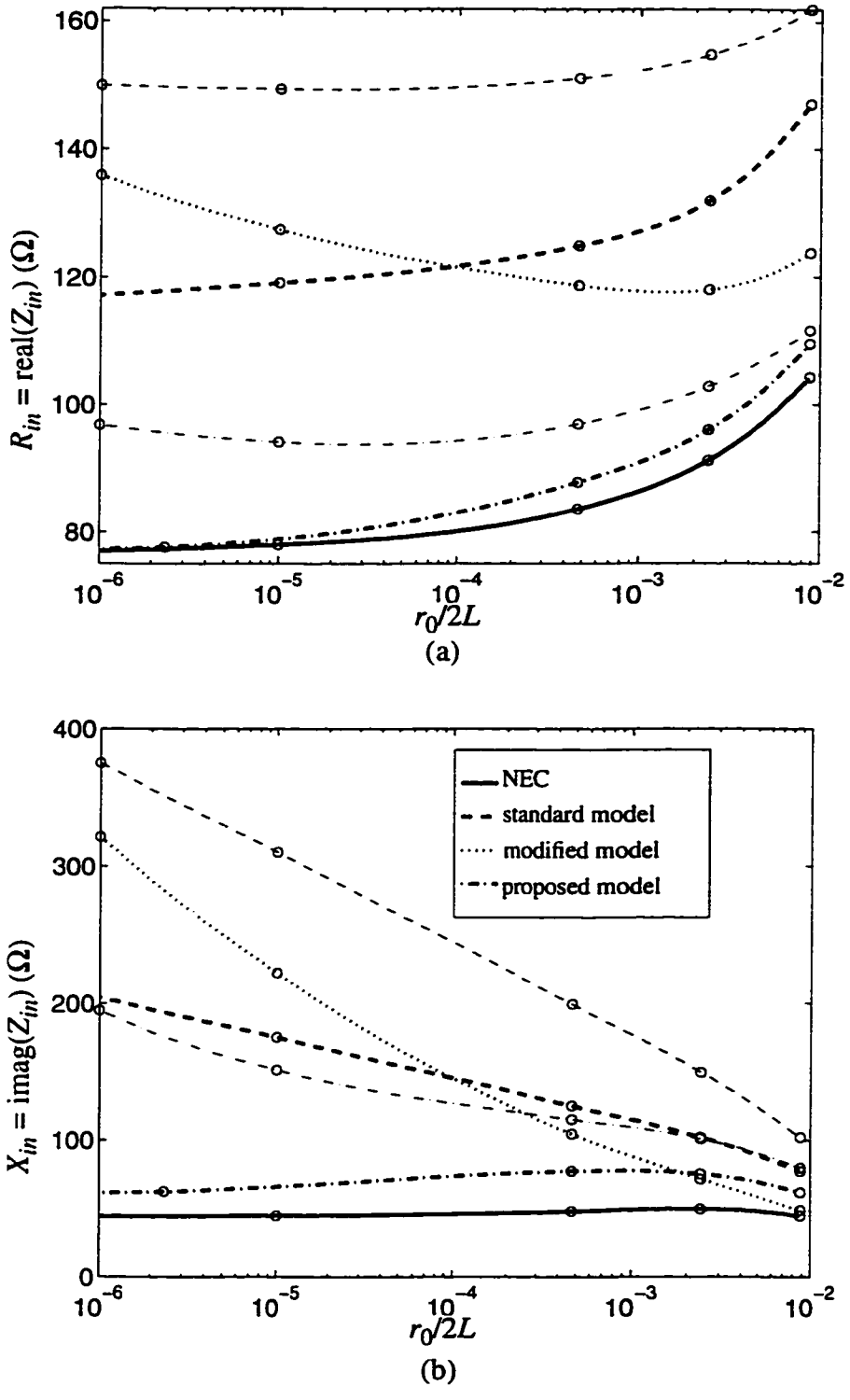

Fig. 6.10 (a) Input resistance and (b) reactance of the dipole antenna at $L = \lambda/2$ calculated by existing and proposed wire models (bold lines are for fine FDTD resolution, thin lines are for coarse resolution).

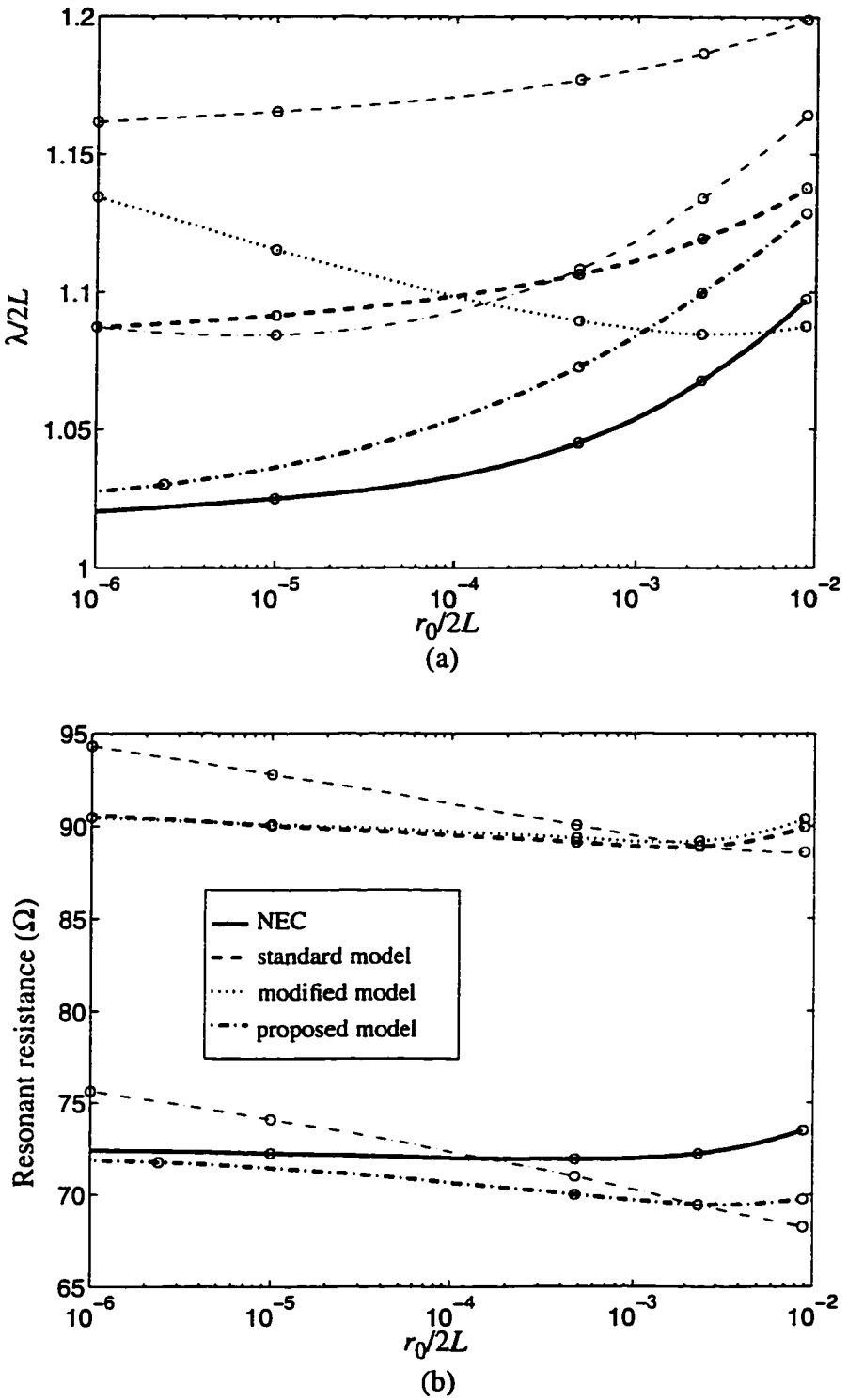

Fig. 6.11 (a) Normalized wavelength and (b) input resistance at the first resonance of the dipole antenna calculated by existing and proposed wire models (bold lines are for fine FDTD resolution, thin lines are for coarse resolution).

6.8 Concluding Remarks

During the dissertation research on the interaction between PCS antennas and the mobile communication environment (Chapter 5), there was an interest in calculating the input impedance of the PCS antennas, in addition to the antenna efficiency, radiation patterns and SAR. Before the FDTD calculations of antenna input impedance could be performed, however, a test was needed to determine their accuracy. The subsequent tests and literature search led to the body of research which is summarized in this chapter.

The literature search revealed that while a number of FDTD thin wire models have been proposed, a thorough investigation and comparison of their accuracy had not been undertaken. Consequently, it was difficult to know how reliable the FDTD wire models are. This research attempts to provide much needed information to this important area. The results of this research are important in many areas of FDTD modeling, including antenna design and the human-antenna interaction for PCS systems.

Two currently-used models were analyzed [79],[108], and the accuracy of both models in calculating the input impedance of a dipole antenna was found to be poor, even though relatively fine spatial resolutions were used in the calculations. While the shapes of the input impedance vs. L/λ curves were similar to those of NEC, the curves were scaled downward in frequency, resulting in significant errors in the input impedance at $L = \lambda/2$ and the wavelength and input resistance at the first dipole resonance.

A new wire model was developed in this chapter. This wire model includes special treat-

ments of the wire ends and the source region, as discussed in Section 6.6. The stability of this wire model was addressed, and a formula was developed for the maximum stability coefficient to be used with this wire model as a function of the wire radius and the spatial resolution selected. This formula can be integrated into an FDTD program to make the use of this wire model easy for the user.

The frequency scaling present in the results of the standard and modified wire models is nearly absent in the proposed wire model results. As a consequence, the proposed wire model is more accurate than the two other wire models for a given spatial resolution. The results also indicate that for the proposed wire model to achieve the same accuracy as the standard wire model, the proposed wire model may use a much coarser spatial resolution, resulting in savings of computer memory and time. The modeling of the field component distributions at the wire ends was the major contributor to the improvement in model accuracy, while the modeling of the source region and the field components along the length of the wire improved the model stability.

The additional computational cost of the proposed wire model to the FDTD method is minimal. The main difference between the proposed and standard wire models is that different factors are used in the update equations for the $\overline{E}$ and $\overline{H}$ field components adjacent to the wire (e.g. C_1 in equation (6.3)). As these factors can be calculated during the pre-processing stage of the FDTD execution, there is no significant change in the computation time of the main FDTD simulation. The added memory of the proposed model is small compared to the total memory requirements of the FDTD program.

Chapter 7 Conclusions and Future Work

7.1 Conclusions

The objective of the dissertation was to add to the current understanding of the electromagnetic interaction between a PCS antenna and the mobile communication environment. Using the FDTD technique, the effects of the user's body and the multipath environment on the antenna performance were investigated. These effects were studied and compared for two antenna configurations representative of linear and microstrip antenna types. The accuracy of FDTD modeling was crucial to the research, and the accuracy of wire modeling was investigated. The original contributions of this research are summarized in the following paragraphs.

The research on antenna configurations emphasized the development of microstrip antennas because of many features which make them attractive for use on PCS handsets. A novel polarization diversity antenna (PDA), first designed by the author during the Master's thesis, was further developed for practical use on PCS devices. The use of the FDTD technique in the design of this antenna allowed for relatively easy modifications of the antenna, and FDTD results provided a complement to measured results. The far-field radiation patterns of the PDA, calculated using the FDTD method, were in good agreement with measured radiation patterns.

An evaluation of the performance of PCS antennas in mobile communication environments was undertaken, also using the FDTD technique. This included the calculation of the far-field radiation patterns, the antenna efficiency and the specific absorption rate (SAR) of energy in the user's body. The radiation patterns were used, together with statistical models of the waves incident on the antenna from the mobile environment, to calculate the mean effective gain of an antenna and the correlation coefficient of a diversity antenna. Anatomically accurate models of the user's head and hand were implemented to evaluate the interaction between the PCS antenna and the user.

The results of the analysis of PCS antennas at frequencies near 900 MHz provided knowledge on how the following factors influence antenna performance and absorbed power in the user: the type of antenna (monopole or PDA), the presence of the user (head and hand) and the type of mobile communication environment (urban outdoor or suburban outdoor). Changing the antenna configuration from the monopole antenna to the PDA significantly affects the antenna efficiency and SAR in the user's body. When the monopole antenna is used, most of the absorbed power is dissipated in the head while a relatively small amount of power is dissipated in the hand. The opposite is true for the diversity antenna. Overall, the PDA performs better than the monopole antenna in terms of the antenna efficiency, the peak averaged SAR in the head, and the MEG. Also, the two modes of the PDA are sufficiently uncorrelated for diversity operation in both environments. However in terms of the MEG, the PDA is more sensitive than the monopole antenna to the presence of the user's body. The presence of the user's body

reduces the antenna efficiency, distorts the far-field radiation patterns, particularly in the direction of the head, and generally increases the magnitude of the cross polarization radiation. The type of mobile communication environment chosen has a pronounced effect on the correlation coefficient of the PDA and on the MEGs of the PDA and the monopole antenna. In urban outdoor environments, vertically-polarized antennas should perform well, while in suburban outdoor environments antennas that strongly receive both vertically-polarized and horizontally-polarized fields should perform better than vertically-polarized antennas. The results showed that the monopole antenna did not perform as well as the PDA, even in the urban environment, because it radiated a significant amount of power towards the ground. Small perturbations in the statistical model of the mobile environment did not greatly change the MEG and correlation coefficient results of either antenna. Thus the antenna performance is not very sensitive to small changes in the mobile environment.

The dissertation work included an in-depth study of the FDTD modeling of thin wires. The accurate FDTD modeling of thin wires and other objects is critical to the development of linear wire antennas (such as the monopole antenna considered in this work) and the research on the interaction between PCS antennas and the environment. A literature search revealed that no thorough investigation of the accuracy of FDTD thin wire models had been undertaken. Furthermore, two currently-used thin wire models were found to be inaccurate after a thorough investigation was performed in this dissertation. An evaluation of the accuracy of FDTD thin wire models was developed in this dissertation, based on the calculation of the input impedance of a dipole antenna

over a broad range of dipole radii. The finding of the errors in the two current wire models motivated the development of a new model. This model includes a special treatment of the field components at the wire ends and the development of a model of the source region. The stability of the wire model was also studied. The proposed wire model is more accurate than the two other wire models for a given spatial resolution. Also, for a given accuracy, the proposed wire model can use a much coarser spatial resolution than either of the two other models, resulting in savings of computer memory and time.

7.2 Future Work

The accurate FDTD thin wire model developed in this dissertation is a valuable tool that can be used to extend the analysis of PCS antennas in mobile communication environments. Using this model, one can evaluate how the presence of the user or the design of the handset changes the input impedance of a PCS antenna. In particular, the effects of the user or the handset design on the antenna resonant frequency or the impedance bandwidth are of interest. Antenna designers can use this information to design an appropriate matching circuit for an antenna or to learn how to use the presence of the user and the handset design to the greatest advantage. As the user's body is in the antenna near field, it should be considered part of the antenna.

The knowledge gained in the development of the thin wire model can also be used to develop accurate FDTD subcell models of other geometries. For example, the modeling of wire bends has not been treated satisfactorily in the literature. An accurate model of

wire bends, based on the near-field physics of the region near the wire bend, is a natural extension of the current work. The subcell modeling of thin slots and thin dielectrics may also be of interest.

In the analysis of the interaction between the PCS antenna and the surroundings, there is increasing interest in understanding how the ground plane formed by the handset affects the antenna performance, especially with the miniaturization of PCS handsets. Of interest is how the shape and size of the handset, the plastic covering and other features affect the electrical parameters of the antenna. The effect of the handset geometry on SAR in the user is also of interest, as the handset may shield the user's head from RF fields for some antenna configurations. A large body of work has been performed on the diffraction of radiated fields by ground plane edges and its effects on antenna characteristics (as reviewed in Chapter 3). However, much of the work has been limited to simple geometries that are analytically solvable (e.g. infinitely thin ground planes and circular geometries), or to experimental measurements, which are limited in terms of measuring near fields and current distributions. Using the FDTD technique, this work could be readily extended to include an analysis of PCS handsets.

Bibliography

Chapter 2

[1] I.J. Bahl and P. Bhartia, *Microstrip Antennas*, Dedham, Massachusetts: Artech-House, 1980.

[2] G.A. Deschamps, "Microstrip microwave antennas," presented at *The 3rd USAF Symposium on Antennas*, 1953.

[3] J. Huang, "Microstrip antennas for commercial applications," in *Microstrip Antennas*, edited by D.M. Pozar and D.H. Schaubert, New York: IEEE Press, pp. 371-379, 1995.

[4] C.A. Balanis, *Antenna Theory: Analysis and Design*, New York: Wiley, pp. 722-784, 1997.

[5] D.H. Schaubert, "A review of some microstrip antenna characteristics," in *Microstrip Antennas*, edited by D.M. Pozar and D.H. Schaubert, New York: IEEE Press, pp. 59-67, 1995.

[6] D.M. Pozar, "A review of bandwidth enhancement techniques for microstrip antennnas," in *Microstrip Antennas*, edited by D.M. Pozar and D.H. Schaubert, IEEE Press: New York, pp. 157-166, 1995.

[7] H. Iwasaki, "Proximity coupled linearly polarized patch antenna for dual frequency use," *Electronics Letters*, vol. 31, no. 15, pp. 1212-1213, Jul. 20, 1995.

[8] H. Iwasaki and Y. Suzuki, "Dual frequency multilayered circular patch antenna with self-diplexing function," *Electronics Letters*, vol. 31, no. 8, pp. 599-602, Apr. 13, 1995.

[9] D. Sanchez-Hernandez and I. Robertson, "Triple band microstrip patch antnenna using a spur-line filter and a perturbation segment technique," *Electronics Letters*, vol. 29, no. 17, pp. 1565-1566, Aug. 19, 1993.

[10] D. Sanchez-Hernandez and I. Robertson, "Analysis and design of a dual-band circularly polarized microstrip patch antenna," *IEEE Transactions on Antennas and Propagation*, vol. 43, no. 2, pp. 201-205, Feb. 1995.

[11] T. Huynh and K.-F. Lee, "Single-layer single-patch wideband microstrip antenna," *Electronics Letters*, vol. 31, no. 16, pp. 1310-1312, Aug. 3, 1995.

[12] K.R. Carver and J.W. Mink, "Microstrip antenna technology," *IEEE Transactions on Antennas and Propagation*, vol. AP-29, no. 1, pp. 2-24, Jan. 1981.

[13] Edward Goff, Personal communication, February, 1997.

[14] R. Waterhouse, "Small microstrip patch antenna," *Electronics Letters*, vol. 31, no. 8, pp. 604-605, April 13, 1995.

[15] Ch. Deleveaud, Ph. Leveque and B. Jecko, "New kind of microstrip antenna: the monopolar wire-patch antenna," *Electronics Letters*, vol. 30, no. 1, pp. 1-2, Jan. 6, 1994.

[16] I.J. Bahl, P. Bhartia and S.S. Stuchly, "Design of microstrip antennas covered with a dieiectric layer," *IEEE Transactions on Antennas and Propagation*, vol. AP-30, no. 2, pp. 314-318, March 1982.

[17] C.A. Balanis, *Antenna Theory: Analysis and Design*, New York: Wiley, p. 63, 1997.

[18] D.A. Paschen, "Practical examples of integral broadband matching of microstrip antenna elements," *Proceedings of the 1986 Antenna Applications Symposium*, pp. 199-217, 1986.

[19] H. An, B. Nauwelaers and A. Van de Capelle, "Broadband active microstrip array elements," *Electronics Letters*, vol. 27, pp. 2378-2379, Dec. 5, 1991.

[20] S. Dey, C.K. Aanandan, P. Mohanan and K.G. Nair, "A new broadband circular patch antenna," *Microwave and Optical Technology Letters*, vol. 7, no. 13, pp. 604-605, Sept. 1994.

Chapter 3

[21] N. Kuster and Q. Balzano, "Experimental and numerical dosimetry," in *Mobile Communications Safety*, edited by N. Kuster, Q. Balzano and J.C. Lin, London: Chapman & Hall, pp. 13-64, 1997.

[22] M.A. Stuchly, "Wireless communications and the safety of the user," *International Journal of Wireless Information Networks*, Vol 1, No. 4, 1994, pp. 223-228.

[23] W.R. Adey, "Bioeffects of mobile communications fields," in *Mobile Communications Safety*, edited by N. Kuster, Q. Balzano and J.C. Lin, London: Chapman & Hall, pp. 95-132, 1997.

[24] C. Polk and E. Postow, *Handbook of Biological Effects of Electromagnetic Fields*, Boca Raton: CRC Press, 1986.

[25] Information Ventures, Inc., *Risk in Perspective: Cellular Telephones and Brain Cancer*, Philadelphia, PA, 19102, 1995.

[26] S.M. Michaelson, "Interaction of nonmodulated fields with living matter," in *Handbook of Biological Effects of Electromagnetic Fields*, edited by C. Polk and E. Postow, Boca Raton: CRC Press, 1986.

[27] U. Bergqvist, "Review of epidemiological studies," in *Mobile Communications Safety*, edited by N. Kuster, Q. Balzano and J.C. Lin, London: Chapman & Hall, pp. 95-132, 1997.

[28] Ministry of Health and Welfare, Canada, *Limits of Exposure to Radiofrequency Fields at Frequencies from 10 kHz - 300 GHz: Safety Code 6*, Ottawa, Canada, 1991.

[29] American National Standards Institute, IEEE C95.1-1991: *IEEE Standard for Safety Levels with Respect to Human Exposure to Radio Frequency Electromagnetic Fields, 3 kHz to 300 GHz*, 1991, Piscataway, NJ 08855-1331, 1991.

[30] A. Taflove, *Computational electrodynamics: The finite-difference time-domain method*, Norwood, MA: Artech House Publications, p. 213, 1995.

[31] K. Karimullah, K-M. Chen and D.P. Nyquist, "Electromagnetic coupling between a thin-wire antenna and a neighboring biological body: theory and experiment," *IEEE Transactions on Microwave Theory and Techniques*, vol. 28, pp. 1218-1225, Nov. 1980.

[32] H.O. Ruoss and F.M. Landstorfer, "Slot antenna for hand held mobile telephones showing significantly reduced interaction with the human body," *Electronic Letters*, vol. 32, no. 6, pp. 513-514, March 1996.

[33] J. Toftgard, S. Hornsleth and J. Bach Andersen, "Effects on portable antennas of the presence of a person," *IEEE Transactions on Antennas and Propagation*, vol. 41, pp. 739-746, 1993.

[34] M.A. Jensen and Y. Rahmat-Samii, "EM interaction of handset antennas and a human in personal communications," *Proceedings of the IEEE*, vol. 83, no. 1, pp. 7-17, 1995.

[35] L. Martens, "Determine the EM fields induced by wireless telephones," *Microwaves & RF*, pp. 161-166, Dec. 1994.

[36] M. Okoniewski and M.A. Stuchly, "A study of the handset antenna and human body interaction," *IEEE Transactions on Microwave Theory and Techniques*, vol. 44, no. 10, pp. 1855-1864, Oct. 1996.

[37] K.R. Foster and H.P. Schwan, "Dielectric properties of tissues," in *Handbook of Biological Effects of Electromagnetic Fields*, edited by C. Polk and E. Postow, Boca Raton, FL: CRC Press, pp. 27-96, 1986.

[38] S. Gabriel, R.W. Lau and C. Gabriel, "The dielectric properties of biological tissues: 3. Parametric models for the dielectric spectrum of tissues," submitted to *Physics in Medicine and Biology*, 1996.

[39] I.G. Zubal, C.R. Harrell, E.O. Smith, Z. Rattner, G.R. Gindi and P.H. Hoffer, "Computerized three-dimensional segmented human anatomy," *Physics in Medicine and Biology*, vol. 21, pp. 299-302, 1994.

[40] P.M. Haskins, P.S. Hall and J.S. Dahele, "Polarisation-agile active patch antenna," *Electronics Letters*, vol. 30, no. 2, pp. 98-99, Jan. 20, 1994.

[41] M.M. Weiner, "Monopole element at the center of a circular ground plane whose radius is small or comparable to a wavelength," *IEEE Transactions on Antennas and Propagation*, vol. AP-35, no. 5, pp. 488-495, May 1987.

[42] J.T. Williams, H.J. Delgado, and S.A. Long, "An antenna pattern measurement technique for eliminating the fields scattered from the edges of a finite ground plane," *IEEE Transactions on Antennas and Propagation*, vol. AP-38, no. 11, pp. 1815-1822, November 1990.

[43] S.A. Long and A.W.C. Chu, "Radiation patterns of a monopole antenna mounted on a cubical conducting box," *IEEE Antennas and Propagion International Symposium Digest*, pp. 654-657, June 1987.

[44] R.G. Fitzgerrell, "Monopole impedance and gain measurements on finite ground planes," *IEEE Transactions on Antennas and Propagation*, vol AP-36, no. 3, pp. 431-438, March 1988.

[45] R.W. Wang and V.V. Liepa, "Reduction of the edge diffraction of a circular ground plane by using resistive edge loading," *IEEE Antennas and Propagion International Symposium Digest*, pp. 769-771, 1985.

[46] M.N.O. Sadiku, *Numerical Techniques in Electromagnetics*, Boca Raton: CRC Press, pp. 309-406, 1992.

[47] C.A. Balanis, *Advanced Engineering Electromagnetics*, New York: Wiley, pp. 743-851, 1989.

[48] J.H. Richmond, "Monopole antenna on circular disk," *IEEE Transactions on Antennas and Propagation*, vol. AP-32, no. 12, pp. 1282-1287, December 1994.

[49] H.M. Ibrahim, "Radiation patterns of a $\lambda/4$ monopole mounted on a small thick circular disc," *International Journal of Electronics*, vol. 68, no. 2, p. 283, February, 1990.

[50] S. Bhattacharya, S.A. Long, and D.R. Wilton, "The input impedance of a monopole antenna mounted on a cubical conducting box," *IEEE Transactions on Antennas and Propagation*, vol. AP-35, no. 7, pp. 756-762, July 1987.

[51] H. Nakano, J. Yamauchi and H. Mimaki, "Backfire radiation from a monofilar helix with a small ground plane," *IEEE Transactions on Antennas and Propagation*, vol. AP-36, no. 10, pp. 1359-1364, October 1988.

[52] H. Nakano, H. Mimaki and J. Yamauchi, "Numerical analysis of a helical antenna with a finite ground plane," *IEEE Antennas and Propagion International Symposium Digest*, pp. 129-132, 1986.

[53] J. Huang, "The finite ground plane effect on the microstrip antenna radiation patterns," *IEEE Transactions on Antennas and Propagation*, vol. AP-31, no. 4, pp. 649-653, July 1983.

[54] A.A. Kishk, L. Shafai, "The effect of various parameters of circular microstrip antennas on their radiation efficiency and the mode excitation," *IEEE Transactions on Antennas and Propagation*, vol. AP-34, no. 8, pp. 969-976, Aug. 1986.

[55] A.K. Bhattacharyya, "Effects of finite ground plane on the radiation characteristics of a circular patch antenna," *IEEE Transactions on Antennas and Propagation*, vol. 38, no. 2, pp. 152-159, February 1990.

[56] S. Rengarajan, "Finite ground plane effects on planar arrays of microstrip patch elements," *IEEE Antennas and Propagion International Symposium Digest*, pp. 741-744, 1984.

[57] W.C.Y. Lee, *Fundamentals of Mobile Communications Design Engineering*, New York: John Wiley and Sons, 1993.

[58] M.G. Douglas, *Diversity Antennas for Hand-Held Radio*, M.Sc. Thesis, University of Calgary, 1993.

[59] M.D. Yacoub, *Foundations of Mobile Radio Engineering*, Boca Raton, FL: CRC Press, 1993.

[60] W.C.Y. Lee, *Mobile Communications Design Fundamentals*, New York: Wiley InterScience, pp. 115-123, 1993.

[61] S.A. Bergmann and H.W. Arnold, "Polarisation diversity in portable communications environment," *Electronics Letters*, vol. 22, no. 11, pp. 609-610, 1986.

[62] T. Taga, "Analysis of correlation characteristics of antenna diversity in land mobile radio environments," *Electronics and Communications in Japan*, Part 1, vol. 74, no. 8, pp. 101-115, 1991.

[63] P.M. Haskins and J.S. Dahele, "Compact active polarisation-agile antenna using square patch," *Electronics Letters*, vol. 31, no. 16, pp. 1305-1306, Aug. 3, 1995.

[64] H. Arai, H. Iwashita, N. Toki and N. Goto, "A flat energy density antenna system for mobile telephone," *IEEE Transactions on Vehicular Technology*, vol. 40, no. 2, pp. 483-486, May 1991.

[65] S. Hosono, N. Goto, and H. Arai, "A flat diversity antenna by disk loaded monopole and three notches," *IEEE Transactions on Vehicular Technology*, vol. 43, no. 2, pp. 353-357, May 1994.

[66] J.B. Andersen and F. Hansen, "Antennas for VHF/UHF personal radio: A theoretical and experimental study of characteristics and performance," *IEEE Transactions on Vehicular*

Technology, vol. VT-26, no. 4, pp. 349-357, 1977.

[67] T. Taga, "Analysis for mean effective gain of mobile antennas in land mobile radio environments," *IEEE Transactions on Vehicular Technology*, vol. 39, no. 2, pp. 117-131, May 1990.

[68] Y.S. Yeh, "Antennas and polarization effects," *Microwave Mobile Communications*, edited by W.C. Jakes, IEEE Press, pp. 152-158, 1974.

[69] W.C.Y. Lee and Y.S. Yeh, "Polarization diversity system for mobile radio," *IEEE Transactions on Communications*, vol. COM-20, no. 5, pp. 912-923, 1972.

[70] W.C.Y. Lee, "Preliminary investigation of mobile radio signal fading using directional antennas on the mobile unit," *IEEE Transactions on Vehicular Communications*, vol. VC-15, pp. 8-15, 1966.

Chapter 4

[71] G.J. Burke and A.J. Poggio, "Numerical Electromagnetic Code (NEC) - Method of Moments," Naval Ocean Systems Center, San Diego, CA, *NOSC Technical Document 116*, Jan. 1981.

[72] M.N.O. Sadiku, *Numerical Techniques in Electromagnetics*, Boca Raton: CRC Press, pp. 179-204, 1992.

[73] K.S. Yee, "Numerical solution of initial boundary value problems involving Maxwell's equations in isotropic media," *IEEE Transactions on Antennas and Propagation*, vol. 14, pp. 302-307, 1966.

[74] C.A. Balanis, *Advanced Engineering Electromagnetics*, New York: Wiley, pp. 2-32, 1989.

[75] K.S. Kunz and R.J. Luebbers, *The Finite Difference Time Domain Method for Electromagnetics*, Boca Raton, FL: CRC Press, Inc., 1993.

[76] *Ibid.*, pp. 347-358.

[77] J-P. Berenger, "A perfectly matched layer for the absorption of electromagnetic waves," *Journal of Computational Physics*, vol. 114, pp. 185-200, 1994.

[78] S. Chebolu and R. Mittra, "The analysis of microwave antennas using the FDTD method," *Microwave Journal*, pp. 134-150, January, 1996.

[79] K.R. Umashankar, A. Taflove and B. Beker, "Calculation and experimental validation of induced currents on coupled wires in an arbitrary shaped cavity," *IEEE Transactions on*

Antennas and Propagation, vol. AP-35, no. 11, pp. 1248-1257, November, 1987.

[80] J.G. Maloney and G.S. Smith, "The efficient modeling of thin material sheets in the Finite-Difference Time-Domain (FDTD) method," *IEEE Transactions on Antennas and Propagation*, vol. AP-40, no. 3, pp. 323-330, March, 1992.

[81] D.J. Riley and C.D. Turner, "Hybrid thin-slot algorithm for the analysis of narrow apertures in Finite-Difference Time-Domain calculations," *IEEE Transactions on Antennas and Propagation*, vol. AP-38, no. 12, pp. 1943-1950, December, 1990.

[82] M.N.O. Sadiku, *Numerical Techniques in Electromagnetics*, Boca Raton: CRC Press, pp. 353-354, 1992.

[83] D.S. Watkins, *Fundamentals of Matrix Computations*, New York: John Wiley & Sons, 1991.

Chapter 5

[84] N.J. Boucher, *Cellular radio handbook: A reference for cellular system operation*, Mendecino, CA: Quantum Publishing, p. 275, 1990.

[85] M.A. Jensen and Y. Rahmat-Samii, "The electromagnetic interaction between biological tissue and antennas on a transceiver handset," *Digest of the IEEE/APS International Symposium*, vol. 1, pp. 367-370, 1994.

[86] R. Mumford, Q. Balzano and T. Taga, "Land mobile systems. II: Pagers, portable phones, and safety," in *Mobile Antenna Systems Handbook*, edited by K. Fujimoto and J.R. James, Artech House, pp. 175-273, 1994.

[87] M.A. Jensen and Y. Rahmat-Samii, "Performance analysis of antennas for hand-held transceivers using FDTD," *IEEE Transactions on Antennas and Propagation*, vol. 42, no. 8, pp. 1106-1113, 1994.

[88] K. Tsunekawa, "Diversity antennas for portable telephones," *IEEE Vehicular Technology Conference Digest*, pp. 50-56, 1989.

[89] G.F. Pedersen and J. Bach Andersen, "Integrated antennas for hand-held telephones with low absorption," *IEEE Vehicular Technology Conference Digest*, pp. 1537-1541, 1994.

[90] T. Taga and K. Tsunekawa, "Performance analysis of a built-in planar inverted F antenna for 800 MHz band portable radio units," *IEEE Journal of Selected Areas in Communications*, vol. SAC-5, no. 5, pp. 921-929, 1987.

[91] Z.D. Liu, P.S. Hall and D. Wake, "Dual-frequency planar inverted-F antenna," *IEEE Transactions on Antennas and Propagation*, vol. AP-45, no. 10, pp. 1451-1458, 1997.

[92] F. Lalezari and R.E. Munson, "Dual polarized, high efficiency microstrip antenna," U.S. Patent, Patent no. 4,464,663, Aug. 7, 1984.

[93] R.H. Johnston and M.G. Douglas, "Polarization/pattern diversity antenna," Patent applications filed in Canada #2,095,305 (April 30/93) and in U.S.A. #08/231,264 (April 22/94).

[94] M.G. Douglas and R.H. Johnston, "A compact two way diversity microstrip Upatch antenna," *IEEE Antennas and Propagation Society International Symposium Digest*, vol. 2, pp. 978-981, 1995.

[95] D. Goulbourne, P. Camwell, A. McGirr, J. McRory and G. Schmidt, "Automated antenna test range for small antennas," *ANTEM'90 Digest*, 1990.

Chapter 6

[96] H.C. Pocklington, "Electrical oscillations in wires," *Proceedings of the Cambridge Philological Society*, pp. 324-332, 1897.

[97] K. Kunz, B.W. Torres, R.A. Perala, J.M. Hamm, M.L. Van Blaricum and J.F. Prewitt, "Surface current injection techniques: a theoretical investigation," *IEEE Transactions on Nuclear Science*, vol. NS-25, pp. 1422-1427, Dec. 1978.

[98] J.G. Maloney, G.S. Smith and W.R. Scott, "Accurate computation of the radiation from simple antennas using the FDTD method," *IEEE Transactions on Antennas and Propagation*, vol. AP-38, pp. 1059-1068, 1990.

[99] W.A. Chamma, L. Shafai and S. Kashyap, "Thin wire modeling in FDTD," *IEEE Antennas and Propagation International Symposium Digest*, pp. 422-425, 1991.

[100] P.A. Tirkas and C.A. Balanis, "Finite-Difference Time-Domain method for antenna radiation", *IEEE Transactions on Antennas and Propagation*, vol. AP-40, no. 3, pp. 334-340, 1992.

[101] A. Taflove, K. Umashankar, B. Beker, F. Harfoush, and K. Yee, "Detailed FD-TD analysis of electromagneic fields penetrating narrow slots and lapped joints in thick conducting screens," *IEEE Transactions on Antennas and Propagation*, vol. AP-36, pp. 247-257, Feb. 1988.

[102] A. Taflove, *Computational electrodynamics: The finite-difference time-domain method*, Norwood, MA: Artech House Publications, p. 282, 1995.

[103] D.B. Shorthouse and C.J. Railton, "The incorporation of static field solutions into the finite-difference time-domain algorithm," *IEEE Transactions on Microwave Theory and Techniques*, vol. MTT-40, pp. 986-994, 1992.

[104] R. Holland and L. Simpson, "Finite-difference analysis of EMP coupling to thin struts and wires," *IEEE Transactions on Electromagnetic Compatibility*, vol. 23, pp. 88-97, 1981.

[105] J.J. Boonzaaier and C.W.I. Pistorius, "Thin wire dipoles - a Finite-Difference Time-Domain approach," *Electronics Letters*, vol. 26, no. 22, pp. 1891-1892, October, 1990.

[106] R. Luebbers, L. Chen, T. Uno and S. Adachi, "FDTD calculation of radiation patterns, impedance and gain for a monopole antenna on a conducting box," *IEEE Transactions on Antennas and Propagation*, vol. AP-40, pp. 1577-1582, Dec. 1992.

[107] C.J. Railton, "The simple rigorous and effective treatment of thin wires and slots in the FDTD method," *24th European Microwave Conference Digest*, pp. 1541-1546, 1994.

[108] J.J. Boonzaaier and C.W.I. Pistorius, "Finite-difference time-domain field approximations for thin wires with a lossy coating," *IEE Proceedings H - Microwaves, Antennas and Propagation*, vol. 141, no. 2, pp. 107-113, 1994.

[109] J.J. Boonzaaier and C.W.I. Pistorius, "Radiation and scattering by thin wires with a dielectric coating - a finite-difference time-domain approach," *Microwave and Optical Technology Letters*, vol. 5, no. 6, pp. 288-291, June 5, 1992.

[110] C.A. Balanis, *Antenna Theory: Analysis and Design*, New York: Wiley, p. 153, 1997.

[111] *Ibid.*, p. 453.

[112] M. Iskander, *Electromagnetic fields & waves*, New Jersey: Prentice Hall, p. 65, 1992.

[113] J.E. Parton, S.J.T. Owen and M.S. Raven, *Applied Electromagnetics, 2nd ed.*, New York: Springer-Verlag, pp. 22-70, 1986.

[114] M.N.O. Sadiku, *Numerical Techniques in Electromagnetics*, Boca Raton: CRC Press, pp. 276-283, 1992.

[115] W.L. Stutzmann and G.A. Thiele, *Antenna Theory and Design*, New York, NY: John Wiley and Sons, Inc., 1981.

[116] C.A. Balanis, *Antenna Theory: Analysis and Design*, New York: Wiley, p. 388, 1997.

[117] R.C. Johnson and H. Jasik, *Antenna Engineering Handbook, 2nd edition*, New York, NY: McGraw-Hill, p. 4-5, 1961.

[118] R.S. Elliot, *Antenna Theory and Design*, Englewood Cliffs, NJ: Prentice-Hall, pp. 299-331, 1981.

[119] J. Van Bladel, *Singular Electromagnetic Fields and Sources*, Oxford, UK: Clarendon Press, p. 131, 1991.

[120] A. Taflove, *Computational electrodynamics: The finite-difference time-domain method*, Norwood, MA: Artech House Publications, pp. 88-90, 1995.